

SIXTH ANNUAL CONFERENCE

AMERICAN SOCIETY OF BIOMECHANICS



University of Washington

Seattle, Washington

October 13 - 15, 1982

SCHEDULE

Wednesday, October 13, 1982

- 2-5 p.m. Registration/check-in
Hutchinson Hall, Room 101
- 2-5 p.m. Informal tours of biomechanics laboratories on the University of Washington campus
- 6:30-9:30 p.m. Registration/check-in and informal get-together at the Waterfront Activities Center, compliments of Kistler Instrument Corporation

Thursday, October 14, 1982*

- 8:00 a.m. Registration/check-in
HUB, room 309
- 8:15 a.m. Opening, welcome, announcements
HUB, room 309A
- 8:30 a.m. Session 1A (309A) Fluid Mechanics
Session 1B (309) Diagnosis
- 10:15 a.m. Coffee (304F)
- 10:40 a.m. Session 2A (309A) Prosthetics and Orthotics
Session 2B (309) Joint Mechanics
- 12:15 p.m. Lunch
Executive Council Meeting (304F)
- 1:15 p.m. Instructional Session 1 (309A)
Analysis of Stress and Strain
- 2:00 p.m. Session 3A (309A) Stress and Strain in Tissue
Session 3B (309) Safety and Performance
- 3:45 p.m. Open
- 6:30 p.m. Buffet Dinner at the Seattle Aquarium and
Instructional Session 2
Biological Biomechanics (Seattle Aquarium)

Friday, October 15, 1982*

- 8:15 a.m. Plenary Session
- 9:40 a.m. Session 4A (309A) Hard Tissue Mechanics
Session 4B (309) Muscle Activity
- 10:40 a.m. Coffee (304F)
- 11:00 a.m. Session 5A (309A) Tissue Mechanics
Session 5B (309) Muscle Action
- 12:25 p.m. Lunch
Executive Council Meeting (304F)
- 1:00 p.m. Instruction Session 3 (309A)
Analysis of Position and Motion
- 1:45 p.m. Business Meeting (309A)
- 2:30 p.m. Session 6A (309A) Kinematics
Session 6B (309) Soft Tissue Mechanics
- 4:30 p.m. Adjournment

*Room numbers refer to meeting rooms on the third floor of the Student Union Building (known as the "HUB") on the University of Washington campus.

CONFERENCE PROGRAM

Thursday, October 14

8:15

OPENING AND WELCOME

8:30-10:15 a.m.

SESSION 1A FLUID MECHANICS

Chairperson: V.C. Mow

8:30

Keynote Lecture: The influence of the ground effect on animal swimming and flight. R. Blake, University of British Columbia

8:55

Motor performance and jet propulsion in the cephalopod *Nautilus Pompilius*. J.A. Chamberlain, Jr., Brooklyn College of the City University of New York

9:05

Asymmetrical particle capture in the marine filter feeder. M.R. Patterson, Harvard University

9:15

Questions

9:20

The pressure and flow patterns inside an aortic bifurcation. S.Ø. Wille, University of Oslo

9:30

Fluid dynamics of aortic stenosis: mechanisms of subvalvular gradient generation. A. Pasipoularides, J.P. Murgo, J.J. Bird, W.E. Craig, Brooke Army Medical Center

9:40

Questions

9:45

The effects of smooth muscle activity on the mechanical and hydraulic properties of the dog aorta. J.-P.L. Dujardin, D.N. Stone, C.D. Forcino, H.P. Pieper, Ohio State University

10:00

Elastohydrodynamic lubrication models for the normal human ankle joint. J.B. Medley, D. Dowson, V. Wright. Universities of Waterloo and Leeds

8:30-10:15 a.m.

SESSION 1B DIAGNOSIS

Chairperson: T.V. How

8:30

Keynote Lecture. Biomechanics and orthopaedics: historical perspectives. D.M. Spengler, University of Washington

8:55

Evaluation of physiologic suspension factors in below knee amputees. F.G. Lippert III, University of Washington

9:05

An analytical investigation on tachographic gait records to explore the factors discriminating handicapped gait from normal gait. D.N. Tibarewala, S. Ganguli, Calcutta University

9:15

Questions

9:20

Evaluation of trunk deformity using light profiles. J.A.A. Miller, D.L. Spencer, A.B. Schultz, University of Illinois at Chicago Circle

9:30

Trunk muscle myoelectric activity in girls with structurally-normal spines and girls with idiopathic scoliosis. M. Reuber, A. Schultz, D. Spencer, T. McNeill, University of Illinois at Chicago Circle

9:40

Questions

9:45

Analysis of the effect of variable strain rate on acoustic emission in bone. R.A. Fischer, M.H. Pope, D.S. Seligson, University of Vermont

10:00

CT obtained bone geometry and density measurements using second order correction. D.D. Robertson, H.K. Huang, Georgetown University and University of California, Los Angeles.

10:40-12:15 p.m.

SESSION 2A PROSTHETICS AND ORTHOTICS

Chairperson: Y.K. Liu

10:40

Biomechanics: research and development at IMA. L.C. Nava, P.A.A. Laura, Instituto de Mecanica Aplicada, Argentina

10:50

Bending stiffness of unilateral and bilateral external fixator frames. F. Behrens, W. Johnson, T. Koch, N. Kovacevic, University of Minnesota and Metropolitan Medical Center

11:00

Questions

11:05

Single-plane X-ray photogrammetry for detecting total joint loosening. F.G. Lippert, R.M. Harrington, S.A. Veress, T. El-Garf, University of Washington and Seattle VA Medical Center

11:15

Origin of knee moments during ambulation and their modification by ankle-foot orthoses. J.F. Lehmann, M.J. Ko, B.J. deLateur, University of Washington

11:25

Questions

11:30

A detailed study of the effects of long term use on a total knee prosthesis. E.H. Coale, S.A. Goldstein, R.R. Reschly, L.S. Matthews, University of Michigan

11:45

PMMA reinforced by hydroxy-apatite crystals—preliminary results: creep analysis. A. Castaldini, A. Cavallini, A. Moroni, R. Olmi, L. Ranieri, University of Bologna

12:00

Fatigue of acrylic bone cement—the influence of strain range and mean strain. E.I. Gates, D.R. Carter, W.H. Harris, Massachusetts General Hospital and Harvard Medical Center

10:40-12:15 p.m.

SESSION 2B JOINT MECHANICS

Chairperson: M.A.R. Koehl

10:40

Muscular power across the knee joint during the pull in Olympic weight lifting. R.M. Enoka, University of Arizona

10:50

Biomechanics of the knee extension exercise. W.J. Sun-
tay, E.S. Grood, D.L. Butler, F.R. Noyes, University of
Cincinnati

11:00

Questions

11:05

Non-sagittal plane movements and forces during dis-
tance running. K.R. Williams, University of California
at Davis

11:15

Intersgmental movement effects on net support mo-
ment. R.H. Deusinger, Washington University

11:25

Questions

11:30

Factors affecting lumbar forces during the clean and
jerk. S.J. Hall, Washington State University

11:45

Analysis of strain in the anterior cruciate ligament of
the human knee. R.A. Fischer, S.W. Arms, R.J. Johnson,
M.H. Pope, University of Vermont

12:00

Torsion in ostrich knees. P.L. O'Neill, Portland State
University

1:15-1:55 p.m.

INSTRUCTIONAL SESSION 1

Analysis of stress and strain. D.R. Carter, Massachusetts
General Hospital and S.L. Woo, University of Califor-
nia, San Diego

2:00-3:45 p.m.

SESSION 3A STRESS AND STRAIN IN TISSUE

Chairperson: J.M. Gosline

2:00

Keynote Lecture: Finite element analysis—what is its
application? R. Crowninshield, University of Iowa

2:20

Vertebral stress distributions and their relationship to
ejection induced spinal injuries. E. Privitser, R.R.
Hosey, Wright-Patterson Air Force Base and Systems
Research Laboratories, Inc.

2:30

An analysis of the human intervertebral joint consider-
ing orthotropic and viscoelastic properties. L. Allen,
A.N. Palazotto, Wright-Patterson Air Force Base

2:40

Questions

2:50

A dynamic finite element model of pole vaulting. P.M.
McGinnis, L.A. Bergman, University of Illinois at Ur-
bana-Champaign

3:00

Analysis of force flow in different artificial knee joints
using the finite element method. H. Röhrle, W. Soll-
bach, J. Gekeler, Tübingen and Friedrichshafen, Ger-
many

3:10

Questions

3:15

A finite-element model of the human head and neck
during oblique-crown impact. R.R. Hosey, J.E. Ryerson,
Y.K. Liu, Systems Research Laboratories, Inc. and Uni-
versity of Iowa

3:30

True stress and strain in mammalian skeletal muscle.
S.C. Bodine, R.F. Zernicke, V.R. Edgerton, R.R. Roy,
D.M. Peller, University of California, Los Angeles

2:00-3:45 p.m.

SESSION 3B SAFETY AND PERFORMANCE

Chairperson: E.M. Burgess

2:00

Keynote Lecture: The influence of biomechanics on the
design of sports equipment. E.C. Frederick, NIKE, Inc.

2:20

Individual subject force production patterns observed
for an isotonic and isokinetic bench press. J.E. Lander,
B.T. Bates, J.A. Sawhill, J. Hamill, University of Oregon

2:30

The prediction of repetition maxima and strength-train-
ing. J.R. Engsborg, J.G. Hay, K. Ueya, University of Iowa

2:40

Questions

2:50

Field measurements in snow skiing injury research. J.K.
Louie, C.Y. Kuo, C.D. Mote, Jr., University of California,
Berkeley

3:00

Force analysis in cross-country skiing. J. Pierce, M. Pope, R. Johnson, D. Punia, University of Vermont

3:10

Questions

3:15

Dynamic simulation of the leg in torsion. L.K. Dorius, M.L. Hull, University of California, Davis

3:30

On the role of joint torques in determining the result of the performance of a motor skill. J.G. Andrews, University of Iowa

6:30-9:00 p.m.

INSTRUCTIONAL SESSION 2

Biological Biomechanics: a guided tour through the Seattle Aquarium. S. Wainwright et al., Duke University

Friday, October 15

8:15-9:35 a.m.

PLENARY SESSION

Chairperson: S. Wainwright

Invited Lectures

8:15 ~~Replacement King Liu~~
Anthropod joints: the benign tyranny of the exoskeleton. J. Currey, University of York ~~Cancelled~~

8:55

The physics of fluid flow in connective tissue. V.C. Mow, Rensselaer Polytechnic Institute

9:40-10:40 a.m.

SESSION 4A HARD TISSUE MECHANICS

Chairperson: ~~A.H. Burstein~~
Woo

9:40

Comparative mechanics of mammalian spines. D.G. Wilder, M.H. Pope, R. Nawojchik, University of Vermont

9:55

The determination and analysis of compressive strength characteristics of squirrel monkey vertebral bodies. S.D. Smith-Lagnese, L. Kazarian, Wright-Patterson Air Force Base

10:10

Effects of X-rays on the mechanical properties of bone. H.S. Ranu, Louisiana Technical University

10:25

The influence of age on rat bone structural and material properties. T.S. Keller, D.M. Spengler, D.R. Carter, VA Medical Center, University Hospital Seattle and Massachusetts General Hospital

9:40-10:40 a.m.

SESSION 4B MUSCLE ACTION

Chairperson: A. Schultz

9:40

The biomechanics of movement in tongues and tentacles. W.M. Kier, K.K. Smith, Duke University

9:55

Quantification of stimulated muscle contractions by Moire surface topography. A.T. Andonian, A.B. Schultz, University of Illinois at Chicago Circle

10:10

Elastic energy storage and power output in squid mantle muscle. J.M. Gosline, R.E. Shadwick, M.E. DeMont, University of British Columbia

10:25

Structural domains of the muscle-tendon-junction. J.A. Trotter, S. Eberhard, University of New Mexico

11:00-12:25 p.m.

SESSION 5A TISSUE MECHANICS

Chairperson: T.R. Nichols

11:00

Regional left ventricular asynergetics: a question of balance between intramyocardial and intracavitary pressure. H.N. Sabbah, P.D. Stein, Henry Ford Hospital

11:25

Mechanical properties of osteopetrotic bone. R.P. Robinson, F. Vosburgh, A.H. Burstein, Mason Clinic, Rockefeller University and Hospital for Special Surgery

11:45

The distribution of tibial trabecular bone properties as determined by computer assisted axial tomography. S.A. Goldstein, L.S. Matthews, E.M. Braunstein, B.W. Marks, University of Michigan

12:05

Acoustic emission: a non-invasive monitoring technique for total joint replacement patients. T.M. Wright, D.L. Bartel, A.H. Burstein, Hospital for Special Surgery

11:00-12:25 p.m.

SESSION 5B MUSCLE ACTION

Chairperson: A. Schultz

11:00

Keynote Lecture: Biomechanics of throwing: projecting into the future. A.E. Atwater, University of Arizona

11:25

Study of the interaction between knee joint position, joint loads, and muscle activity at the knee. T.P. Andriacchi, G.B.J. Andersson, R. Ortengren, R. Mikosz, Rush-Presbyterian-St. Luke's Medical Center

11:45

Muscular work in selected ankle extensors of the cat during unrestrained locomotion. W.C. Whiting, R.J. Gregor, R.R. Roy, C.L. Hager, University of California, Los Angeles

12:05

The two-burst pattern revisited. M.H. Sherif, R.J. Gregor, L.M. Liu, R.R. Roy, C.L. Hager, University of California, Los Angeles, University of Illinois, Chicago

1:00-1:40 p.m.

INSTRUCTIONAL SESSION 3

Tom And.

The analysis of position and motion. ~~E.S. Grood~~, University of Cincinnati, J. Dapena, University of Massachusetts

1:45-2:25 p.m.

BUSINESS MEETING

2:30-4:24 p.m.

SESSION 6A KINEMATICS

Chairperson: A.E. Atwater

2:30

Segment interaction during the swing phases of walking and running. C.A. Putnam, Dalhousie University

2:45

Linearized approximations for the simulation of swing leg motion during gait. W.H. Lee, J.M. Mansour, Harvard Medical School

3:00

Mechanics of orientation in sea pens: a rotational one link joint. B.A. Best, Duke University

3:15

A new method for describing the motion of the knee. H. Kurosawa, P.S. Walker, Brigham and Women's Hospital, VA Medical Center

3:30

Evaluation of data smoothing techniques for biomechanical data. R.J. Bentham, Dalhousie University

3:48

A triple pendulum model of the golf swing. K.R. Campbell, University of Illinois

4:06

Speed-correlated changes in limb orientation, stride frequency and movement components in a generalized lizard. J.A. Peterson, University of California, Los Angeles

2:30-4:24 p.m.

SESSION 6B SOFT TISSUE MECHANICS

Chairperson: ~~S.L. Woo~~

2:30

Coping with stress and strain: the mechanics of feeding with extensible tentacles (*Eupolymnia heterobranchia*). A.S. Johnson, University of California, Berkeley

2:45

Mechanical properties of human neck/torso skin and vessel replications. W. Goldsmith, L.J. Frankel, University of California, Berkeley

3:00

Mechanical properties of the Liverpool artery: I. Uniaxial properties. T.V. How, R.M. Clarke, D. Annis, University of Liverpool

3:15

Mechanical properties of the Liverpool artery: II. Multi-axial properties. R.M. Clarke, T.V. How, University of Liverpool

3:30

Mechanical properties of cephalopod arteries. R. Shadwick, J. Gosline, University of British Columbia

3:48

Mineral Deposits in connective tissues: the mechanical design of spicule-reinforced animals. M.A.R. Koehl, University of California, Berkeley

4:06

Ionic regulation of tissue modulus: electrostatic or chemical? J.P. Eylers, A.R. Greenberg, Duke University, University of Colorado

INDEX OF PARTICIPANTS

Abstracts are arranged in the order in which they appear in the program. Those included from pages 78-93 are listed alphabetically by first author and are presented at this conference by title only.

ALLARD, P	91	EYLERS, JP	77
ALLEN, L	32	FERGUSON, AB	80
ANDERSSON, GBJ	49	FISCHER, RA	13, 27
ANDONIAN, AT	46	FORCINO, CD	6
ANDRES, R	81	FRANCIS, PR	78
ANDREWS, JG	43	FRANKEL, LJ	72
ANDRIACCHI, TP	49	FREDERICK, EC	37
ANNIS, D	73	GANGULI, S	10
ARMS, SW	27, 92	GATES, EI	21
ATWATER AE	44	GEKÉLER, J	34
BARTEL, DL	62	GOLDSMITH, W	72
BATES, BT	38, 78	GOLDSTEIN, SA	19, 57
BEHRENS, F	16	GOSLINE, JM	47, 75, 79
BENTHAM, RJ	68	GREENBERG, AR	77
BERGMAN, LA	33	GREGOR, RJ	50, 61
BERTRAM, JE	79	GROOD, ES	23, 63
BEST, BA	66	HAGER, CL	50, 61
BIRD, JJ	5	HALL, SJ	26
BLAKE, R	1	HAMILL, J	38
BODINE, SC	36	HARRINGTON, RM	17, 86
BRAUNSTEIN, EM	57	HARRIS, WH	21
BROWN, TD	80	HAY, JG	39
BURGER, CP	93	HOSEY, RR	31, 35
BURSTEIN, AH	56, 62	HOW, TV	73, 74
BUTLER, DL	23	HUANG, HK	14
CAMPBELL, KR	69	HUBBARD, M	84
CARTER, DR	21, 29, 55	HULL, ML	42
CASTALDINI, A	20	JOHNSON, AS	71
CAVALLINI, A	20	JOHNSON, RJ	27, 41, 88
CHAFFIN, DB	81	JOHNSON, W	16
CHAMBERLAIN, JA2, 82	KAZARIAN, L	53
CLARKE, RM	73, 74	KELLER, TS	55
COALE, EH	19	KIER, WM	45
CRAIG, WE	5	KINOSHITA, H	78
CROWNINSHIELD, R	30	KO, MJ	18
CURREY, J	51	KOCH, T	16
DAPENA, J	63	KOEHL, MAR	76
DELATEUR, BJ	18	KOVACEVIC, N	16
DEMONT, ME	47	KRIELLARS, DJ	85
DEUSINGER, RH	25	KUO, CY	40
DONNERMEYER, DD	92	KUROSAWA, H	67
DORIUS, LK	42	LANDER, JE	38
DOWSON, D	7	LAURA, PAA	15
DUJARDIN, J-PL	6	LEE, K	81
EBERHARD, S	48	LEE, WH	65
EDGERTON, VR	36	LEHMANN, JF	18
EL-GARF, T	17	LING, SC	89
ENGIN, AE	83	LIPPERT, FG	9, 17, 86
ENGSBERG, JR	39	LIU, LM	61
ENOKA, RM	22	LIU, YK	35

Participants
 6th ASB Conference
 Page 2

LOUIE, JK	40	ROBERTSON, DD	14
MANSOUR, JM	65	ROBINSON, RP	56
MARKS, BW	57	RÖHRLE, H	34
MATTHEWS, LS	19, 57	ROY, RR	36, 50, 61
MCGINNIS, PM	33	RYERSON, JE	35
MCINTYRE, DR	87	SABBAH, HN	49, 60
MCNEILL, T	12	SAWHILL, JA	38
MEDLEY, JB	7	SCHEIRMAN, GL	86
MEDOFF, H	88	SCHULTZ, AB	11, 12, 46
MIKOSZ, R	49	SHADWICK, RE	47, 75
MILLER, JA	11	SELIGSON, DS	13
MOORE, WA	82	SHERIF, MH	61
MORONI, A	20	SIMON, MR	90
MOTE, CD	40	SIROIS, JP	91
MOW, VC	58	SMITH, KK	45
MURGO, JP	5	SMITH-LAGNESE, SD	53
MUTSCHLER, TA	80	SOLLBACH, W	34
NAVA, LC	15	SPENCER, DL	11, 12
NAWOJCHIK, R	52	SPENGLER, DM	8, 55
NEWELL, SG	86	STEIN, PD	59, 60
NGUYEN, L	89	STOKES, IAF	92
NOYES, FR	23	STONE, DN	6
OLADUNNI, J	83	SUNTAY, WJ	23
OLMI, R	20	THIRY, PS	91
O'NEILL, PL	28	TIBAREWALA, DN	10
ORTENGREN, R	49	TRINKLE, JC	84
PALAZOTTI, AN	32	TROTTER, JA	48
PASIPOULARIDES, A	5	UEYA, K	39
PATTERSON, MR	3	VERESS, SA	17
PELLER, DM	36	VOLOSHIN, AS	93
PETERSON, JA	70	VOSBURGH, F	56
PHUNG, PK	89	WALKER, PS	67
PIEPER, HP	6	WHITING, WC	50
PIERCE, JP	41, 88	WILDER, DG	52, 92
PILLSBURY, SW	82	WILLE, SØ	4
POPE, MH	13, 27, 41, 52, 88, 92	WILLIAMS, KR	24
PRIVITZER, E	31	WOO, SL	29
PUNIA, D	41, 88	WOODLE, AS	86
PUTNAM, CA	64	WOSK, J	93
RALEY, BF	87	WRIGHT, TM	62
RANIERI, L	20	WRIGHT, V	7
RANU, HS	54	YOUNG, Y	89
RESCHLY, RR	19	ZERNICKE, RF	36
REUBER, M	12		

THE INFLUENCE OF THE GROUND EFFECT
ON ANIMAL SWIMMING AND FLIGHT

Robert Blake
Department of Zoology
University of British Columbia
Vancouver, B.C. CANADA

MOTOR PERFORMANCE AND JET PROPULSION IN THE CEPHALOPOD

NAUTILUS POMPILIUS

by

John A. Chamberlain, Jr.
Department of Geology
Brooklyn College of the
City University of New York
Brooklyn, NY 11210

and

Osborn Laboratories of Marine Sciences
New York Aquarium
Brooklyn, NY 11224

Strain gauge measurements of propulsive force and pressure in swimming Nautilus pompilius show that for adult animals (body wt \approx 600 - 1200 gm) a mean propulsive force of about 5×10^4 dynes is produced by a mantle cavity pressure of about 3×10^3 dynes/cm², and with a jet velocity of about 250 cm/sec. Swimming velocity is about 30 cm/sec. This performance is achieved with propulsive muscles totalling about 10% of the animals body weight. Juveniles have correspondingly smaller output and size, although maximum swimming velocity is not much less than in the adults. Cinematography of locomotory behavior suggests that periodic inward-outward movements of the body produced by action of the paired adductor muscles generates much of the propulsive force. Equilibrium control is achieved through the inherently high static stability of the shell. Comparison of propulsive muscle output, and mass, and of propellant volume and velocity, among fish, marine mammals, and cephalopods shows that Nautilus is much more weakly powered and inefficient than these other swimmers. Estimates of swimming speed in fossil cephalopods, based on the data for Nautilus, indicate that most were slower than Nautilus. The relative ineffectiveness of the propulsion mechanism of shelled cephalopods like Nautilus, is due mainly to the retention of the shell as a major feature of adaptive design. The evolutionary history of swimmers (i.e. shelled cephalopods, soft bodied cephalopods, and fish) seems to be governed by advances in the sophistication of buoyancy and propulsion mechanisms. Shelled cephalopods have declined partly because their unique buoyancy system, based on the retention of a heavy shell, has prevented them from developing an efficient means of propulsion comparable to that of fish and soft bodied cephalopods.

Asymmetrical Particle Capture in a Marine Filter Feeder

Mark R. Patterson
 Biological Laboratories
 Harvard University
 Cambridge, MA 02138

The application of fluid mechanics to the study of filtration behavior in marine invertebrates is very recent. Aerosol filtration theory has been shown to correctly model suspension feeding in a brittle star at the level of the filter elements (LaBarbera 1978), but little attention has been paid to the properties of arrays of filter elements -- colonies -- in marine passive suspension feeders. Filtration behavior of whole colonies of a New England octocoral, Alcyonium siderium, was examined in a flow tank using neutrally buoyant particles (200 μm diam.) for a variety of filter shapes over a range of flow speeds (2-20 cm/s).

Mapping of particle impaction sites indicates that angular position of capture on colonies with bilaterally symmetric geometries is a function of flow speed (Figure 1). At low speeds ($U < 5$ cm/s), capture of particles is predominantly on the upstream side of the colony, but shifts to the downstream side as flow increases. This effect holds for arborescent, ellipsoidal, and spherical colonies. This asymmetry of particle retention in a whole colony filter may result from two velocity dependent processes: 1) increasing mechanical deformation of upstream filter elements (polyps) into an orientation unfavorable for particle capture and retention, and 2) differential particle concentrations in the boundary layer of the colony over the downstream coordinate due to particle migration in shear fields, this effect being greatest at low speeds. Optical measurements of polypal deformations and particle availability in the boundary layer of the colony over the downstream coordinate show that both are appropriate functions of flow speed to explain the asymmetrical particle capture phenomenon.

LaBarbera, M. 1978. Particle capture by a Pacific brittle star: experimental test of the aerosol suspension feeding model. Science 201: 1147-1149.

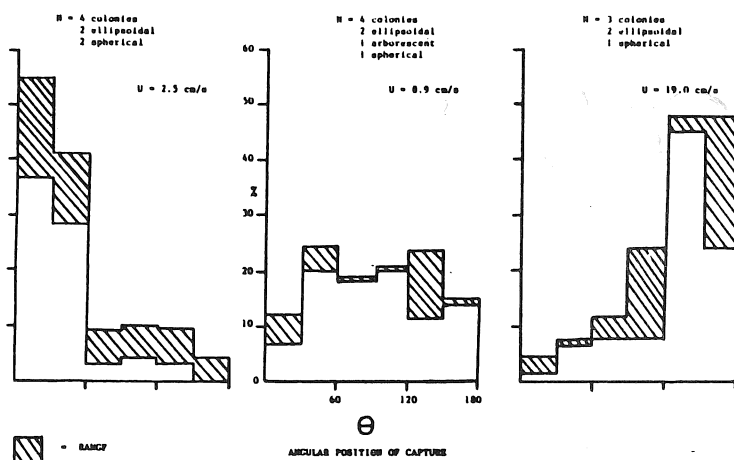


FIGURE 1. DOWNSTREAM SHIFT IN POSITION OF CAPTURE OF ARTEMIA CYSTS BY ALCYONIUM WITH INCREASING CURRENT SPEED. LEADING EDGE OF COLONY IS AT $\theta = 0$. ORDINATE IS PERCENT TOTAL NUMBER OF CYSTS CAUGHT WITH $N = 150, 267, 489$ CYSTS FOR VELOCITY = 2.5, 8.9, 19.0 CM/S RESPECTIVELY.

THE PRESSURE AND FLOW PATTERNS INSIDE AN AORTIC BIFURCATION

Sven Øivind Wille
 Institute of Informatics
 University of Oslo, Norway.

The mechanical interaction between the moving blood and the vessel wall has been agreed to play an important role in atherogenesis. Two major theories have been suggested in order to explain the early development of the disease. One which states that early atherosclerosis is developed at sites in the arterial system where high shear forces are acting on the vessel wall, and thus damaging the endothelium layer. The other suggests that early atherosclerosis is coincident with regions with low shear, while the development of atheroma is retarded in those regions in which wall shear rate is expected to be high. These theories appear to be in conflict with each other. In order to more fully understand the mechanism behind atherogenesis, both the flow patterns and the localisation of early atherosclerosis have to be known.

The equations governing three dimensional fluid flow are given by the Navier-Stokes equations together with the continuity equation. The assumptions made by applying these equations for the description of blood flow are : The blood is a homogeneous, incompressible, newtonian fluid and the flow is laminar and steady. The vessel wall is assumed to be rigid.

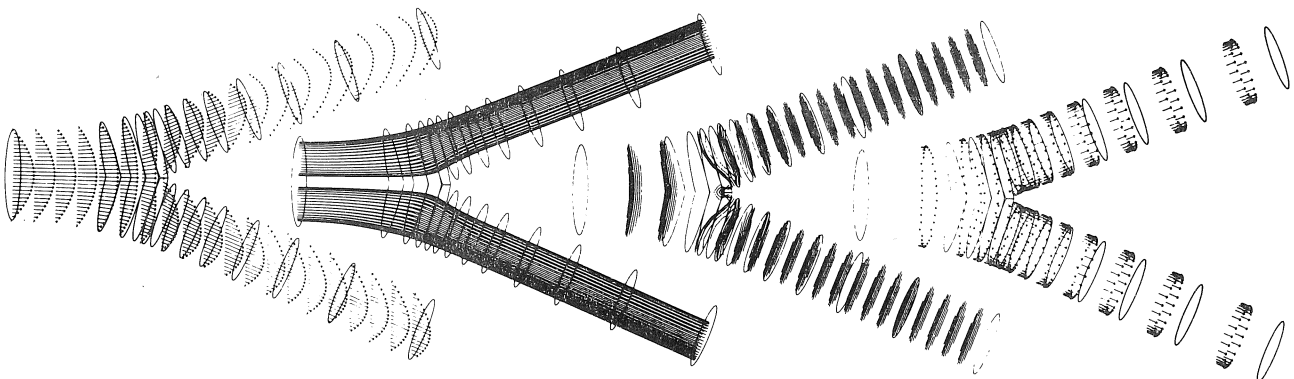
$$\frac{1}{\rho} \frac{\partial p}{\partial x} - \mu \left(\frac{\partial^2 u}{\partial x^2} + \frac{\partial^2 u}{\partial y^2} + \frac{\partial^2 u}{\partial z^2} \right) + u \frac{\partial u}{\partial x} + v \frac{\partial u}{\partial y} + w \frac{\partial u}{\partial z} = 0$$

$$\frac{1}{\rho} \frac{\partial p}{\partial y} - \mu \left(\frac{\partial^2 v}{\partial x^2} + \frac{\partial^2 v}{\partial y^2} + \frac{\partial^2 v}{\partial z^2} \right) + u \frac{\partial v}{\partial x} + v \frac{\partial v}{\partial y} + w \frac{\partial v}{\partial z} = 0$$

$$\frac{1}{\rho} \frac{\partial p}{\partial z} - \mu \left(\frac{\partial^2 w}{\partial x^2} + \frac{\partial^2 w}{\partial y^2} + \frac{\partial^2 w}{\partial z^2} \right) + u \frac{\partial w}{\partial x} + v \frac{\partial w}{\partial y} + w \frac{\partial w}{\partial z} = 0$$

$$\frac{\partial u}{\partial x} + \frac{\partial v}{\partial y} + \frac{\partial w}{\partial z} = 0$$

The Navier-Stokes equations for three dimensional steady flow are solved for an aortic bifurcation model, which is constructed from a cast of a typical human aortic bifurcation. The finite element method is used to obtain the solutions of the equation system. The results of the numerical analysis is presented as three dimensional plots of velocity vectors, streamlines, pressure isobars and wall shear vectors, respectively, as shown below.



FLUID DYNAMICS OF AORTIC STENOSIS: MECHANISMS
OF SUBVALVULAR GRADIENT GENERATION

Ares Pasipoularides, M.D., Ph.D., Joseph P. Murgu, M.D., COL, MC
Julio J. Bird, M.D., MAJ, MC, William E. Craig, M.D., MAJ, MC

Cardiology Service, Department of Medicine
Brooke Army Medical Center, Fort Sam Houston, Texas 78234

Intraventricular flow velocity patterns and pressure gradients measured by high-fidelity multisensor catheters in patients with isolated valvular aortic stenosis (AS) were analyzed. In 12 patients with AS, valve area $1.0 \pm 0.3 \text{ cm}^2$, measured intraventricular (subvalvular) pressure drops were $42 \pm 16 \text{ mmHg}$ and transvalvular ones were $59 \pm 22 \text{ mmHg}$. A fluid dynamic model for ejection through the tapering subvalvular field was developed to assess the contributions by dissipative and non-dissipative mechanisms to the large subvalvular gradients and transvalvular pressure drops in AS. It identified the contributions by geometric taper and ejection velocity patterns to convective and local acceleration mechanisms: The striking augmentation of pressure gradients in the immediate vicinity of the stenotic orifice is underlain mainly by the intensification of the convective acceleration effect. Whereas the convective acceleration component requires a tapering flow field, the local acceleration component is always operative with a pulsed flow. At peak flow, when the local acceleration $\partial V/\partial t$ is zero, only convective gradients are operative along the tapering region and account fully for the measured pressure drops. For negative values of $\partial V/\partial t$, corresponding to flow deceleration following peak ejection, the contribution of the local acceleration effect to the total instantaneous pressure drop values is negative; it thus opposes the simultaneous effect of the convective component, whereas they both act in the same sense prior to peak ejection when $\partial V/\partial t$ is positive. The influence of the enhanced streamwise taper in AS is much stronger on convective than on local acceleration gradients, since the former depend on the square whereas the latter on the square root of the ratio of downstream to upstream flow-section areas of the tapering subvalvular region. Thus, in AS pressure drops and ejection velocities are more in-phase as opposed to normal ejection dynamics. The measured subvalvular gradient values are shown to depend strongly not only on the applying geometric taper and ejection velocity patterns, but also on the distance between and the exact placement of the pressure measuring sensors along the highly tapering subvalvular region. Viscous losses make only a small contribution to the subvalvular pressure gradients. They preclude recovery of pulsatile pressures as stream cross-section reexpands beyond the stenosed valve and are thus responsible for large transvalvular pressure drops.

THE EFFECTS OF SMOOTH MUSCLE ACTIVITY ON THE MECHANICAL AND HYDRAULIC PROPERTIES OF THE DOG AORTA

Jean-Pierre L. Dujardin, Dana N. Stone, C. Douglas Forcino and Heinz P. Pieper
Department of Physiology, The Ohio State University, Columbus, Ohio 43210.

In previous experiments it was shown that after hemorrhage, at any given pressure P , the diameter D of the descending thoracic aorta decreased, while dP/dD increased, indicating a change in activity of the smooth muscle. Volume expansion had the opposite effects.

The present experiments were undertaken to determine the effects of changes in smooth muscle activity on the elastic wall properties of the aorta and to clarify the role of these changes in the hemodynamic adjustments to hemorrhage and volume expansion. The experiments were performed on anesthetized male dogs ventilated with a positive pressure respirator. A left thoracotomy was performed at the level of the 4th intercostal space and 2 piezoelectric crystals (4 mm diameter) were attached across the thoracic aorta using cyanoacrylate glue. The transit time for a burst of ultrasound to pass from one crystal to the other was measured by means of a sonomicrometer. The voltage output of this instrument was proportional to the transit time and thus also to the external aortic diameter. Aortic pressure was measured in the cross-section of the crystals by means of a catheter-tip transducer (Millar Instruments, PC-360). Aortic pressure and diameter were digitized at a rate of 1000 samples per sec and displayed on a digital oscilloscope (Nicolet Explorer III). In order to obtain aortic pressure and diameter in a wide range, a sinusoidal piston pump was attached to the abdominal aorta by means of a cannula inserted into the left femoral artery. When operating, this pump produced slow oscillations in aortic pressure and diameter with a cycle of 5 sec. In all experiments, recordings were made under the following conditions: under control conditions, after hemorrhage (-15% of the estimated blood volume), after reinfusion (new control conditions), after volume expansion (+15% of the estimated blood volume) and 30 min after α -blockade with phenoxybenzamine (5 mg/kg). For each condition, the pump was operated for at least 10 sec. During this period, the pressure and diameter signals were recorded on magnetic disk. At a later time, the diastolic pressure-diameter relationship was analyzed by determining D and dP/dD at 0.5 kPa pressure intervals.

In order to draw conclusions about the effects of the changes in smooth muscle activity on the material properties, the incremental elastic modulus E was calculated and plotted as a function of the normalized diameter $D^* = D/D_{13.3}$ (where $D_{13.3}$ is the diameter of the aorta at 13.3 kPa under control conditions) for the different conditions. Hemorrhage caused E to increase by an average of 11.4% when compared to the control values at the same normalized diameter. Volume expansion and α -blockade caused E to decrease respectively by 10.2 and 24.2% when compared to control.

In order to draw conclusions about the functional significance of the changes in smooth muscle activity, the characteristic impedance of the proximal aorta Z_c was calculated and plotted as a function of pressure. The curves relating Z_c to pressure showed a minimum in the physiological pressure range and were well described by parabolas under all conditions. Under control condition, the minimum was located close to the mean arterial pressure. Hemorrhage increased Z_c at each pressure level (average 10.8%), while volume expansion as well as α -blockade reduced Z_c at all pressure levels (average respectively 7.8 and 12.8%). Since Z_c is the main determinant of the arterial opposition to pulsatile flow, it was concluded that reflex contraction or relaxation of the aortic smooth muscle could significantly alter left ventricular afterload.

Elastohydrodynamic Lubrication Models for the Normal Human Ankle Joint

J.B. Medley; Department of Mechanical Engineering, University of Waterloo, Waterloo, Canada.

D. Dowson, Institute of Tribology, Department of Mechanical Engineering, University of Leeds, Leeds, England.

V. Wright, Rheumatism Research Unit, Department of Medicine, University of Leeds, Leeds, England.

The geometry, friction and lubrication of normal human ankle joints have been investigated. The joints exhibited converging-diverging surfaces in the direction of motion. The cylindrical form of the measured surface contours indicated that a reduced radius of about 0.35 m gave a good representation of the ankle joint geometry.

Human ankle joint specimens were tested in a joint simulator. Although considerable difficulties were encountered in the measurement of the very small coefficient of friction between the cartilage surfaces, an upper limit of about 0.01 was identified for this important tribological feature of synovial joints.

An equivalent bearing to represent the ankle joint was proposed which consisted of a rigid cylinder covered with a compliant layer sliding on a rigid plane (Fig. 1). The dimensions for this geometry were based on the measurements of the present study. Theoretical models were developed to estimate the cyclic variation in elastohydrodynamic film thickness and coefficient of friction for the ankle during walking.

Theoretical minimum film thicknesses of about $1 \mu\text{m}$ were estimated along with coefficients of friction up to 0.001. The theoretical predictions of the cyclic variation of film thickness remained small compared with the magnitude of the film thickness itself. Furthermore, the theoretical film thicknesses were smaller than the measured Ra roughnesses for cartilage which appear in the literature. When a very considerable increase in the bulk viscosity of the lubricant was introduced into the calculations film thicknesses of about $18 \mu\text{m}$ and coefficients of friction up to 0.01 were estimated. This value for film thickness was sufficient to separate the surface asperities of healthy articular cartilage.

Unless thin film mechanisms, such as an increased lubricant viscosity or micro-elastohydrodynamic lubrication act, the present study indicated that full fluid film lubrication cannot be sustained. However, the predicted film thicknesses were not much smaller than the surface roughness of cartilage and the ability to generate and preserve fluid films was found to be greatly enhanced by the entraining and squeeze film action. Thus, the modes of lubrication for normal human ankle joints must include a significant contribution from elastohydrodynamic lubrication.

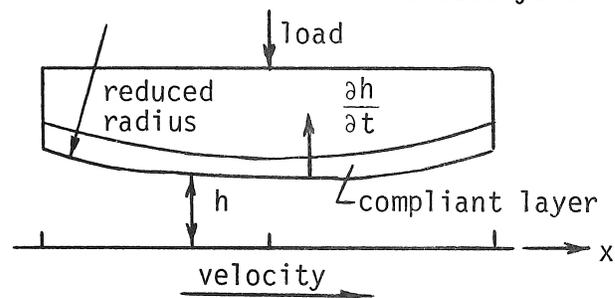


Fig. 1: An equivalent bearing representing the ankle

Dan M. Spengler, M.D.
Associate Professor
Department of Orthopaedics, RK-10
University of Washington

Biomechanics in Orthopaedics: Historical Perspectives

During this presentation, the author will review the development of orthopaedic biomechanics. The significant impact of Carl Hirsch and his many proteges will be presented. In addition, the contributions of Evans, Bonfield and Lee, and Frankel and Burstein will be highlighted. The author hopes to relate the significant contributions of the past to the many technological advances presently being utilized in orthopaedic biomechanics of the 1980's.

EVALUATION OF PHYSIOLOGIC SUSPENSION FACTORS IN BELOW KNEE AMPUTEES

The functional capacity of below knee amputees is directly related to the suspension, stability and proprioception provided by the prosthesis. Suspension is provided by ancillary and physiologic mechanisms some of which also contribute to stability and proprioception. Decrease in ancillary suspension would reduce venous obstruction and help cosmesis, skin irritation, and associated maintenance problems. We have found physiologic suspension to be a function of prosthetic socket and residual limb contour, skin motion, muscle expansion and compliance, and the dimensional relationships between the residual limb and the socket. The purpose of this study is to report the significance of training techniques and individual suspension factors on physiologic suspension.

Evaluation of 17 patients with 21 limbs included contour, dimensional, and tensile slippage measurements. Subjective evaluation of prosthetic function, training, activity level and ability, and physiologic suspension were obtained. Regression analysis was used to establish the significance of individual parameters.

One third of the subjects were able to generate a tensile retention force equal to the weight of their prosthesis with less than one half inch of slippage. Mean maximum tensile retention force was over three times greater than mean prosthesis weight. At least 50% of subjects demonstrated improved tensile retention ability due to a training program involving isometric muscle contractions within the environment of their own prosthesis. This agreed with the results of the subjective evaluation.

Contraction of the stump musculature can apply useful force vectors to the prosthetic socket. The suspension potential of below knee amputees can be predicted clinically by our study protocol. Training amputees within the environment of their own prosthesis shows promise in improving ambulatory function. Surgical contouring and prosthesis fitting taking into account the factors identified in this study, may offer additional functional improvement to the myoplastic below knee amputee.

Frederick G. Lippert, III, M.D.
Associate Professor
Department of Orthopaedics
University of Washington
Chief, Department of Orthopaedics
V.A. Hospital and Medical Center
Seattle, Washington 98108

AN ANALYTICAL INVESTIGATION ON TACHOGRAPHIC GAIT RECORDS TO
EXPLORE THE FACTORS DISCRIMINATING HANDICAPPED GAIT FROM NORMAL GAIT

D.N. TIBAREWALA and S. GANGULI
Bioengineering Unit, University College of Medicine (Goenka Hospital)
Calcutta University, 145 Muktagram Babu Street, Calcutta 700 007, India

The graphonumerical method of analysing the tachographic gait curves--the curves obtained by recording the time variations in the instantaneous velocity of body's centre of gravity, as developed by present authors, postulates a set of eight parameters to represent the gait characteristics of an individual. Such representation of gait by a parameter set has been found to be capable of discriminating the handicapped gait from the normal gait with reasonable accuracy.¹ Nevertheless, the underlying factors which may be responsible for the discrimination remained unexplored and the present investigation was an attempt to bridge this gap. In this attempt, the principal component analysis of the gait data of different types of subjects has been carried out, and the intergroup differences in gait have been explored in terms of the derived components.

For the purpose of this investigation, altogether 790 gait cycles were recorded from different types of subjects and subsequently analysed to determine the sets of eight gait parameters (mentioned as 'gait parameters' hereafter) for each cycle by the method developed by present authors. Out of the 790 gait cycles investigated upon, 225 were recorded from normal subjects whereas the rest were obtained from different types of lower extremity handicapped persons, namely, below-knee amputees using ptb prostheses (200 cycles), above-knee amputees using a particular type of prostheses (98 cycle), axillary crutch-users (81 cycles), post-polio rehabilitees (101 cycles), and cases having a history of femoral neck-fracture.

Observations on the correlation coefficients between various pairs of gait parameters indicated that these gait parameters were not independent of each other, and therefore, it might be possible to derive a lesser number of uncorrelated variates to represent the gait characteristics. Further, since some of the observed correlations were common to all types of gait and some others were specific to particular type of disability, the intergroup differences are likely to be prominent in the derived variates. In order to derive such uncorrelated variates, the above-mentioned gait data were segregated into six groups according to type of subjects whose gait records have been analysed and standard procedures of principal component analysis were applied to each group. The varimax method of rotating the reference axes maintaining their orthogonality was used on the derived principal components to facilitate the appraisal of the results. Simultaneously, the contributions of the principal components to the total variance within the corresponding groups were also determined.

While subjecting the gait data to the principal component analysis, it has been hoped that the derived components will reveal dimensions of variability in the data more basic than the observed parameters. The expectations have been very closely attained by the present observations whereby only 4 or 5 principal components could explain almost whole of the variances originally contributed by eight gait parameters. Besides, the inter-group gait differences were readily observable in these derived components with regards to two aspects, namely, distribution of variance among the principal components and the correlations of these derived components with the gait parameters determined through graphonumerical analysis of tachographic gait curves.

Observations on distribution of the variances indicate that the major portion of the total intragroup variability could be accounted for by a single principal component in the handicapped gait patterns, and the value of such proportion has been found to increase with the severity of the disability. The distribution pattern has been observed to be homogeneous in the normal gait whereas a heterogeneous distribution has been a characteristic of handicapped gait. Therefore, it may be concluded that the dependence of the causes of intra-group variability on a single biomechanical factor which controls the principal component contributing maximum to the variance increases with the severity of the handicap. As a result, the variations of the other biomechanical factors or the contribution of the principal components controlled by these factors towards intra-group variance is diminished with an increase in the degree of disability. Consequently, a reduction in capability of attaining the optimum normal gait is observed in the lower extremity disabled.

Further, the principal components which contributed maximally to the intragroup variance of each group should have been representing those biomechanical factors which could be adjusted most easily to approach the optimum gait. As such, since there has been a little difference in the contribution to intragroup variances of first four principal components of normal gait, almost all the gait parameters could be effectively controlled by the normal persons giving rise to optimum normal gait. In contrast to this, the easily controllable factors have been very few in the case of the handicapped gait as indicated by one or two principal components contributing a major portion of the intragroup variance.

On the other hand, the principal components whose contribution to the intragroup variance is minimum, may be considered as invariant for the particular group. And therefore, such principal components may be identified as representatives of the characteristic features of gait of the corresponding type of subjects.

In all the above derivations, the identity of the principal components have been defined by their correlation coefficients with the gait parameters obtained from tachographic gait curves.

¹Tibarewala D.N. (1980): Ph.D. thesis, University of Calcutta.

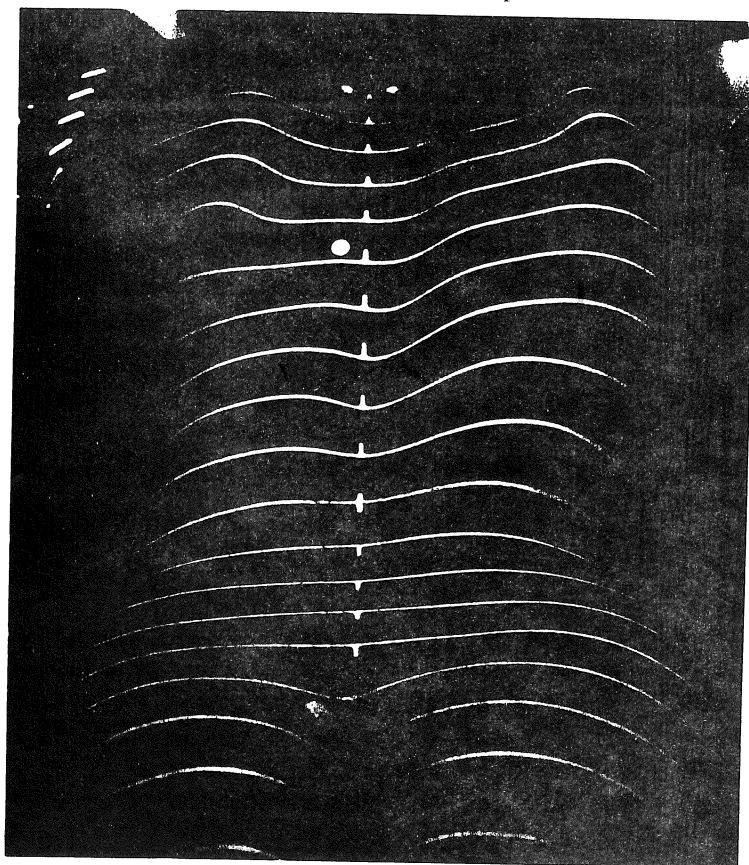
EVALUATION OF TRUNK DEFORMITY USING LIGHT PROFILES.

James A.A. Miller, D.L. Spencer⁺ and A.B. Schultz⁺
Departments of Materials Engineering and Orthopaedics,
University of Illinois at Chicago, Chicago, IL 60680.

The evaluation and treatment of scoliosis involve taking multiple radiographs over the course of several years. Radiation hazard considerations have created a demand for alternative, non-invasive methods for evaluating the deformity. One approach is to evaluate the surface topography of the trunk as a means of deducing the underlying deformity of the spine and rib cage. The Moire fringe contour technique is an example of this approach, and it has gained some acceptance in recent years, but the complexity of the Moire image has hampered attempts to automate data analysis. Such automation may be necessary to examine the complex geometry of the trunk in ways which yield useful information on the underlying skeletal deformity.

We are developing an alternative method that gives simple, high quality images (see figure) from which surface topography can be quantified. These images readily lend themselves to automated opto-electronic scanning techniques. A light grating is projected onto the body while the resulting profiles are viewed from a given angle to the projector axis. Profile images so obtained can be related to surface anatomy. When this viewing angle is 90° a true body profile results, but the curved surfaces of the back usually require use of a smaller angle (we use 70°). The technique requires only readily available, inexpensive photographic equipment.

We used the technique to evaluate trunk deformity in 41 girls from 9 to 19 years of age with untreated, idiopathic scoliosis. An initial study of how well trunk rotation relative to the pelvis correlated linearly with spine lateral deviation (Cobb measure) yielded an overall correlation coefficient of 0.6 and a coefficient of 0.7 for the 11 single curves. These correlations are about the same as that found by users of the Moire technique. In our technique, however, an angular measure of trunk rotation is obtainable directly from the photographs.



TRUNK MUSCLE MYOELECTRIC ACTIVITY IN GIRLS WITH STRUCTURALLY-NORMAL SPINES AND GIRLS WITH IDIOPATHIC SCOLIOSIS. M. Reuber, A. Schultz, D. Spencer, and T. McNeill (Department of Materials Engineering, University of Illinois at Chicago Circle, Box 4348, Chicago, IL 60680).

Introduction: Idiopathic scoliosis is a disease in which the spine develops a lateral curvature which often progresses. Its cause is unknown, and if left untreated it may result in gross trunk deformity. Asymmetric trunk muscle myoelectric activity has been reported in girls with idiopathic scoliosis. To examine this phenomenon in greater depth, we studied trunk muscle myoelectric activity in 12 girls with structurally-normal spines and 20 female patients with mild-to-moderate idiopathic scoliosis, in biomechanically-well-defined experiments.

Subjects: Subject ages ranged from 10 to 15 years, with a mean age of approximately 13.5 years in both groups. Patients had lateral curves with a mean Cobb measure of 23.7 degrees. Nine of these girls were untreated, seven were being treated by electrical muscle stimulation and four were being treated with a brace at the time of testing. There were 12 double curves, four single thoracic curves, two single lumbar curves, and two thoracolumbar curves. Seven curves had progression documented by roentgenographs. Curves increases of ten degrees or more over a period of five or more months occurred in one patient prior to testing and in two patients after testing. Curve increases between five and ten degrees occurred in one additional patient prior to, and in three additional patients after testing.

Methods: Bipolar surface electrodes picked up activity in the erector spinae and the latissimus dorsi on both sides at the T9 level; and in the erector spinae, the rectus abdominus and each of the lateral portions and the anteromedial portions of the external abdominal oblique muscles on both sides at approximately the L3 level.

Each girl performed 15 ten-second duration isometric exercises while standing. These included relaxed standing, voluntary tensing of trunk muscles, and resisting horizontal loads applied to a helmet worn by the subjects. Flexion, extension, and right and left pull resist tasks were imposed through cables attached to the helmet and a system of pulleys and weights. All exercises were performed both with the pelvis free, and with the pelvis belted against a support board.

Results: (1) Both the healthy girls and the patients showed significant individual variations in myoelectric signal amplitudes and degree of lateral asymmetry in these signals. For example, some normal girls had twice as much myoelectric activity on one side compared to the other. (2) Myoelectric activity under pelvis-belted and pelvis-free conditions was not significantly different. (3) Patients with curves of more than 25 degrees had myoelectric signals which were significantly **more asymmetric** than those of normal girls ($p < .01$). Lumbar level myoelectric signals were higher on the convex sides in the erector spinae muscles while resisting flexion, and in the external abdominal oblique and the rectus abdominus muscles while resisting lateral bending. No other statistically significant differences between the myoelectric activity in normal and scoliotic girls were found. (4) Myoelectric activity in patients whose lateral curves progressed, either before or after testing, was not significantly different from activity in patients who did not progress. Patients with documented progression who had curves of 25 or fewer degrees showed no significant difference in myoelectric activity from that of structurally-normal girls.

Conclusions: Moderately asymmetric trunk muscle myoelectric activity occurs in girls who have structurally-normal spines as well as in girls who have scoliosis. Substantial asymmetries in trunk muscle myoelectric activity arose only in patients with curves larger than 25 degrees, suggesting that they resulted from rather than helped create those lateral curves.

ANALYSIS OF THE EFFECT OF VARIABLE STRAIN RATE ON ACOUSTIC EMISSION IN BONE.
 Fischer RA, Pope MH, Seligson DS: Department of Orthopaedics and Rehabilitation,
 University of Vermont College of Medicine, Burlington, Vermont 05405.

Acoustic emissions (AE) are elastic stress waves that stem from sudden energy release in a material. It has been shown that AE is affected by strain rate in materials other than bone.¹ This study investigated the AE response in tensile tests of machined cortical bone specimens, at varying strain rates.

Test Method: Bovine metatarsals were stripped of soft tissue and were machined into cortical bone specimens of standard size. The dimensions of these specimens were: length 13.97 cm, width 2.54 cm, thickness 3.30 mm, gauge length 31.75 mm, width of specimen neck 5.59 mm and radius of curvature from body to neck 9.53 mm. These specimens were gripped in parallel wedge grips in an MTS machine and were preloaded 22.68 Kg, in tension, to prevent initial slippage. A Dunegan Endevco 3000 series AE system was used to obtain data on total emission counts and amplitude distribution of the acoustic response. Two miniature transducers (Model S 1000 BM) were attached to the bone 6.35 cm apart. The locate mode was utilized to cancel out all signals except those emanating from the gauge length of the bone specimen. The strain rate, in tension, for the three groups were: Group 1 (N=5) $.0001 \text{ sec}^{-1}$; Group 2 (N=5) $.001 \text{ sec}^{-1}$; and Group 3 (N=5) $.01 \text{ sec}^{-1}$. In addition, the AE responses of partially decalcified specimens (N=5), in tension, at a strain rate of $.001 \text{ sec}^{-1}$ was studied. Gains of 50 Db/channel and a threshold of 30 Db were used during all tests.

Results A statistically significant ($p < .01$) difference was found between the number of acoustic events in Group 1 (\bar{x} 25, S.D. 8.86), and Group 2 (\bar{x} 60.2 S.D. 20.66). However, the amplitude distributions of the acoustic events in these two groups were not statistically different. There was no statistically significant difference in the mean number of events or amplitude distribution between Group 2 and Group 3. Slow strain rates characteristically result in low amplitude, continuous AE, while fast strain rates tend to produce higher amplitude, burst-type emissions. These types of emissions represent the extremes on a continuum. In this study, despite different total numbers of events between Groups 1 and 2, there was no difference in amplitude distribution between the three groups. This information is important to researchers using AE technology for the study of bone fracture mechanics in the laboratory, as well as clinically. It appears from this study that if AE in bone is affected by strain rate, extremes in strain rate greater than $.0001 \text{ sec}^{-1}$ to $.01 \text{ sec}^{-1}$ will be necessary to demonstrate this.

1. Pollock AA: An introduction to acoustic emission and a practical example. J Environ Sci 39-41, 1979.

CT OBTAINED BONE GEOMETRY AND DENSITY
MEASUREMENTS USING SECOND ORDER CORRECTION

D. D. Robertson
H. K. Huang

Department of Physiology and Biophysics
Georgetown University Medical School
3900 Reservoir Road, N.W.
Washington, D.C. 20007

Department of Radiological Sciences
UCLA
Los Angeles, CA 90024

The early detection of bone loss or gain is of paramount import in the diagnosis and treatment of many metabolic bone diseases. Several non-invasive methods have been developed and modified, however to date no method provides the required sensitivity, precision, versatility of choice of bony sites, and easy availability to clinicians necessary to be helpful to the millions of patients with metabolic bone disease. The use of a second order bone correction algorithm for X-ray beam hardening allows computed tomography (CT) to meet the above requirements. This paper describes a series of experiments performed to establish the accuracy and usefulness of a second order bone correction.

CT scans of embalmed human cortical (femur, humerus, radius, ulna) and trabecular bone (lumbar vertebrae, distal femur) were performed and images reconstructed with and without second order correction. Comparisons of cortical bone's total cross sectional area, medullary canal area, and bone density, with and without correction were done. Comparisons between corrected and uncorrected trabecular bone density were also done. All the CT obtained values were compared to the bone's real area and density as determined by physical methods. Results show that second order bone correction significantly corrects CT generated values of bony geometry (especially the medullary canal area) and CT generated density values of cortical and trabecular bone. In view of these results we feel that second order correction can be used as an important adjunct in the diagnosis and evaluation of treatment of metabolic bone disease.

Biomechanics: Research and Development at IMA.

by L.C.Nava and P.A.A.Laura
Instituto de Mecánica Aplicada
Base Naval Puerto Belgrano
8111 - Argentina

Crutches and canes constitute some of most basic engineering elements which provide assistance and satisfy the fundamental desire to be mobile to the disabled. On the other hand, the design of crutches and canes has not varied to a great extent since their original conception..., and in the case of a crutch this is quite remarkable since it has been in use for almost 5000 years!.

From a modern engineering viewpoint one must consider crutches or canes as dynamic mechanical systems which act in an active manner in order to complement the disabled human body. Take, for instance, the case of canes or walking-sticks. When used correctly "they provide several possibilities for support and recovery from stumbling and they transmit from the arms energy for voluntary push-off conspicuously lacking in the artificial ankle joint", (Reference 1).

The present paper describes some of the developments accomplished recently at IMA and the resulting experiences: retractile, anti-shock, non slipping crutches; variable length, non slipping canes; angle-adjustable fore-arm crutches, etc.

The paper deals also with elements specially developed for disabled children, for instance, a crutch-toy which consists in a crutch which can be used as a "rifle" by the child.

Reference

1. E.F.Murphy, "Lower Extremity Components", Chapter 5 of Orthopaedic Appliances Atlas (Vol.2: Artificial Limbs). J.W.Edwards -Ann Arbor, Michigan, 1960.

BENDING STIFFNESS OF UNILATERAL AND BILATERAL EXTERNAL FIXATOR FRAMES

by

Fred Behrens, M.D., F.R.C.S.(C), Wes Johnson, B.S.M.E.,
Tom Koch, B.S.Ag.Eng., and Neb Kovacevic, M.S.A.E.
Departments of Orthopaedic Surgery, St. Paul-Ramsey Medical Center
and the University of Minnesota; and
the Orthopaedic Biomechanics Laboratory, Metropolitan Medical Center,
Minneapolis, Minnesota

In the past decade external skeletal fixation has become the preferred method for the immobilization of severe open tibial fractures and skeletal infections. Among a number of different fixators, the "Vidal-Hoffmann" apparatus has proven most popular. These frames and many of the newer fixators are exclusively used in bilateral configurations (two or more transfixion pins are inserted into each main bony fragment and then connected on each side of the limb by one or more longitudinal rods). Recently McCoy, et al¹, investigated the mechanical behavior of the bilateral configurations of six different fixators under conditions of axial loading, AP and lateral bending, and torsion. All frames were most sensitive to bending moments. It was particularly disturbing that they were three times less stiff in the anterior-posterior than in the lateral plane because such simple activities as contraction of dorsi- and plantar flexors of the foot, elevation of a leg from a bed, and level walking² induce anteroposterior bending moments which are considerably larger than those exerted in the lateral plane.

This study was undertaken to test our hypothesis that unilateral frames (two or more pins inserted into each main fragment and connected by one longitudinal bar), particularly when applied in an anterior position, would be more successful in controlling AP bending moments. We therefore examined different unilateral and bilateral frame configurations which were built with the Hoffmann apparatus (4 mm. pins, 8 mms. connecting rods, universal joints) and the ASIF "tubular" fixator (5 mm. pins, 11 mm. tubular connecting rods, independent joints). The Hoffmann unilateral (UL) configuration consisted of three half-pins in each main bony fragment and one longitudinal rod, while the Hoffmann bilateral (BL) frame utilized transfixion pins and two longitudinal rods on each side (the "Vidal-Hoffmann" configuration). The universal joints limited the spread between the most proximal and distal pins in each fragment to 4.4 cm. The frames erected with the ASIF "tubular" fixator had only two pins in each main fragment, and in the case of the bilateral configuration only one longitudinal bar on each side. As each pin is connected over an independent articulation, frames with 4.4 cm. and 9.0 cm. pin spread were erected. Unilateral frames were applied in a straight anterior and lateral position while, as in the clinical situation, bilateral frames were limited to a lateral application. Anteriorly applied frames were tested at two bone-rod distances of 2.5 and 8.0 cm. All lateral applications were limited to an 8 cm. bone-rod distance as clinically the leg musculature prevents a closer placement. The fixator frames were assembled on a cylindrical model bone of laminated linen with an outside diameter of 2.54 cm. and a wall thickness of 0.64 cm. As the modulus of elasticity for laminated linen is 31 GPa this model bone closely approximated the structural properties of a tibial diaphysis. The experimental study was conducted on an MTS Model 812 materials testing machine. As the exact loading modes at the fracture site are presently unknown, all fixator frames were tested in 4-point bending. The model bone fragments were angularly displaced at a constant rate of 1.27°/second up to a displacement of 3.8°. Angulation of the model bone fragments and the applied bending moments were recorded on an x-y plotter, and the stiffness of the fixator frames determined from the slope of the recorded curve and expressed in N.m./degree of angulation.

FRAME TYPE	PIN-PIN (cm)	TABLE 1		AP BEND. (N.m.) degree	LAT BEND. (N.m.) degree
		BONE-BAR (cm)			
<u>Lateral Appl.</u>					
-Hoffmann UL	4.4	8.0	1.0	9.7	
-Hoffmann BL	4.4	8.0	1.9	10.4	
-ASIF UL	4.4	8.0	1.7	11.5	
" "	9.0	8.0	2.8	13.4	
-ASIF BL	4.4	8.0	2.0	15.4	
" "	9.0	8.0	5.8	18.3	
<u>Anterior Appl.</u>					
-Hoffmann UL	4.4	2.5	3.2	2.9	
" "	4.4	8.0	9.7	1.0	
-ASIF UL	4.4	2.5	9.7	4.9	
" "	4.4	8.0	11.5	1.7	
-ASIF UL	9.0	2.5	13.0	7.2	
" "	9.0	8.0	13.4	2.8	

It is hoped that the information from this study will help in choosing the most appropriate frame configuration for anteroposterior and lateral bending, which are two weakest loading modes of most fixator frames:

- For laterally applied frames, the ASIF BL frame with 9 cm. pin-pin spread was stiffest in both anterior and lateral bending. The ASIF UL frame with the shorter pin spread was almost equally as rigid as the Vidal-Hoffmann frame; this is impressive considering the simplicity of this configuration.
- All but one of the anterior frames were considerably stiffer in AP bending than the lateral frames, but only the ASIF UL with 9 cm. pin-pin spread approached the lateral frames in lateral bending rigidity.
- The traditional clusters of three 4 mm. pins per bony fragment should be abandoned as they were consistently weaker than two 5 mm. pins.
- An increase in the spread from pin to pin in each fragment improved both anterior and lateral bending stiffness in all frames.
- Increase in the bone-rod distance in anterior frames consistently increased anteroposterior and decreased lateral rigidity.

References

1. McCoy, M.T., Briggs, B.T., Chao, E.Y.; Orthop. Res. Soc. Trans. 5:173, 1980.
2. Faul, J.P.; Proc. R. Soc. London Ser. B 192:163-172, 1976.

SINGLE-PLANE X-RAY PHOTOGRAMMETRY FOR DETECTING TOTAL JOINT LOOSENING. F.G. Lippert and R.M. Harrington, Dept of Orthopaedics, Seattle VAMC; S.A. Veress and T. El-Garf, Civil Engineering, Univ of Washington, Seattle, WA 98195

X-ray photogrammetry is an accurate method of measuring displacements in the skeletal system. For clinical use 0.9 mm spherical stainless steel markers are implanted in the bones to serve as accurately observable landmarks. Two different systems for obtaining three-dimensional displacements have been developed and tested to determine their accuracy (Lippert, 1982). The primary use of these systems has been to measure the displacements of total hip and total knee implants relative to the surrounding bone. Both systems measure relative motions with a root mean square error of 0.1 mm or less in model testing and 0.2 mm in human subjects.

In order to develop a screening test which can be more widely adapted for use in hospital radiology departments, a single-plane (two-dimensional) x-ray photogrammetry method is being tested. A single-plane measurement could detect such motions as pistoning and toggling of the femoral component of total hip implants, or loosening of the acetabular cup or tibial plateau which also have stainless steel markers implanted in them. The orthopaedist will be able to choose measurements in one or more planes based on clinical examination.

The basic principle of the two-dimensional system is to establish an accurate calibration frame with four landmarks whose coordinates are known. These four points establish a plane which is positioned to pass through the volume of space occupied by the structures to be measured (Fig. 1). X-ray exposures are made with the total joint in two different loading conditions such as weightbearing/nonweightbearing or varus/valgus force. The calibration frame is attached to the subject so that it maintains its relative position to the markers in bone if the subject rotates or moves closer or further away from the x-ray film while changing from one load condition to another. The relative distances between markers are calculated in the calibration plane. Loosening of the total joint component will cause relative displacement of the markers in the bone and implant under different loading conditions.

The accuracy of the system depends on the accuracy with which coordinates are determined for the calibration markers and the bone markers. This accuracy depends upon several factors: marker size, digitizer accuracy and resolution, human operator accuracy and resolution, calibration frame marker coordinate accuracy, soft tissue scattering of the x-ray beam, and attachment of the calibration plane to the subject. Testing of each of these factors has been performed, along with a comparison of displacements measured with the two-dimensional and three-dimensional systems.

The goal of this system is to use a commercially available digitizer, microcomputer, and a calibration frame which can be applied by the x-ray technician to perform screening tests on total joint implant patients. This screening will allow orthopaedists to follow implant loosening or settling. Pain evaluation, activity restrictions, and replacement surgery decisions will be based on more objective data than is currently available.

Reference: Lippert, F.G., Harrington, R.M., Veress, S.A., Fraser, C., Green, D., and Bahniuk, E. (1982) A comparison of convergent and bi-plane x-ray photogrammetry systems used to detect total joint loosening. *J. Biomechanics* (in press).

Research funded by the Veterans Administration.

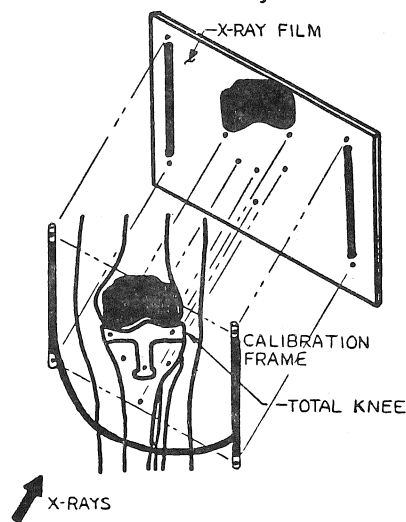


FIG. 1

ORIGIN OF KNEE MOMENTS DURING AMBULATION AND
THEIR MODIFICATION BY ANKLE-FOOT ORTHOSES

by

Justus F. Lehmann, M.D., Michael J. Ko, M.S., Barbara J. delateur, M.D., M.S.
University of Washington
Seattle, WA 98195

OBJECTIVE - This study examines the origin of knee moments during normal gait, the changes caused by wearing an ankle-foot orthosis, and the clinical importance of knee moments.

METHOD - In normal subjects, force plate data and kinematic data from film of the subject were used to derive moments during normal walking and with an ankle-foot orthosis adjusted to allow only 5° dorsiflexion or 5° plantarflexion. The total knee moment was analyzed, as well as moment contributions of the fore-aft shear and vertical forces.

RESULTS - The knee moment components, due to the fore-aft shear and vertical forces, tend to counterbalance each other, minimizing the magnitude of the total knee moment, which demonstrated a flexion peak at toe-strike, changing to an extension peak after heel-off. The fore-aft shear moment was most affected by the magnitude of the fore-aft shear force rather than its moment arm, while the vertical force moment was most affected by the length of the moment arm rather than the vertical force. The flexion moment peak at toe-strike was greater than normal for both adjustments of the orthosis. With 5° plantarflexion, the increase was a result of a larger forward shear force; and with 5° dorsiflexion, it was due to a larger moment arm relative to the vertical force.

CONCLUSION - In normal gait, the total knee moment is minimized; but any factor, including adjustment of an ankle-foot orthosis, can increase the knee moment creating knee instability and increasing the muscular effort needed during ambulation. This study shows the importance of the total knee moment and its components in the analysis of gait, gait abnormalities and the prescription of orthoses.

A DETAILED STUDY OF THE EFFECTS OF LONG TERM USE
ON A TOTAL KNEE PROSTHESIS

Edward H. Coale, M.S., Steven A. Goldstein, Ph.D., Ronald R. Reschly, M.D. and
Larry S. Matthews, M.D.
Biomechanics Laboratory, Section of Orthopaedic Surgery, University of Michigan

The first patient treated with Spherocentric arthroplasty at our institution donated her knee for research at her death. She was seventy years old at the time of arthroplasty for degenerative arthritis. No special cement techniques were used. Her arthroplasty was a clinical success for the 6.5 years until her death. Evaluation at six month intervals for pain, stability, range of motion, walking ability, and use of supports had documented very satisfactory continuous use of the prosthesis. Her weight had increased from 81.8 to 100 Kg (180 to 220 lbs). She was extremely active and subjected the prosthesis treated knee to an estimated 12 million cycles at loads ranging up to 364 Kg (800 lbs) during the evaluation period.

The knee joint was carefully removed, preserving the bone-cement interface, surrounding soft tissue, and the supporting trabecular bone. Thirty separate soft tissue specimens were prepared for standard light, phase contrast, and polarized microscopy with special attention to possible observation of methacrylate or UHMWPE particles, macrophage proliferation, or inflammation.

The metaphyseal regions were sliced longitudinally and transversely at 6 mm intervals. The slices were examined for trabecular bone remodeling, viability of bone and bone marrow near the methacrylate, and for the presence or absence of an interface membrane. Special thin ground specimens were thoroughly examined for interdigitation of cement with trabecular bone, for membrane formation, and tissue viability.

The polyethylene components were evaluated for wear and/or deformation by utilizing a computer actuated precision x-y table and a LVDT Gage Head along a z-axis. Wear-deformation contour maps were generated. Scanning electron micrographs were made of the bearing surfaces of the plastic parts.

Conclusions

The trabecular bone remodeling and absence of a membrane proves that a durable load transferring interface is possible. In spite of documented wear and deformation there was no evidence of an inflammatory reaction to particulate material. The location of the observed wear or deformation emphasizes the extreme bearing conditions that exist at the extreme range of allowed motion for this constrained prosthesis.

PMMA REINFORCED BY HYDROXY-APATITE CRYSTALS
PRELIMINARY RESULTS: CREEP ANALYSIS

A. Castaldini¹, A. Cavallini¹, A. Moroni², R. Olmi², L. Ranieri²

¹Physics Institute of the University of Bologna.

²III Orthopedic Clinic of the Rizzoli Orthopedic Institute, Univeristy of Bologna.

The importance of the use of acrylic cements in prosthetic surgery has induced study of the behaviour of compound cements for strengthening of the prosthetic implant.

The Authors have, therefore, seen it opportune to add synthetic hydroxy-apatite crystals to a PMMA base commercial cement (Surgical Simplex) keeping in mind, besides normal criteria (e.g. non-toxicity), its affinity with the great quantity of crystalline units of hydroxy-apatite present in the bone.

A study was therefore carried out to determine deformation in the reinforced cement using various percentages of hydroxy-apatite. In order to examine the variation of the plastic deformability from the moment of mixing, creep tests were subsequently made from the polymerization moment.

FATIGUE OF ACRYLIC BONE CEMENT--THE INFLUENCE OF STRAIN RANGE AND MEAN STRAIN

Evalyn I. Gates, Dennis R. Carter, William H. Harris

Orthopaedic Research Labs, Massachusetts General Hospital and
Harvard Medical School, Boston, MA 02114

Acrylic bone cement is used in total joint arthroplasty to securely anchor the prosthesis to the bone. After implantation it is exposed to many loading cycles during normal patient activity, and therefore its fatigue behavior is a fundamental design consideration. Stress analyses of joint implants indicate that in many *in vivo* applications, bone cement will be cyclicly loaded under constant strain rather than constant stress conditions and that both tensile and compressive strains may be imposed. To study the influence of mean strain and strain range we conducted strain controlled fatigue tests of acrylic bone cement in both zero-tension and tension-compression loading configurations.

Standard, waisted specimens were tested in an axial loading mode in a wet environment at 37 degrees celsius. A constant strain rate of 0.02 s^{-1} was used, which resulted in physiologic loading frequencies. An extensometer was attached to the specimen gauge length so that strain could be controlled and monitored during testing. Stress vs. time and strain vs. time histories were continuously monitored on a strip chart recorder. Thirty-nine specimens were tested in a fully reversed tension-compression mode 40, in a zero-tension loading mode and 11 specimens were subjected to monotonic tensile tests to failure. Fatigue failure was defined as either complete fracture or the point at which the stress range fell below 70% of the stress range on the first loading cycle, whichever occurred first.

The fatigue strength of individual specimens could usually be related to the presence of voids, which were evident in roentgenograms taken prior to testing. The variability in void size and void distribution contributed strongly to the data scatter seen in our results. Regression analysis of the data plotted as strain range vs. cycles to failure and stress range vs. cycles to failure revealed less scatter for the strain curve, implying that the fatigue behavior of cement is more strongly governed by strain than by stress. Regression analysis of the data plotted as maximum tensile strain vs. cycles to failure, showed no statistical difference between the zero-tension and tension-compression loading modes. The monotonic tensile tests resulted in ultimate strains of 0.015 (S.D. 0.004). Fatigue tests with a maximum cyclic tensile strain of about 0.005 caused failure in 10,000 cycles. A Weibull statistical analysis of the data was used to quantify the distribution of specimen survival probability under specific test conditions. Using the 20% survival probability levels from the Weibull analysis, a modified Goodman diagram was constructed. Our data fell below the Goodman line, with a calculated n value in the modified Goodman equation of less than one. These results suggest that fatigue failure is more strongly influenced by maximum cyclic tensile strain than the cyclic strain range. This finding is in direct contrast to the fatigue behavior of most metals, and may be related to the fact that the monotonic compressive strength of cement is more than twice the tensile strength. The study emphasizes the critical role that cement tensile strains may play in cement failure and implant loosening.

Supported by the Firestone Foundation, The William H. Harris Foundation and NIH RCDA AM 00960.

MUSCULAR POWER ACROSS THE KNEE JOINT DURING THE PULL IN OLYMPIC WEIGHTLIFTING

Roger M. Enoka

Department of Physical Education, University of Arizona, Tucson, Arizona

The rate of mechanical energy flowing into or out of muscles, power absorption and production respectively, is often thought to limit human performance, especially if the event is of short duration (e.g., Wilkie, *Ergonomics*, 3:1, 1960). The intent of this investigation was to evaluate the relevance of this premise to Olympic weightlifting by examining the influence of skill and load on the muscular power produced by experienced weightlifters. The analysis focused on the segment of the lift in which the barbell was displaced from the floor to approximately waist height. Over this range of motion the dominant musculature has been demonstrated to be that about the knee joint (Enoka, *Med. Sci. Sports*, 11:131, 1979).

Six competitive weightlifters, three of whom were more skillful than their counterparts, were each tested on two occasions. A testing session comprised one lift at 80%, one at 90% and three at 100% of a coach-specified maximum load (100%). At the time of testing the 100% loads represented $86 \pm 3\%$ and $86 \pm 4\%$ ($p > .10$) of the estimated maximum capabilities for the skilled and less skilled groups, respectively. Each lift was filmed (≈ 100 Hz) and the ground reaction force measured (sampled at 500 Hz). The cinematographically derived position-time records were filtered (symmetric second order Butterworth digital filter, cutoff frequency = 6 Hz) and the segmental acceleration-time histories obtained by double-differentiation (first order finite differences). Muscular power across the knee joint was determined with respect to the mass of the leg as the product of the resultant muscle torque, calculated by Newtonian mechanics, and the absolute angular velocity of the leg.

The angular displacement about the knee joint comprised two periods of extension, separated by an interval of flexion. Concomitantly, the instantaneous power-time histories were characterized by alternating periods of power production and absorption. The mean profiles differed across loads (80, 90, and 100%) for the skilled subjects with the number of production-absorption epochs increasing with load. In addition, the profiles differed between skill level in that the less skilled 100% pattern was more similar to that developed by the skilled subjects with the 90% rather than the 100% load. Each profile contained at least an initial and subsequent period of power production and absorption, respectively, which collectively accounted for between 66 (100% skilled) to 100% (80% skilled) of the movement duration. The duration of the initial period of power production, however, was relatively constant among the profiles ($42 \pm 3\%$). The peak instantaneous power and its temporal location, as a percentage of movement duration, was not significantly different ($p > .05$) across loads (80, 90, and 100%) for the skilled subjects during either of these first two periods. Conversely, the peak instantaneous power produced by the less skilled subjects during the initial period (31.0 ± 14.2 W/kg) was significantly greater ($t_{.05}(2), 29 = 2.37, p < .05$) than that produced by the skilled subjects (21.7 ± 5.8 W/kg). Since these maxima did not differ in temporal location, these observations suggest that the ability to produce muscular power across the knee joint, at least with loads up to 86% of maximum capability, was not a limiting factor over the range of motion examined.

Supported by Biomedical Sciences Support Grant 61-2300 and RR-07096 NIH awarded to the Department of Kinesiology at the University of Washington and by the University of Arizona Computer Center.

BIOMECHANICS OF THE KNEE EXTENSION EXERCISE

W.J. Suntay, E.S. Grood, D.L. Butler, F.R. Noyes
Giannestras Biomechanics Laboratory, Department of Orthopaedic Surgery
University of Cincinnati, Cincinnati, OH 45267

The purpose of this study was to measure directly the mechanical advantage of the quadriceps mechanism, the effects of cutting the anterior cruciate ligament, and the addition of weights to the foot during the knee extension exercise.

Five whole cadaveric lower limbs were studied. The femur was mounted horizontally, and supported on the posterior surface with the leg hanging freely at 90 degrees flexion. The quadriceps were dissected and attached to the load cell and actuator of an Instron via a wire cable and pulleys. Actuator motion was used to load the quadriceps and bring the leg to extension. Three dimensional knee motion was measured using an instrumented chain (1).

The chain was mounted across the knee, one end to the femur and the other end to the tibia, using three 1/8 inch stainless steel pins, which form an exoskeleton. The position of the chain ends relative to coordinate systems located in both bones were determined using a bi-planar x-ray technique (2).

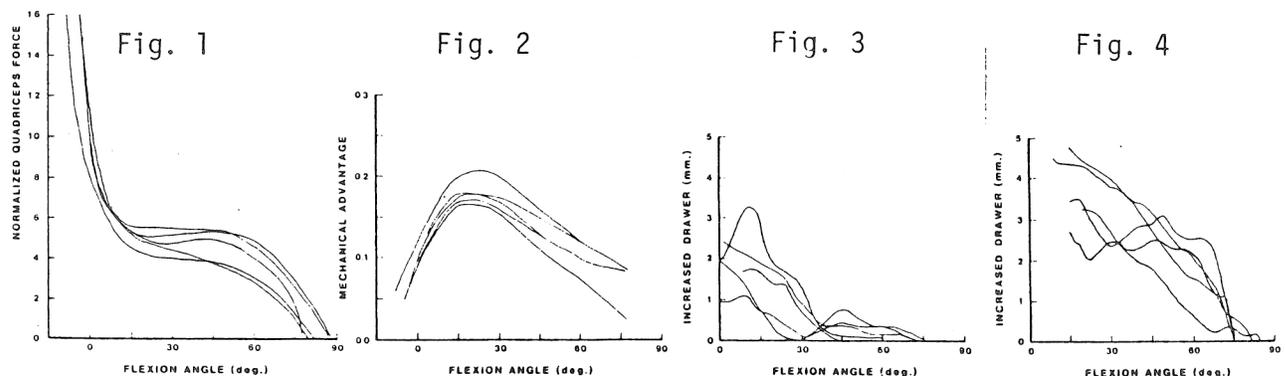
Joint motion was described in terms of clinical rotations and translations using a nonorthogonal coordinate system (3). Modelling the quadriceps mechanism as a lever, we determined its mechanical advantage.

Results from five specimens are shown in figures 1-4. The quadriceps force required to extend the leg is shown normalized with respect to leg weight in Figure 1 for the intact knee. The initial rise in force with extension is due to an increase in the moment arm of the leg's center of gravity. The plateau between 50 and 15 degrees reflects an increased mechanical advantage of the extensor mechanism shown in Figure 2. With extension past 15 degrees, there was a rapid increase in quadriceps force reflecting a reduction in mechanical advantage plus resistance of the ligaments to hyperextension.

Cutting the anterior cruciate ligament had no effect on the quadriceps force. The addition of a 32 newton, 7 lbs., weight on the foot required an average additional force of 240 newtons, 54lbs., to reach within 30 degrees of full extension. This corresponds to 7.5 lbs. of additional quadriceps force for each pound added at the foot.

Figure 3 shows changes in anterior drawer relative to the intact knee resulting from sectioning the anterior cruciate ligament. A significant anterior shift of the tibia was seen towards extension. This is consistent with our prior studies which showed the ligament to be a primary restraint to anterior drawer (4). With the addition of 7 lbs. to the foot a marked increase in anterior drawer (Figure 4) was evident over the entire flexion range.

References. 1. Kinzel, G.L., et al.: J. Biomech. 5:93-105, 1972. 2. Brown, R.H., et al.: J. Biomech. 9:355-356, 1976. 3. Grood, E.S., et al.: 25th ORS p.80, Feb., 1979. 4. Butler, D.L., et al.: J.B.J.S. 62-A:259-270, 1980. This work supported in part by NIH Grant 1R01AM21172.



Non-Sagittal Plane Movements and Forces During Distance Running

Keith R. Williams
Physical Education Department
University of California at Davis
Davis, California 95616

Analyses of distance running performed in the past have usually involved planar cinematography with the camera orientated to give a sagittal plane view of the runners. The inherent assumption made is that movements out of the sagittal plane are small and their contribution to kinematic parameters generally can be neglected. While movements out of the plane are usually small in comparison to those in the plane, they may be important when subtle variations in running style are examined. The present paper utilized three-dimensional cinematography and a force platform analysis to examine a number of parameters characteristic of distance running which involve movements and forces out of the sagittal plane.

Thirty-one subjects were filmed using four cameras operating at 100 fps while running overground. Subsequent analyses of the data provided three-dimensional coordinates of twenty landmarks and joint centers on the body which were used to evaluate various kinematic parameters of one running cycle for each subject. From this three-dimensional data non-sagittal plane kinematics could be extracted. Ground reaction forces and center of pressure patterns were measured and averaged over five foot contacts both left and right feet. This enabled medio-lateral forces and center of pressure movements to be evaluated in comparison to kinematics. Additionally, front view film was taken at 50 fps while subjects ran on a treadmill and were analyzed to obtain a measure of the position of foot contact relative to a midline of the run, a parameter labeled cross-over.

Analysis of kinematic results enabled a number of descriptive parameters pertaining to non-sagittal plane movements to be quantified. These include for one cycle of running measures such as the mean range of medio-lateral movements of the wrists (13.0 ± 4.2 cm), knee (8.0 ± 2.2 cm), ankle (11.1 ± 2.3 cm), and total body center of mass ($1.91 \pm .91$ cm), the total amount of rotation at the shoulders ($26.7 \pm 4.9^\circ$) and hip ($24.3 \pm 7.7^\circ$), and the amount of cross-over (1.0 ± 1.4 cm) where positive values place the foot lateral to the midline. The relative importance of some of these medio-lateral movements is exemplified by putting the mean range of wrist movements (13.0 cm) in contrast to the ranges in the antero-posterior (A-P) direction (30.9 ± 5.7 cm, relative to the body center of mass) and the vertical direction (13.0 ± 4.4 cm).

A number of interesting relationships were uncovered involving non-sagittal plane parameters. For example, a significant correlation of -0.65 was found between the measure of cross-over obtained and the integral of the medio-lateral forces. The further the foot landed medially, the greater the net impulse in the medial direction. A further high correlation was found between the A-P position of initial contact of the foot and the peak of the laterally directed forces. The further forward on the foot that initial contact was made, the greater the lateral forces. These results help to explain the source of the often confusing medio-lateral forces which result during running.

These and other results indicate that non-sagittal plane movements and forces may be important to a complete description of the mechanics of distance running, particularly for some individuals. If kinematic or kinetic parameters are being related to other quantities, such as metabolic energy expenditures or the effects of fatigue, and particularly if the magnitude of variation between subjects or conditions is small, it may be very important that a three-dimensional analysis be employed so that errors due to sagittal plane assumptions are circumvented.

INTERSEGMENTAL MOVEMENT EFFECTS ON NET SUPPORT MOMENT

Robert H. Deusinger, P.T., Ph.D.
Program in Physical Therapy
Washington Univeristy School of Medicine
660 South Euclid Avenue, St. Louis, MO 63110

The net support moment principle is an algebraic summation of all extensor moments at the ankle (M_a), knee (M_k), and hip (M_h) sufficiently positive during stance to provide support and suggests that muscle groups with the most pronounced net moment activity are the major contributors to support. Since most human movement involves interaction of two or more segments, each influencing motion of the others, it could be expected that a large component of a NJM is due to moment influences of adjacent segments. Therefore, the purpose of this paper was to determine for the net support moment principle (M_s) whether major net joint moments (NJM) of the lower extremity stance phase of gait are due primarily to muscle generated moments at the respective joint or to relative moment contributions at adjacent joints.

With the lower extremity modelled as a three link system in the sagittal plane, a kinetic analysis was applied to 5 normal and 2 pathological subjects to determine M_a , M_k , M_h during stance phase of walking. Thirty-five mm. interrupted light photography, anthropometric data, and computer applications were used and the net support moment was determined. Subsequently, segment velocities and accelerations were zeroed in successive order to determine the percent moment contribution by each segment to the total net moment produced at the ankle, knee, and hip. The moment contributions were expressed as a percentage change in moments. Therefore, the segment with the largest negative percentage change identified that segment contributing most to the NJM produced at a given segment.

Results demonstrate for both groups of subjects that a major portion of NJM ascribed to muscular activity by M_s are often due to submaximal moment contributions of adjacent joints. This suggests, for example, that treatment rationale for patients not able to produce a sufficient knee extensor moment include activities that emphasize sequenced movement of the major lower extremity segments (i.e. coordination) but more specifically, that attention be given to strengthening muscle groups of segments adjacent to the injured or diseased joint.

FACTORS AFFECTING LUMBAR FORCES DURING THE CLEAN AND JERK

By Susan J. Hall
Washington State University

Factors influencing axial and shear forces and moment of force at the L5/S1 intervertebral joint were examined for 9 different weight magnitude/lifting time combinations of the clean and jerk as performed by 10 female subjects. Weight magnitudes utilized were 40%, 60%, and 80% of each subject's maximum lifting capability, with designated lifting times of 1.5, 3.5, and 7 seconds.

A simple five link model of the human body was designed to enable approximations of axial force, shear force, and reactive torque at L5/S1 from digitized high speed film data. Other variables examined included intra-abdominal pressure, vertical and antero-posterior ground reaction forces, and myoelectric activity at the first and fifth lumbar levels and in the lateral obliques

Pearson correlations, calculated for each of the 90 trials, revealed positive relationships between lumbar myoelectric activity and both reactive torque and shear force at L5/S1, as well as between myoelectric activity in the lateral obliques and compressive force at L5/S1. The Pearson correlations were generally negative between myoelectric activity at the lateral oblique site and both reactive torque and shear force at L5/S1, and between lumbar myoelectric activity and compressive force at L5/S1. Relations between intra-abdominal pressure and the other variables were inconsistent.

The respective effects of weight magnitude and lifting time were assessed through two-way analyses of variance and subsequent Scheffe tests. Weight level was a significant influence with $p < .001$ for mean compressive force and mean shear force at L5/S1, as well as for maximum lumbar EMG amplitudes. The F ratios for lifting time were significant with p 's ranging from .001 to .05 for both mean and maximum values of compressive force, shear force, and reactive torque at L5/S1; as well as for mean and maximum lumbar myoelectric activity.

ANALYSIS OF STRAIN IN THE ANTERIOR CRUCIATE LIGAMENT OF THE HUMAN KNEE. R.A. Fischer, M.D.; S.W. Arms, B.S.; R.J. Johnson, M.D.; and M.H. Pope, Ph.D.; Department of Orthopaedics and Rehabilitation, University of Vermont College of Medicine, Burlington, VT 05405

Introduction: The repair, reconstruction and rehabilitation of injury to the anterior cruciate ligament depend on a knowledge of the normal mechanical behavior of this structure. We have devised a 10mm long strain transducer which, when attached directly to the ACL, can accurately measure strain to within .002cm. The objectives of this study were to: (1) Refine a technique for measuring strain over small segments in the human ACL, (2) establish the strain pattern in the ACL from full extension to 120° of flexion, with and without a 44.5N valgus force at the medial malleolus and with and without 13.6Nm of internal and external rotation torque on the tibial shaft...(a) when the leg is passively raised by lifting the foot, (b) when a quadriceps pull on the patellar mechanisms is simulated, (3) establish the strain in the ACL during simulated isometric contraction of the quadriceps.

Methods: Our strain transducer employs the Hall effect to detect linear displacement of a .5mm diameter magnet sliding within a tube. This device is sutured to the ligament with minimal influence on its physiologic behavior. This study was carried out on a limited number of autopsy specimens. In each case, the femur was rigidly secured to the autopsy table via skeletal fixation pins. A metal stirrup was then attached to the ipsilateral distal tibia and foot via skeletal pin fixation. A coupling protrudes from the plantar aspect of this stirrup so that its longitudinal axis aligns with that of the tibia. Access for transducer attachment to the ACL was gained via a medial parapatellar incision. An electrogoniometer was attached to the femur and tibia, to measure knee flexion angle. This angle was changed via "passive" lifting of the foot and by "active" raising of the leg via pulling on the quadriceps insertion on the patella. Using two techniques, the knee was subjected to a range of motion from 0° to 120° of flexion. These were then performed with a 44.5N valgus force at the medial malleolus, and with 13.6Nm internal rotation and external axial rotation torques on the tibial shaft coupling.

Results: During "passive" range of motion, ACL strain decreased from full extension to a minimum at 20° - 30° of flexion, and then increased to its maximum level at full flexion. During simulated quadriceps leg raising, the strain in the ACL decreased from a maximum in full extension to a minimum at 50° - 60° of flexion, and then increased with further flexion to 90°. Therefore, maximum strains in the ACL for "passive" motion occur in flexion while maximum strains in the ACL during simulated quadriceps leg raising occur in extension. During simulated isometric contraction of the quadriceps, maximum strain in the ACL occurred from 0-40° of flexion and these were the greatest strains observed during the study. Strain in the ACL was potentiated by the valgus force and internal rotation torque.

Discussion: Numerous authors have described methods for evaluating strain in the human ACL. This study describes the difference in strain in this structure as a result of "active" vs "passive" methods of knee extension. In light of these results, previous and future studies must be interpreted carefully. The position of least strain in the ACL and the immobilization angle postoperatively appears to be between 50° and 60° of knee flexion. The greatest strains in the ACL in this investigation were observed during a simulated isometric contraction of the quadriceps between 20° and 40° of knee flexion. Conclusions from this study, similar to those of Paulos et al.¹, indicate that isometric or isotonic quadriceps contraction in the early postoperative phase may subject ACL repairs and reconstructions to damaging effects.

1. PAULOS, L et al.: Knee Rehabilitation After Anterior Cruciate Ligament Reconstruction and Repair. Am J Sports Med, Vol. 9, No.3, 1981, pp.140-149

TORSION IN OSTRICH KNEES

Patricia L. O'Neill
Department of Biology
Portland State University
P.O. Box 751
Portland, Oregon 97207

Ratite birds (ostrich, rheas, emus and cassowaries) and human beings are the only large bipedal organisms which walk and run. Ratite birds have been bipedal for about 65 million years longer than humans and their hominid ancestors. Nevertheless, human and ostrich knees are similar in size and share many structural similarities. This study determined the rotatory laxity, strength and behavior of the ligaments of ostrich knees loaded in torsion.

In normal standing posture when the knee was maximally extended, the femoral-tibial angle was 130° . Further extension was prevented by the large cremial crest. Full flexion averaged 63° .

The knee was primarily stabilized by the cruciate ligaments and collateral ligaments. The cruciate ligament complex was composed of 3 ligaments which originated on the anterior, interior, and posterior portions of the tibia and shared a common femoral insertion. The capsular ligament was loose and poorly defined.

Knees were rotated in a specially built torsion machine until dislocation occurred. Force vs. angular displacement relations were J-shaped until the yield point. 114 Newton-meters were required to dislocate knees with all ligaments intact. Failure occurred as fracture of the cruciate ligament complex at the femoral insertion. Damage to menisci was virtually absent. With the cruciate ligaments sectioned, 59 Newton-meters were required to dislocate the knee. 49 Newton-meters were sufficient for dislocation when both collateral ligaments were sectioned.

The intact knee displayed 14° of rotatory laxity at full extension. Sectioning the cruciates increased the laxity to 41° ; sectioning the collaterals allowed 49° of laxity.

Bird knees generally allow more rotational freedom than the human knee. Rotatory laxity is necessary since rotation of the leg occurs at the knee instead of the hip as it does in the human gait.

ANALYSIS OF STRESS AND STRAIN

Dennis R. Carter
Orthopaedic Research Laboratories
Massachusetts General Hospital
Boston, MA

Savio L. Woo
Department of Orthopaedic Surgery
University of California, San Diego
San Diego, CA

FINITE ELEMENT ANALYSIS
WHAT IS ITS APPLICATION

30

Roy D. Crowninshield, Ph.D.
Biomechanics Laboratory
Orthopaedic Surgery Department
University of Iowa

The finite element method is a generally applicable method for obtaining numerical solutions to continuum mechanics problems. Problems of stress analysis, heat transfer, fluid flow, electric fields and others have been solved by finite elements. The method is applicable to linear, planar and three dimensional geometries. The solutions obtained are a finite approximation to the physical behavior of the continuum. The method typically uses digital computer executed matrix algebra to solve systems of equations describing the continuum's physical behavior. Biomechanical applications of finite element analysis include stress analysis, heat transfer and fluid flow.

Finite element stress analysis has been used in orthopaedic implant design development. Stress distribution throughout the implant, bone cement and surrounding bone can be studied by this method. Information useful in understanding implant loosening, implant failure and bone remodeling has resulted.

The transfer of heat generated by the exothermal curing of PMMA bone cement has been studied by finite element analysis. These studies have investigated the possibility of thermally induced bone necrosis surrounding total joint replacement components.

Other biomechanical application of the finite element method include modeling of blood flow, skin closure around wounds, stress development in soft tissue during sitting and impact loading of the head. Many past productive uses of the method have been reported and considerable promise for future applications exist.

VERTEBRAL STRESS DISTRIBUTIONS AND THEIR RELATIONSHIP TO EJECTION
INDUCED SPINAL INJURIES

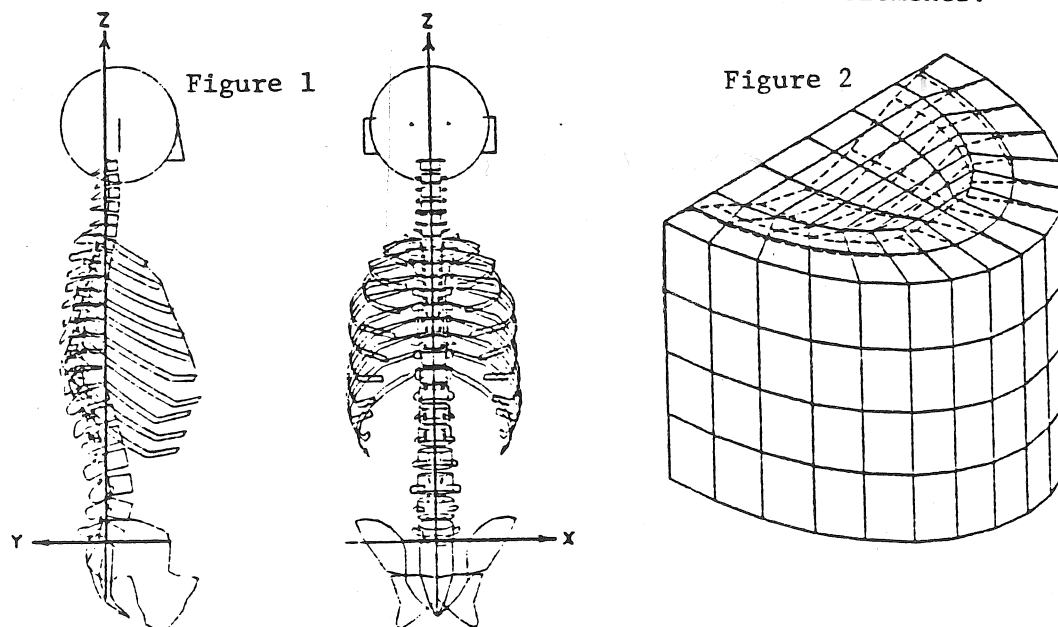
EBERHARDT PRIVITZER⁽¹⁾ AND RONALD R. HOSEY⁽²⁾

The Air Force Aerospace Medical Research Laboratory (AFAMRL) has developed a 3-dimensional model of the human head-torso system for evaluation of ejection system design (Figure 1). The injury prediction capability of this model treats each vertebra of the thoracolumbar spine as a right-elliptical cylinder having a homogeneous isotropic core of trabecular bone surrounded by a thin shell of cortical bone. The predicted peak cortical shell compressive stresses are compared to the compressive yield strength of cortical bone to obtain an indication of the likelihood of spinal injury.

As part of the injury prediction validation process, finite-element analysis of a generic vertebral body are being performed in order to (1) determine the validity of the simplifying assumptions used in the formulation of the injury-prediction capability and (2) improve our insight into the functional relationships between vertebral stress distributions and arbitrary 3-dimensional endplate loadings. To this end, we have been investigating the effects that variations in geometry and material distribution have on vertebral body stress for a variety of prescribed surface traction and displacement boundary conditions.

A number of finite element meshes have been generated in which the trabecular core is modeled with a set of either 8 or 27 node, isoparametric, hexahedral elements and the endplates and cortical shell with a set of thin-shell elements. In addition, separate meshes have been generated for the isolated trabecular core and the isolated cortical shell with and without endplates. The non-linear finite-element program, MAGNA, is being used to perform the analyses.

Figure 2 shows the initial and deformed (dotted) geometry of the isolated cortical shell with endplates that result from the application of a uniform pressure to the superior endplate (inferior endplate fixed) using linear analysis. Complex loading conditions will also be treated. The effects of geometric variations will be considered by (1) varying the thickness of the cortical shell and endplates and (2) varying the curvature of the cortical shell. The effects of variation in material distribution are included in this study by modifying a transition zone between the cortical and trabecular bone elements.



- (1) AFAMRL, Wright-Patterson Air Force Base, Ohio 45433
(2) Systems Research Laboratories, Inc., Dayton, Ohio, 45440

AN ANALYSIS OF THE HUMAN INTERVERTEBRAL JOINT
CONSIDERING ORTHOTROPIC AND VISCOELASTIC PROPERTIES

Capt Leslie Allen, Instructor, USAF Academy and
Anthony N. Palazotto, Professor,
Aeronautics and Astronautics Department
Air Force Institute of Technology
WPAFB, Ohio 45433

ABSTRACT

The United States Air Force has taken a great deal of interest in the study of extreme gravitational forces on air-crew members. Spinal injuries, due to aircraft ejection, and the study of disc degeneration, are just two of the related problems brought about by high g forces. This study was undertaken in order to construct a model of the intervertebral joint using the finite element approach.

Experiments have shown that healthy intervertebral joints exhibit creep when subjected to axial load. A previous study of this time dependent behavior employed a simplified visco-elastic model of the disc which neglected its inhomogeneity. Though the homogeneous model successfully simulated the externally observed response of its joint, it could not adequately portray the internal response of the disc, especially the interaction of the annulus fibrosis and the nucleus pulposus.

The focus of this investigation is the behavior and interaction of the nucleus and annulus under loading, noting in particular, the role of the annulus as a restraining mechanism on the nucleus. An axisymmetric finite element model is employed, which incorporates a linear visco-elastic constitutive relation for the annulus and nucleus based upon a three-parameter Kelvin solid. The visco-elastic constants are found by matching one-dimensional axial experimental data with this two-dimensional model. The nucleus, which is composed of a series of concentric lamellae of collagen fibers, has been modelled as a 12 ply structure of orthotropic material. The cortical bone, trabecular bone, and the bony end plate are assumed to be isotropic and linearly elastic.

Results indicate that the orthotropic material properties of the annulus have a significant impact upon its time dependent behavior and should be included when modelling the joint.

A DYNAMIC FINITE ELEMENT MODEL OF POLE VAULTING

Peter M. McGinnis and Lawrence A. Bergman
Department of Physical Education and Department of
Theoretical and Applied Mechanics, University of Illinois,
Urbana, Illinois 61801

Finite element methods have been used extensively in biomechanics to model and analyze biological tissues and prostheses. Few studies have used the finite element method to analyze human-implement interactions in sport. This study was designed to demonstrate the use of the finite element method in the analysis of a human movement involving an implement. The pole vault was dynamically modeled using the finite element analysis program ABAQUS* which was capable of dynamic and geometric nonlinear analyses. The pole model consisted of twenty pipe elements and the vaulter model consisted of seven cylindrical elements. The vaulter was hinged to the pole at the node representing the wrist joint. Hinges were also used to model the vaulter's shoulder and hip joints. Concentrated moments representing the muscular torques produced by the vaulter at the wrist, shoulder and hip were applied to the corresponding nodes of the model. Film of a 5.29 meter competitive vault provided the necessary data for the initial conditions of the analysis. Torque histories similar to those reported in the literature were input as the concentrated moments at the wrist, shoulder, and hip nodes. The trajectories of the mass center of the actual vaulter and the model vaulter were compared and found in close agreement. It was concluded that the finite element method may be used to accurately model pole vault dynamics.

*ABAQUS was developed by Hibbitt, Karlsson & Sorensen, Inc.
35 South Angell St., Providence, R.I. 02906

ANALYSIS OF FORCE FLOW IN DIFFERENT ARTIFICIAL KNEE JOINTS
USING THE FINITE ELEMENT METHOD

H. Röhrle, W. Sollbach Dornier GmbH D-7990 Friedrichshafen
J. Gekeler Orthopädische Universitätsklinik
D-7400 Tübingen

Detailed knowledge of the force flow resp. stress distribution in the endoprosthesis-bone compound is among other things important for the design and evaluation of artificial knee joints.

We present finite element analysis based on the use of tetrahedron volume element for different systems of the human knee:

- natural knee
- artificial knee with shaft and fixed axis
- artificial knee with shaft and movable axis
- artificial knee without shaft and with movable axis (sledge endoprosthesis).

The comparison of the stresses in the living bone of the artificial knee joints with the stresses in the natural knee shows the more or less unphysiological deviations. At this we use a new interpretation of the Wolf's law:

The quality of an endoprosthesis and endoprosthesis-bone compound is the higher the less the mechanical stress in the bone deviates from that of the healthy bone.

Different attributes of the artificial knee joint influence the stresses:

- The stiffening effect of the shaft
- The dislocation of the axis
- The ventral or dorsal dislocation of the endoprosthesis
- The local concentration of pressure transfer

We present this influences for the load cases -symmetrical knee bend and -horizontal walking.

A FINITE-ELEMENT MODEL OF THE HUMAN HEAD AND NECK DURING
OBLIQUE-CROWN IMPACT

R. R. Hosey,⁽¹⁾ J. E. Ryerson,⁽¹⁾ and Y. King Liu⁽²⁾

A finite-element model for head and neck injury has been developed by Hosey and Liu (1982) based on the general-purpose finite-element program SAP4. This morphologically "exact" model includes the skull, dura, cerebrospinal fluid space, cervical spine, cerebrum, brainstem, and spinal cord (Figure 1). A 6 ms simulation of an occipital impact was performed with the model. Reasonable agreements with the cadaveric data of Nahum et al. (1977) and the rhesus monkey data of Ommaya et al. (1971) were obtained for the contact-impact duration of approximately 4 ms.

Crown, or supero-inferior (SI), impact is important because contact-impact in that particular direction is one of the major causes of partial or complete spinal cord transection. Examples of such violent contacts are: diving accidents, American football, and various traumatic episodes involving self-propelled vehicles in which the crown comes in contact with a solid body. The special vulnerability of the neck to a dynamic supero-inferior impact to the skull is due to the fact that the neuromusculature plays a negligible protective role for the cervical vertebral column because the muscles cannot contract to absorb energy. Furthermore, compressive preload only adds to the dynamic buckling load experienced by the cervical spine.

The results of a 6 ms simulation of vertical-crown impact of 1500 N magnitude and 4 ms contact-impact duration indicate that the effect of crown load in the brain region is not quite as severe as from occipital impact. More of the impact energy from the crown load is absorbed by the spinal column as evidenced by high disc and vertebral body compressive stresses of approximately 5 MPa. Corresponding pressures in the brain region did not exceed 20 MPa. Maximum horizontal displacements of approximately 2.8 mm were observed in the C4 region of the spine. Figure 2 illustrates the buckling effect of the spine under a vertical-crown load of magnitude 6000 N.

We are currently studying oblique-crown impact. Preliminary results from a 1500 N crown impact at a 45° angle of incidence (horizontal load component toward the anterior) show that the maximum buckling deflection of the spine is shifted superiorly to the C2 level. The maximum horizontal displacement is 2.7 mm. Peak pressure values in the frontal and occipital regions of the brain were slightly higher than those in the region of the load. Further work will include the effects of a 45° crown-impact load applied to the region of the frontal bone (anterior to the coronal suture). This load condition better characterizes the contact-impact of athletic events.

References:

1. Hosey, R.R. and Liu, Y.K. (1982), "A Homeomorphic Finite Element Model of the Human Head and Neck," Chap. 18, Finite Elements in Biomechanics, (Eds: R.H. Gallagher, B.R. Simon, P.C. Johnson, and J.F. Gross), John Wiley & Sons, pp. 379-401.
2. Nahum, A.M., Smith, R., and Ward, C.C. (1977), "Intracranial Pressure Dynamics During Head Impact," 21st Strapp Car Crash Conf., SAE, Warrendale, PA, 15096, pp. 337-336.
3. Ommaya, A.K., Grubb, R.L., Jr., and Neumann, R.A. (1971), "Coup and Countercoup Injury: Observations on the Mechanics of Visible Brain Injuries in the Rhesus Monkey," J. Neurosurg., 35:5:506-516, 1971.

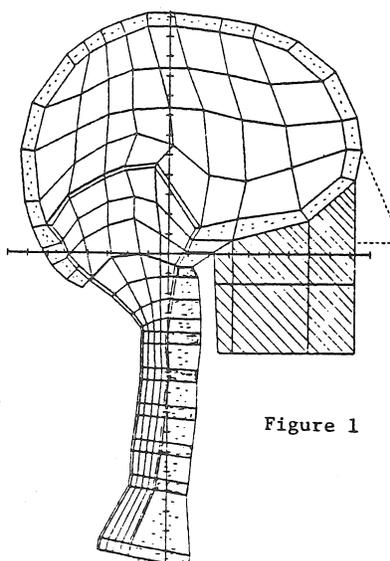


Figure 1

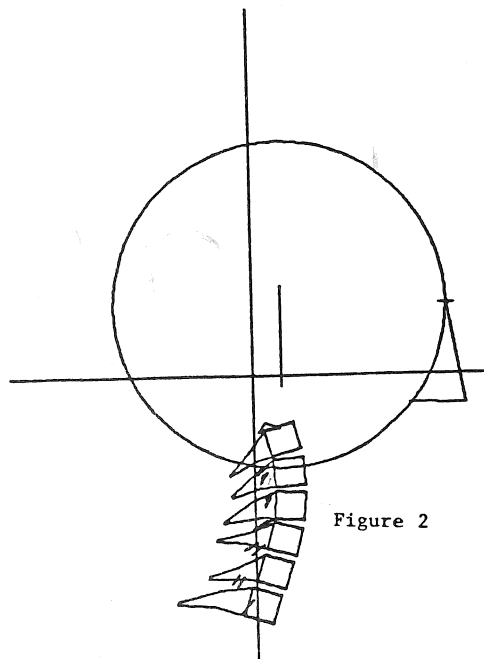


Figure 2

(1) Systems Research Laboratories, Inc., Dayton, Ohio 45440
(2) Dept. Biomedical Engineering, University of Iowa

TRUE STRESS AND STRAIN IN MAMMALIAN SKELETAL MUSCLE

BODINE, S.C., ZERNICKE, R.F., EDGERTON, V.R., ROY, R.R. and PELLER, D.M. Biomechanics and Neuromuscular Research Labs, Department of Kinesiology and Brain Research Institute, University of California, Los Angeles, California, 90024

True stress and strain are inherently difficult to obtain in actively contracting muscle, and typically engineering stress and strain are calculated as estimates of material properties. The purpose of this investigation was to determine intra-contraction true stress and strain for skeletal muscle and subsequently contrast true material properties with engineering stress and strain. The cat semitendinosus (ST) has a septum of dense fibrous connective tissue which separates the muscle into proximal (STp) and distal (STd) compartments, attached in series. The STp constitutes 1/3 and the STd 2/3 the length of the total muscle. STp and STd have separate nerve trunks which permit independent or combined activation of the contractile elements of the two parts of the muscle. The in series structure and activation combinations of the ST produce a unique model for quantifying passive and active mechanical properties of skeletal muscle. The in situ contractile properties were determined for isometric and for isotonic contractions at different loads. Force and displacement were recorded, via a pneumatic lever system, as STp and STd were stimulated separately or simultaneously. Markers were attached to the surface of the muscle, along the line of the fibers; kinematics of the STp, STd, and ST were determined with high-speed (200 fr/s) cinematography and were synchronized with analog data from force and displacement. For each contraction, structural and material properties of STp, STd, and ST were calculated as continuous functions of time. STp shortened and STd lengthened during isometric contractions in which STd and STp were simultaneously stimulated. At resting length, cross sectional areas of STp and STd were not significantly different, but as a consequence of the differential length changes in STp and STd, the cross sectional areas and, thus, true stresses differed. Isotonic conditions at high force, low shortening velocities produced mechanical behavior analogous to the isometric conditions. At low force and high velocities, STp and STd both shorten, but at different absolute velocities; thus, dissimilar true stresses were developed in the STp and STd. The existence of an endogenous in series muscle arrangement provides an intriguing experimental preparation for examining the passive and dynamic mechanical properties of skeletal muscle. The results of this study highlight the non-uniform mechanical interactions which may occur in muscle-tendon units as a consequence of passive and active components.

Supported by NIH Grant NS16333.

THE INFLUENCE OF BIOMECHANICS ON THE DESIGN OF SPORTS EQUIPMENT

E.C. FREDERICK, DIRECTOR OF RESEARCH AND DEVELOPMENT, NIKE, INC.
EXETER, NEW HAMPSHIRE 03833

The principles of biomechanics and, in many cases, the results of biomechanical experiments, form the basis for the design of many articles of sports equipment. Some examples of this relationship between biomechanics and sports equipment design are: new ergogenic bicycle designs, aerodynamic javelins, compound archeries, tennis racquets with ergogenic grips and enlarged sweet spots, long flying and non-hooking golf balls, improved golf club designs, properly banked and compliant running tracks, wind suits for high velocity sports and last but not least sport shoes designed for specific applications and to improve running economy. The development of most of our sport shoes is influenced by the biomechanical experiments that are performed in our Sport Research Laboratory, as well as by the published work of other scientists. As one example of how biomechanics finds its way into the design of sports equipment, let me show you how the process works at NIKE.

Our biomechanics research focuses on two interrelated problems; defining human needs and finding the optimal solution to those needs. The principal techniques we use to study these two problems include: high speed cinematography with computer digitization, force plate analysis, accelerometry, impact testing with dynamic load displacement analysis, flexibility testing, mechanical wear testing, oxygen uptake measurements, in vivo foot temperature measurements and field testing.

In our basic research, we use these techniques most commonly to study three needs shared by most sports: cushioning, stability and economy of movement. Our research has helped us to define cushioning requirements for athletes with various body dimensions, running at a range of speeds and with various patterns of footstrike. We are also interested in the functional anatomy of the foot and in the biomechanical consequences, including range of rearfoot movement, of different foot types. Our studies with economy of movement have focused on understanding the causes of inter- and intra- individual variations in the oxygen cost of running.

Our applied research program uses these same techniques to determine the performance characteristics of various prototype and production shoes. The most common measurements we make on those models are: cushioning, (in vitro and in vivo), rearfoot control (in vivo), flexibility (in vitro) and oxygen cost.

Our own basic and applied research findings along with input from a team of consultants are used to guide the development of new shoes and to make certain that the intended functional design specifications of new models are being achieved. Our efforts have allowed us to improve our understanding of human needs and in many cases helped us to find better solutions to those needs.

INDIVIDUAL SUBJECT FORCE PRODUCTION PATTERNS OBSERVED FOR AN ISOTONIC AND ISOKINETIC BENCH PRESS

J.E. Lander, B.T. Bates, J.A. Sawhill, and J. Hamill, Biomechanics/
Sports Medicine Lab., University of Oregon, Eugene, OR, 97403

Since the development of isokinetic training devices in the 1960's researchers and practitioners alike have argued the merits of these devices compared with isotonic or free weight training. The purpose of the study was to measure and compare selected parameters describing isotonic (IT) and isokinetic (IK) bench press technique.

Six highly skilled college age males performed five IT trials at 90% of their maximum single repetition ability (1RM) followed by five trials at 75% 1RM with adequate rest between trials. Speed settings for two comparable IK conditions for each subject were established based upon average movement speeds achieved during the IT trials. Each subject performed five trials at a slow speed (25-50 deg/sec) and five trials at a fast speed (50-95 deg/sec). Parameters describing the IT condition were generated from cinematographic data (150 fps). The data for the IK conditions were obtained using an instrumented Cybex Power Bench Press. Only the vertical component of force was evaluated. The data presented are for the slow IK and heavy IT conditions. Similar results were observed for the fast IK and light IT trials.

Visual examination of the Cybex force vs time data curves suggested the use of three patterns of force production. Subjects 2 and 4 exhibited a moderately large first peak value (1871.0 N) and a very large second peak value (2308.0 N). Consequently, the peak 1 to peak 2 ratio was low (0.81). Subjects 1 and 5 exhibited generally flat force vs time curves with a small first peak value (1671.9 N) and a small second peak value (1651.9 N) resulting in a ratio of 1.02. Subjects 3 and 6 exhibited a large first peak value (2086.6 N) and a small second peak value (1648.3 N) yielding a ratio of 1.26. The three patterns related to the 1RM strength capabilities of the subjects. The order of performance from strongest to weakest was 2, 4, 1, 5, 6, 3 with mean 1RM values of 1523.8 N, 1366.1 N, and 1222.5 N for the three subgroups respectively.

A subject's performance on an IK device is primarily a function of strength. Free weight performance (IT) is not only influenced by strength but requires additional technique to stabilize the bar in the horizontal direction. For this reason, mean IK force values throughout the activity were in general approximately 10% greater than the corresponding IT values.

Although all subjects were highly skilled based upon a strength criterion, technique differences were apparent. Subjects 1 and 5 used a relatively wide grip and maintained a large arm-trunk angle (ATA) of approximately 90 deg throughout the lift. This type of grip makes explosiveness at the beginning of the lift difficult due to anatomical constraints and appears to limit the overall success of the lift. In contrast, subjects 3 and 6 used a relatively narrow grip and maintained a small ATA (~45 deg) throughout the lift. This better enables the lifter to explode at the beginning of the lift, but hinders force production near the end. Subjects 2 and 4 exhibited "classic" bench press technique, using a moderate grip width which allows for a small ATA at the beginning of the lift and a corresponding explosiveness. As the activity progressed, ATA was increased to approximately 90 deg to take advantage of body structure, enabling the generation of large second peak values.

The results of the study suggest that a relationship exists between technique and IT performance capabilities that appears to be reflected by the ratio of the two peak forces observed during the IK performances.

"The Prediction of Repetition Maxima in Strength-Training," by Jack R. Engsborg, James G. Hay, and Kiyomi Ueya, Biomechanics Laboratory, Department of Physical Education, University of Iowa, Iowa City, Iowa, 52242.

Strength training studies often require the investigator to determine the maximum load with which a subject can perform a given number of repetitions, i.e., a repetition maximum (RM). Most investigators determine RMs on a trial and error basis. This process has several shortcomings--it can be very time consuming, fatigue can influence the results if the required RM is not found after a few trials, and the accuracy of the results obtained is governed by the magnitude of the load increases or decreases.

Those responsible for the development and implementation of strength training programs are often concerned about the maximum number of repetitions that can be performed with a certain percentage of the 1 repetition maximum (1RM). They are concerned, for example with questions like "How many repetitions can a person be expected to perform with 60% of his or her maximum load?" The available literature provides little guidance on such issues.

The purposes of this study were (1) to evaluate an alternative procedure for determining repetition maxima, and (2) to determine the maximum number of repetitions that can be performed with selected percentages of a 1RM load.

Sixteen male college students from an advanced weight training class were used as subjects. 1RMs were determined for bench press, arm curl and squat exercises using the trial and error method. In addition, the maximum number of repetitions that could be performed with each of six different loads was determined for each exercise. Linear regression was used to obtain a line of best fit for these latter data for each subject and each exercise. The equations for these lines were then used to predict the corresponding 1RMs. The equation of a straight line passing through extreme values recorded for the number of repetitions performed was also determined for each subject and each exercise. These equations were then used to predict the corresponding values of the 1RMs.

No significant differences were found between the mean 1RMs determined by the trial and error method and those determined by the prediction methods (p<.05).

To determine the maximum number of repetitions that could be performed at selected percentages of 1RM, linear regression was used to obtain a line of best fit for the combined data of all subjects on each exercise.

Evaluations were made of the individual cases in which 1RMs determined by the trial and error method differed by more than 10% from those determined by the first prediction method. Results indicated that for the lift with which the subjects were most familiar (the bench press), there was only one case in which the 1RM determined by the trial and error method differed from that determined by the prediction method by more than 10%. For the lift with which the subjects were least familiar (the squat), there were six such cases.

The prediction methods appear to offer some advantages over the trial and error method. The trial and error method yields a value for the repetition maximum of interest. The prediction methods yield an equation which can be used to compute repetition maxima over the entire range of interest. Thus, when a single repetition maximum is needed, any one of the methods can be used to obtain that value. When more than one repetition maximum is needed, the trial and error method must be used repeatedly if it is to yield the same information that can be obtained from a single use of a prediction method.

The results obtained from this study appeared to warrant the following conclusions:

1. The prediction method provides an acceptable alternative to the traditional trial and error method for determining repetition maxima.
2. The prediction method appears to provide a more realistic value for the 1RM than the trial and error method, especially if the subject is not completely familiar with the exercise.
3. The prediction method can yield nRMs (n=1,15) whereas the trial and error method determines only a single RM.

FIELD MEASUREMENTS IN SNOW SKIING INJURY RESEARCH

J. K. Louie
C. Y. Kuo
Graduate Students

C. D. Mote, Jr.
Professor

Department of Mechanical Engineering
University of California
Berkeley, California 94720

Abstract

Severe lower extremity injuries continue to occur during snow skiing, particularly to the ligaments at the knee. The use of a modern ski release binding fixing the boot to the ski reduces the possibility of tibia fractures and ankle injuries, but a reduction in injuries at the knee has not been reported.

Field measurements during skiing experiments simultaneously recorded the complete excitation of the toe and heel of one foot (12-dynamometers), the absolute spatial orientation of the pelvis and the foot (6-rate-gyros), muscle activity at the hip, knee and ankle (6-integrated EMG probes), and the complete rotation of the femur relative to the tibia across the knee (3-goniometers) in three subjects. Data were transmitted from test subjects by a 100K bit/sec. FM-PCM system and recorded in digital form.

Preliminary analyses of early field data show the magnitude of the loading applied to the lower extremity during normal skiing often exceeds the ultimate strength of the tibia as measured in quasi-static experiments. Anterior-posterior bending of 600 N-M has been recorded. Longitudinal rotation across the knee was in-phase with, though not proportional to, the applied torsion at the foot, and it often exceeds 20 degrees during normal skiing. Increased complexity of the injury and protection problems is indicated in these early results.

FORCE ANALYSIS IN CROSS-COUNTRY SKIING

Javin Pierce; Malcolm Pope, PhD; Robert Johnson, MD; David Punia, BSEE
Department of Orthopaedics & Rehabilitation
University of Vermont College of Medicine

The purpose of this study was to construct a portable recording system to dynamically quantify the propulsive forces created in cross-country skiing in order to understand and improve racing technique.

Strain gauges were mounted on one ski pole to measure compressive force, and force plates were attached to the opposite ski to measure axial heel loads, axial forefoot loads and anterior-posterior shear at the forefoot. Force plates and binding assemblies added 250 g to the test ski, and a dummy plate of the same size and weight was added to the opposite ski. A backpack was worn by the skiers which contained strain conditioning and amplification. The force signals were converted to multiplexed frequencies by a voltage to frequency converter; also in the backpack, the four separate signals were then sent to a SONY TCD5 stereo cassette recorder that was strapped to the skier's chest. This system is self-contained and weighs 6.4 kg.

Test Methods. In one series of tests a soft snow track was set in a field with a slight incline followed by a slight decline. A world class racer was instrumented and asked to ski five runs up the incline in a diagonal stride, and to continue down the other side, twice double poling and three times double poling with an alternating "kick".

Results. We found that the magnitude, duration and relationship of forces in time could all be accurately measured with this system without significantly altering the skier's form or the properties of the ski. Table 1 illustrates the differences in average peak forces due to stride and terrain changes. The heel transducer sensed the most force in double poling with a kick. This could be accounted for by the strong backward pole thrust resulting in a rearward weight shift. Surprisingly, a kick force was generated in the double pole maneuver, although no actual "kick" occurred. However, this is highly plausible in soft conditions due to the sudden upward and forward thrusting of the skier's body after the crouching double pole release.

Table 1. Average Peak Forces in % of Body Weight - Soft Snow

<u>Measured Forces</u>	<u>Stride Type</u>		
	<u>Diagonal</u>	<u>Double Pole</u>	<u>Double Pole with Kick</u>
R Pole	11	14	13
L Heel	61	68	72
L Forefoot	162	38	154
Ant. forefoot (glide)	10	10	14
Post. forefoot (kick)	14	8	8

This system will be employed with a synchronized high speed photography system devised by Dr. Charles J. Dillman, Biomechanics Director of the U.S. Olympic Committee, for use with the U.S. Ski Team.

DYNAMIC SIMULATION OF THE LEG IN TORSION

by

L. K. Dorius
Graduate Student

M. L. Hull
Assistant Professor

Department of Mechanical Engineering
University of California
Davis, California 95616

The proliferation of lower extremity injuries from sporting accidents, especially snow skiing, has stimulated research into lower extremity injury mechanisms under dynamic loading. Although the injury site most common is the knee, the majority of injury mechanism research has focused on the tibia. Accordingly, little information exists about how ankle, knee, and tibia injuries are influenced by dynamics of the leg. One objective of this study is to analyze the role of torsional leg system dynamics on these injuries. A second objective is to explore the effects of thigh tissue compliance on injury dynamics. The final objective is to define a release decision algorithm for snow ski bindings.

The biomechanical model used in this study (see Fig. 1) consists of four lumped inertias connected by piecewise linear springs and linear dissipative elements. Note that the connection between the femur bone and thigh tissue is compliant. The parameters for the model were obtained from the literature. Reference 1 tabulates the parameter values and their sources. Injury criteria consisted of the quasi-static fracture strength of the tibia in torsion and axial rotations beyond the primary stiffness region for the joints.

Results were obtained by first deriving the equations of motion and solving for the ankle and knee displacements and the tibial moment half way up the shank. Then a torque input $M_Z(t)$ having a haversine pulse form was applied with the resulting time response of the failure variables determined by numerical integration. A typical result is illustrated in Figure 2 which plots the non-dimensionalized applied moment for tibial, ankle, and knee failure versus pulse duration.

Conclusions from the study include the following:

1. Ankle, knee, and tibial injury responses are similar and approximate the shock spectrum response of a single degree-of-freedom system.
2. The similarity above is neither affected by variations in parameter values nor thigh tissue compliance.
3. A single degree-of-freedom system can be used to calculate both the tibia loading and the response of the joint with the lower injury threshold.

References:

1. Dorius, L.K. and Hull, M.L., "Transient Response of the Leg in Torsion," 1981 Advances in Bioengineering, ASME, pp. 25-28.

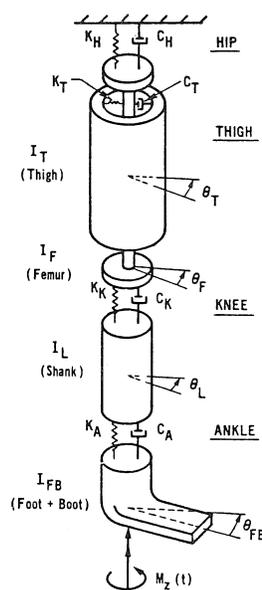


Figure 1

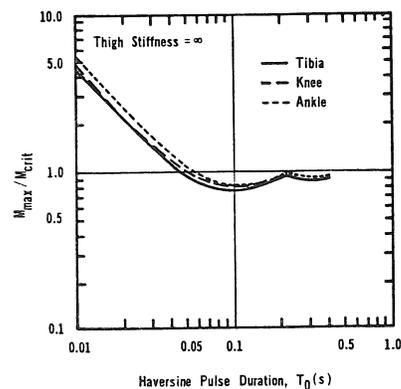


Figure 2

On the Role of Joint Torques in Determining the
Result of the Performance of a Motor Skill

James G. Andrews
Division of Materials Engineering and
Department of Physical Education (FH)
University of Iowa, Iowa City, IA 52242

In evaluating the performance of a motor skill, and in making recommendations for improving that performance, it is essential to have a thorough understanding of all those factors which influence the performance, as well as their relative order of importance. One common method used by biomechanists to analyze human movements consists of constructing a mechanical model of the body, deriving the equations governing model behavior, and then studying how the solution of these equations (i.e., the system's kinematic performance) is influenced by the kinetic factors (i.e., the external forces and torques) which determine that response. The purpose of this paper is to investigate the role that joint torques and other kinetic factors play in determining the result of the performance of a motor skill.

When standard rigid body modeling techniques are used to represent the performer, the characteristic equations that relate model performance to the kinetic factors which produce that response are Lagrange's equations. Newton's equations are not utilized because they include the effects of all workless constraints, and the Lagrangian formulation makes it clear that these reaction forces do not influence the unconstrained motion of the system. In terms of Lagrange's equations, the influence of any external kinetic factor on the system's kinematic performance can be determined by examining the generalized forces. These forces are obtained by calculating the virtual work done on the system, and therefore they will depend, in general, upon the segment weights, the joint forces, the joint torques, and the external forces acting on the system where it contacts the external environment.

Examination of the virtual work expression in common practical situations leads to the following observations concerning the role of the joint torques and other kinetic factors in determining the result of the performance of a motor skill. (1) If the joints are modeled as points fixed in both the involved segments, as is often the case, then the joint forces will not influence system performance. Conversely, if joint translations can occur, then the joint forces will generally effect system response. (2) If, as is usually the case, joint segments rotate relative to each other, then the torques at the corresponding joints will generally influence system performance. (3) If the system contacts external surfaces which are smooth and fixed in an inertial reference frame R , then these contacts will not effect system performance. (4) If the system contacts external surfaces which are smooth but not fixed in R , then these contacts will generally influence system response. (5) If the system contacts external surfaces which are rough and if sliding occurs, then these contacts will generally effect system performance whether the external surfaces are fixed in or move relative to R . (6) If the system encounters air resistance and the associated drag forces are non-negligible, then this contact will also influence system performance.

In conclusion, joint torques will generally play a key role in determining the result of the performance of a motor skill. They will be the sole mechanical determinants of system performance only in those circumstances when the segment weights, the joint forces, and the forces resulting from contact with the external environment do no virtual work on the system.

BIOMECHANICS OF THROWING: PROJECTING INTO THE FUTURE

Anne E. Atwater

Department of Physical Education, University of Arizona, Tucson, Arizona

The skill of throwing is a common element in a wide range of sports. As distinguished from the more simultaneous joint actions of the arm during a push, the throwing motion involves properly timed accelerations and decelerations of body segments in a sequence progressing from the contralateral foot to the throwing hand. The objective of the throw in many sports is to achieve an optimum hand speed and direction at release so as to impart that speed and direction to the object released by the hand.

Descriptions of the throwing motion, particularly the patterns of motion used in projecting a ball or javelin, have been clarified by position-time studies of subjects ranging in ability from skilled to novice. However, kinematic analyses have not been extensive to date due to the recognition that the throwing motion clearly is three-dimensional and that appropriate techniques of three-dimensional cinematographic analysis have not been readily available until recently.

This presentation focuses on the overarm throwing motion and will include the following topics: differentiation between overarm and sidearm throws, examination of the ball path and resultant velocity prior to and at release (Figures 1 and 2), description of joint actions associated with changes in ball path and resultant velocity, analysis of joint actions involved in applying spin to the ball, and identification of potential relationships between throwing mechanics and injuries in the throwing arm.

Future research on the biomechanics of throwing should build upon the existing kinematic data base through more extensive application of three-dimensional analysis techniques. And further, kinetic analyses should be conducted with emphasis on the contributions of individual body segments and on the quantification of resultant joint forces and muscle torques.

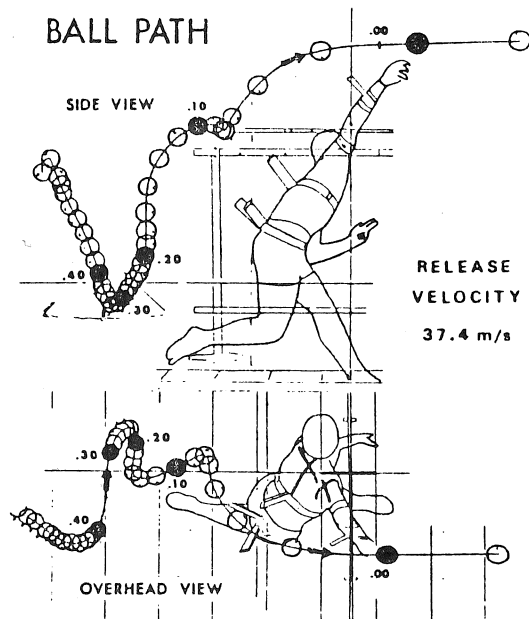


Figure 1

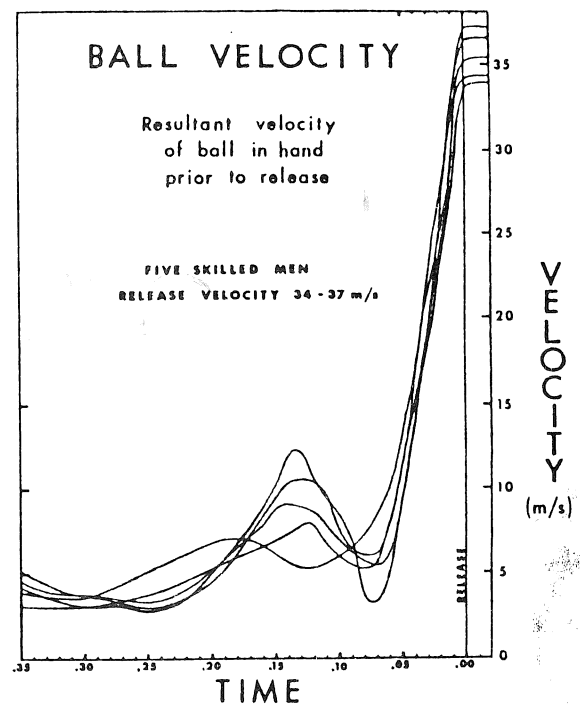


Figure 2

William M. Kier and Kathleen K. Smith

Departments of Zoology and Anatomy, Duke University, Durham, North Carolina

Skeletal support systems interact with the muscular system of animals in a number of ways. These include transmission of force, structural support and provision for joints or pivot points. There are, in general, two major categories of skeletal support in the animal kingdom. The first is characterized by hardened internal or external skeletal elements as seen in the echinoderms, arthropods and vertebrates. The second is characterized by hydrostatic skeletons, typically a fiber-reinforced container surrounding a fluid-filled cavity as seen in polyps and vermiform animals. We wish to consider a group of structures which lack the characteristics of these two categories of skeletal support: the arms and tentacles of cephalopods and the tongues of vertebrates. These structures are composed entirely of muscle, thus muscle acts both as the effector of movement and as the skeletal support system.

Here we will model the biomechanics of three major types of movement in this unique system: change in length, bending and torsion or twisting around the long axis. These models will be supported by comparative behavioral (high-speed cinematography, cineradiography and electromyography) and morphological (gross dissection, histology and electron microscopy) investigations on a number of animals possessing these characteristics.

One of the most important biomechanical characteristics of these muscular structures is that they are of constant volume. Therefore, any decrease in one dimension must result in increase in another dimension. For instance, increase in length has been observed in cephalopod tentacle extension and tongue protrusion in reptiles. This movement is produced by contraction of muscles arranged so to decrease the cross-sectional area of the structures, such as transverse or circular muscles. Such arrangements have been observed in both of these animals.

Bending requires unilateral activity of longitudinal muscles, but in order for bending to occur, longitudinal compression caused by the contraction of these muscles must be prevented. In most animals the resistance is provided by skeletal structures. In these systems support is provided by simultaneous activity of muscles arranged so as to resist increase in diameter and therefore decrease in length. Torsion, or twisting along the long axis is caused by contraction of a sheet of muscle fibers which wraps these structures in a helical fashion. Structures such as squid tentacles which twist in both directions possess both left and right-hand helical musculature.

QUANTIFICATION OF STIMULATED MUSCLE CONTRACTIONS BY MOIRE SURFACE TOPOGRAPHY

A.T.Andonian and A.B.Schultz

University of Illinois at Chicago Circle

The ability to treat scoliosis (a lateral deformity of the spine) via surface-stimulated trunk muscle contractions is now being evaluated at several treatment centers. In order to make biomechanical analysis of the procedure, so that the technique can be used optimally, data are needed to quantify the muscle contractions produced by different sets of electrical stimulation parameters and different electrode locations.

We evaluated the use of moire topography to quantify muscle contractions resulting from electrical stimulation applied to the surface of the back in a healthy subject. Moire photographs of the subject before and during electrical stimulation were made using twelve stimulation electrode sites (Fig.1). The optical data were then fed into a computer so that cross-sectional profiles could be generated after rigid body rotations were removed (Fig.2). Differences in back surface shapes shown by these back profiles were then examined to see if muscular contractions could be quantified. Back surface contour bulges as large as 15mm were observed in these studies. It appears that the study objectives are achievable.

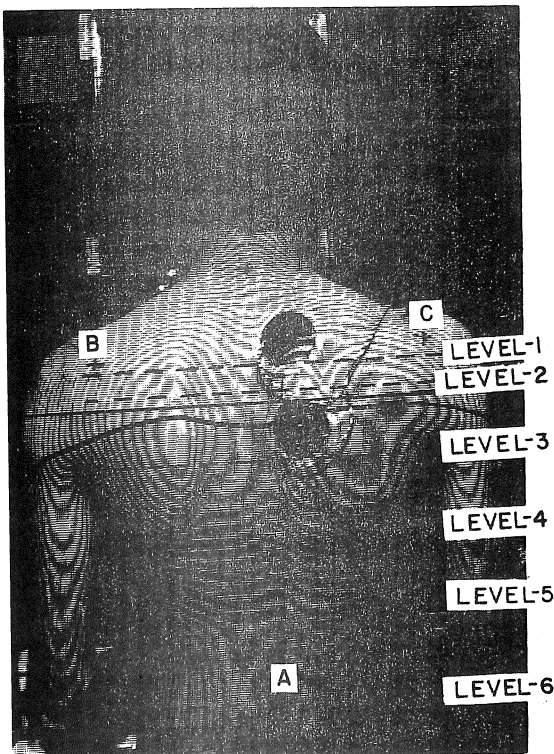


Figure 1

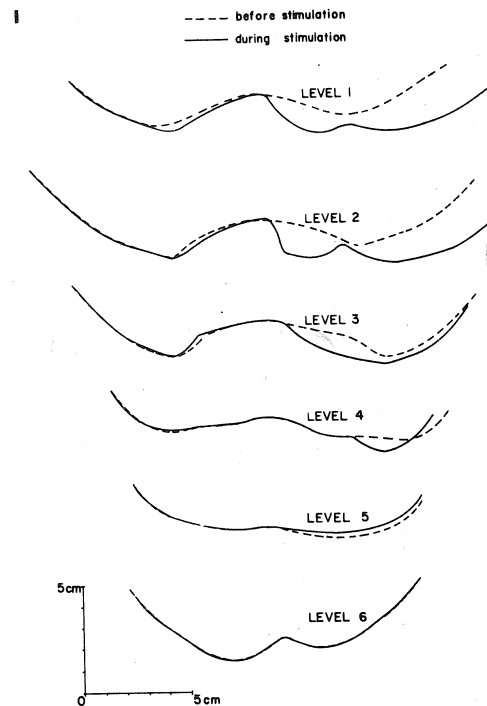


Figure 2

ELASTIC ENERGY STORAGE AND POWER OUTPUT IN SQUID MANTLE MUSCLE

J.M. Gosline, R.E. Shadwick and M.E. DeMont
Department of Zoology, University of British Columbia,
Vancouver, British Columbia, Canada

The propulsive phase of the squid jet cycle is powered by the contraction of a single set of circular mantle muscles. The refilling phase of the cycle, however is powered by two systems; (1) contraction of radially oriented muscles and (2) elastic energy stored in a network of collagen fibers during the propulsive phase. In this study we attempt to determine the relative importance and mechanical significance of the two systems powering the refilling phase. Our findings indicate that elastic recoil provides the major component of the refilling costs. Thus the circular muscles which power the jet also provide most of the power for refilling. Our analysis indicates that this use of elastic energy storage allows the animal to maximize the utilization of the circular muscle's power output, and hence minimize the mass of additional (ie. radial) muscles necessary for jet locomotion.

STRUCTURAL DOMAINS OF THE MUSCLE-TENDON-JUNCTION

John A. Trotter and Susan Eberhard, Department of Anatomy, University of New Mexico School of Medicine, Albuquerque, New Mexico 87131

The contractile force of skeletal muscle fibers, generated intracellularly by the shearing of myosin and actin filaments, is transmitted to extracellular structures at the muscle-tendon junction. It is therefore important to understand the structural and mechanical properties of this region. Ultrastructural and experimental studies currently underway on murine muscles have revealed that the muscle-tendon-junction consists of at least four domains. 1. The "internal lamina" is comprised of thin filaments continuous with the actin filaments that arise from the most distal A-band. These thin filaments are approximately parallel to one another and to the direction of force. They are linked together by connecting filaments which are oriented approximately perpendicular to them. Stereo electronmicroscopic techniques are presently being employed to more precisely define the relations of these elements. Present knowledge of the structure of the internal lamina suggests that stress applied to any of the thin filaments will be distributed throughout the internal lamina, and that the elastic modulus of the internal lamina is relatively high. These considerations are important for understanding how force is transmitted. They are also important for an understanding of the mechanisms by which sarcomeres are added to and subtracted from myofibrils during growth and remodeling of muscle fibers. Present evidence indicates that new sarcomeres are added at the muscle-tendon-junction. The internal lamina must therefore provide mechanical strength and, at the same time, must be capable of adding and subtracting components. 2. Removal of the lipids of the plasma membrane with a nonionic detergent (Triton X-100) leaves the muscle-tendon-junction functionally intact (Trotter *et al*, 1981, *Anat. Rec.* 201, 293) and reveals fine threads, 2-7nm in diameter, oriented approximately perpendicular to the direction of force and to the plane of the plasma membrane. These threads are up to 60nm long and provide a morphological connection between the internal lamina and the external lamina. They traverse the space occupied in the native muscle by the plasma membrane. Some portion of each thread must therefore be "intramembranous". Extraction of muscle under different conditions reveals that each thread is composed of at least two components which meet at level of the plasma membrane. These threads are considered to play an important role in the transmission of force. They may act in concert with a layer of hydrated glycosaminoglycan associated with the external cell surface. 3. The external lamina is composed of type IV collagen, which has the structure of indefinitely long flexible polymers covalently cross-linked in non-parallel fashion (Timpl *et al*, 1981, *Eur. J. Biochem.* 102, 203). It is expected that this structure will have mechanical properties similar to those of vulcanized rubber. The external lamina also contains laminin, a glycoprotein which interacts with type IV collagen and may modify its mechanical properties. 4. The external lamina is linked to collagen fibers of the tendon indirectly by as yet undetermined structural elements.

These observations suggest that each domain has distinct ultrastructural and mechanical properties. They further suggest that the muscle-tendon-junction is a significant series-elastic element important as a mechanical damper in the transmission of contractile force.

by

T.P. Andriacchi, G.B.J. Andersson, R. Ortengren, and
R. Mikosz

The knee joint relies on muscles to provide stability as well as movement. As such, the muscles contribute a major portion of the forces acting at the knee joint. The muscle control motion through a combination of agonist and antagonistic activity and stabilize the joint by producing moments to maintain equilibrium. An understanding of the factors that influence level of muscle contraction, muscles synergy, and the presence of an antagonistic activity about the knee is an important component in the analysis of the internal mechanics of the joint. The purpose of the present study was to investigate the relationship between external moments acting at the knee, knee flexion angle, and the myoelectric activity of 12 muscles surrounding the joint.

The twelve muscles included in this study were the biceps femoris, semi-tendinosus, semi-membranosus, sartorius, tensor fascia latae, gracilis, vastus lateralis, vastus intermedius, vastus medialis, and rectus femoris. Fine wire electrodes of 0.5 millimeters in diameter was inserted into each muscle. The myoelectric activity of all muscles were measured as external moments were applied in directions tending to produce flexion, extension, and combined loads of flexion-adduction, flexion-abduction, extension-adduction, and extension-abduction. The tests were performed at 10, 20, and 40° of knee flexion.

The results indicate that the action of both the flexor and extensor muscle groups at the knee were highly dependent on the angle of knee flexion. Quadriceps muscles all had their largest activity when the knee was near full extension and the activity was reduced by nearly a factor of 2 as the knee approached 40° of flexion under constant loading. Conversely, the activity of the knee flexor were reduced under constant load as the knee moved from a flexed position to full extension.

There was also significant antagonistic muscle activity in the gastrocnemius lateralis and gastrocnemius medialis when the quadriceps muscles were active. The addition of the adduction moment caused the tensor fascia latae activity to increase indicating its stabilizing effect to this loading.

The results of this study tend to indicate that the level of muscle activity cannot be predicted from external moments acting about the joint in a simple manner. Some of the explanations for this phenomena can be described in purely mechanical terms. First, the patellar mechanism acts to change the moment arm of the quadriceps mechanism which changes with knee flexion angle. Secondly, the contact point between the femur and the tibia can be moved posteriorly with increasing flexion, increasing the mechanical advantage of the extensor mechanism and reducing the mechanical advantage of the flexor mechanism with increasing flexion angle. Thus, there is not necessarily a linear relationship between extrinsic moment magnitudes and muscle activity. This non-linear response seems to be influenced to some extent by a combination of the presence of antagonistic muscle activity as well as subtle shifts in the moment arm of the individual muscles.

Rush-Presbyterian-St. Luke's Medical Center
Department of Orthopedic Surgery
1753 West Congress Parkway
Chicago, Illinois 60612

MUSCULAR WORK IN SELECTED ANKLE EXTENSORS OF THE CAT DURING UNRESTRAINED LOCOMOTION

Whiting, W.C., R.J. Gregor, R.R. Roy and C.L. Hager
Biomechanics and Neuromuscular Research Laboratories - Department of Kinesiology
University of California, Los Angeles, California 90024

Muscle function in a seemingly simple activity such as locomotion is a complex phenomenon. The purpose of this study was to investigate several aspects of this complexity by considering the force produced by skeletal muscle and the work performed in vivo during unrestrained treadmill locomotion in cats.

Mechanical muscular work (W) was defined as the product of muscle force monitored at the tendon (F) times the length change of the muscle (d). Two cats were surgically implanted with buckle force transducers (as previously reported (1)) on the medial gastrocnemius (MG) and soleus (SOL) tendons, and with bone screws in the femur and tibia near the origins of the MG and SOL, respectively. Electrical activity (EMG) was monitored simultaneously in both muscles. The cats were trained to walk and run on an enclosed treadmill at three speeds. A two camera three-dimensional film technique was used to estimate muscle lengths during the testing sessions (2).

Force values in the MG and SOL agreed with previously reported data (3). Peak forces were greater at the slower speed for the SOL. Relatively greater length changes at the higher speeds resulted in greater mechanical work at the medium and fast speeds (Figure 1). A brief period of negative work was observed just after paw contact at all speeds, followed by a rapid transition to positive work during the remainder of the stance phase. Minimal work was exhibited during the swing phase. Exemplar active and passive periods of muscle activity are shown for the SOL at medium speed in Figure 2.

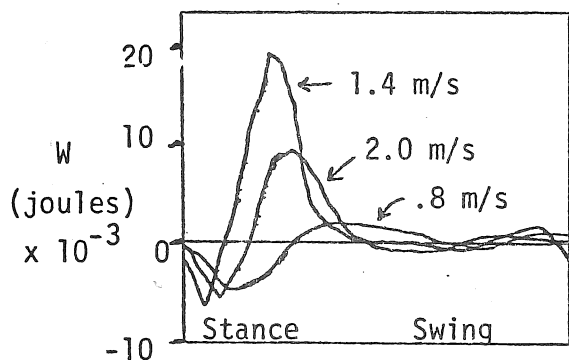


Figure 1
SOL Work at 3 speeds

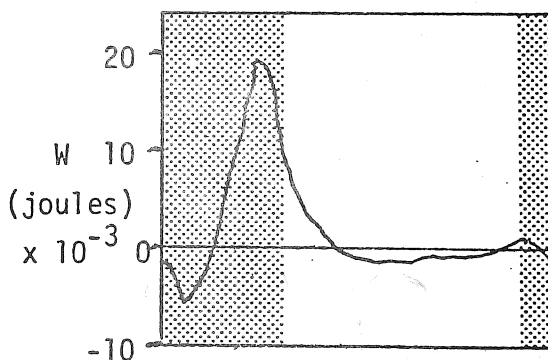


Figure 2
SOL at 1.4 m/s (shaded
area indicates muscle active)

- (1) Gregor, R.J., C.L. Hager & R.R. Roy. *In vivo* muscle forces during unrestrained locomotion. *J. Biomechanics*, 14(7):489, 1981.
- (2) Whiting, W.C., R.J. Gregor & R.R. Roy. 3-D estimates of muscle length changes during cat locomotion. *Med. Sci. Sports & Exercise*, 14(2):144-5, 1982.
- (3) Walmsley, B., J.A. Hodgson & R.E. Burke. Forces produced by medial gastrocnemius and soleus muscles during locomotion in freely moving cats. *J. Neurophysiol.*, 41:1203-1216, 1978.

ARTHROPOD JOINTS: THE BENIGN

TYRANNY OF THE EXOSKELETON

John Currey
Department of Biology
University of York
York, England

COMPARATIVE MECHANICS OF MAMMALIAN SPINES

David G. Wilder, MSME, Malcolm H. Pope, PhD, Robert Nawojchik, BS
University of Vermont, Department of Orthopaedics & Rehabilitation
Burlington, VT 05405

The purpose of this work was to analyze the spines of various mammals by comparing the size and shape of the vertebral body with the loads on the body and the normal motion of the animal. We utilized a photographic apparatus along with direct measurements to record the dimensions of the vertebral bodies in three orthogonal directions of selected mammals from the Smithsonian collection.

At least one family in each of 18 orders of mammals was measured. In addition, families of the orders Marsupialia (5 families), Primates (10 families), Odontoceti (4 families) and Artiodactyla (7 families) were measured. Loads in the caudo-cephalad and ventral-dorsal directions were computed for mammals standing erect, in a quadruped stance, and tree climbing posture where appropriate. Loads were compared to joint areas and vertebral body section properties. Several hypotheses were tested and of these the following were found significant.

The weight was proportional to the sum of the area of the facets and the end plates in the caudo-cephalad direction ($r^2 = .97$). It appeared that the area of the facets increased more as a function of weight ($r^2 = .77$) than did end plate area. The shear load was proportional to the ventral-dorsal plan area of the facets ($r^2 = .81$). Other relationships that were not significant will be discussed.

These data suggest a strong form and function relationship between the size and shape of the vertebral bodies and the animal's size and shape. Hence, if the determining factors for the shape of the vertebral bodies can be found, then models for vertebral body shape could be formulated.

THE DETERMINATION AND ANALYSIS OF COMPRESSIVE STRENGTH
CHARACTERISTICS OF SQUIRREL MONKEY VERTEBRAL BODIES

S.D. SMITH-LAGNESE AND LEON KAZARIAN
AIR FORCE AEROSPACE MEDICAL RESEARCH LABORATORY
WRIGHT-PATTERSON AIR FORCE BASE, OHIO 45433

The present effort was initiated to ascertain the rate, position, and geometry dependent strength characteristics of isolated Squirrel Monkey vertebral bodies. These results will contribute to the establishment of an interspecies scaling relationship to allow description and validation of biomechanical effects. Previous techniques utilized for insuring a uniform load distribution pattern proves to be unsuccessful for smaller specimens.

The spinal columns of eight male squirrel monkeys were dissected en masse. The vertebral bodies were separated from one another by cutting through the intervertebral disks and articular processes. All transverse and posterior elements were removed. Fifteen vertebral bodies were obtained from each spine. The remaining centra were carefully cleaned of all soft tissue. To insure consistent uniaxial compressive loading application, a Buelher Isomet was used to shave select material from the superior and inferior surfaces of the specimens. The specimens were loaded to 30% strain using an Instron screw-type test machine at 0.1, 1.0, and 2.0 in./min. displacement rates according to a pre-existing test matrix. The resultant force/displacement data were analyzed on a PDP-11/34 for strength characteristics including ultimate load, displacement to ultimate load, energy to ultimate load, stiffness, and yield effects. The results were compared to results obtained on unshaven specimens subjected to the identical test protocol.

No significant effect of shaving on the original average height of the specimens was noted. Slenderness ratio increased linearly with vertebral level.

Column position had the most obvious effect on the measured strength characteristics indicating proportional increases in ultimate load, stiffness, and yield load with position and slight increases in associated energy. The displacement data varied from no observed effect to slight decreases with increased position.

Rate effects were not as dramatic but indicated the greatest variations when comparing data having at least a one order of magnitude difference in the displacement rates. Ultimate and yield loads showed slight increases with rate, while stiffness remained relatively constant.

Comparisons to the unshaven specimen data revealed significant differences in stiffness, energy, and displacement results particularly when considering positional effects. The differences can be described by the loading mechanisms and failure patterns. Ultimate load and yield load comparisons revealed no significant differences between the test groups. In this presentation the quantitative strength parameters and variations in fracture patterns will be compared.

EFFECTS OF X-RAYS ON THE MECHANICAL PROPERTIES OF BONE

by

Harcharan Singh Ranu
Department of Biomedical Engineering
Louisiana Tech University
Ruston, Louisiana 71272

In recent years extensive use has been made of X-rays in the treatment of cancer. Currently, one of the most important problems in radiotherapy is to gain a fuller understanding of the changes induced by ionizing radiations on normal tissue. Therefore, this study was undertaken in order to evaluate the response of X-rays on the mechanical behaviour of rat's bone.

Femoral shaft of the right leg of six groups (six rats in each group) of two month old femal Sprague Dawley rats were irradiated with single exposures (1000, 2000 and 3000R) of X-rays, while the other leg was used as a control. Half the animals were sacrificed after an interval of 50 days and the other half were sacrificed after 190 days. Their femurs were carefully dissected and prepared for testing. Then a three point bending test up to fracture was carried out at physiological rate of loading in a universal testing machine. Maximum fractured load and deformation were recorded. Bone density and ash contents of both irradiated and unirradiated specimens were also measured.

The results show that the load carrying capacity of the bone decreases as the exposure increases for the both post-irradiation periods. Exhibiting a shoulder in exposure response curves. Maximum deformation also decreased with exposure. Bone density and percentage ash content also show a decrease with exposure.

Conclusions drawn from this investigation are that the strength of bone, deformation, density and ash content are all dependent on exposure and time. Similar trends have also been observed on the mechanical properties of rat, mouse and human skin when exposed to irradiation, Ranu (1975 and 1981).

Ranu, H. S. (1975) Effects of Ionizing Radiation on the Mechanical Properties of Skin. Doctoral Thesis, CNAAL, London, England.

Ranu, H. S. (1981) Radiotherapy Response of Human Skin Evaluated in Terms of Structural and Physical Characteristics. Proceedings of Third International Symposium on Bioengineering and the Skin. Philadelphia, U.S.A. (In Press).

THE INFLUENCE OF AGE ON RAT
BONE STRUCTURAL AND MATERIAL PROPERTIES†

Keller, T.S.*, Spengler, D.M.**, and Carter, D.R.***

An in vitro torsional testing procedure was used to elucidate the effect of animal age and weight on the structural, geometric, and material properties of rat femora. Sprague-Dawley rats ranging in age from 21 days to 200 days (40 to 500g) were examined. The specimens were excised immediately following sacrifice and the proximal and distal portions of the left femur were potted in methylmethacrylate, which acts as a grip for the test fixture. Rosette strain gages were bonded to the anterior surface of the femora at mid-diaphysis. The test specimens were kept moist (at room temperature) during the potting, gaging and test procedures, which require approximately 3 hours. A Burstein-Frankel torsion testing device (1) was used to conduct failure tests. The torque (T) versus angle (ϕ) curve was recorded on a storage oscilloscope and strains from the rosette gages were recorded on a strip chart recorder. Nonfailure calibration torsion tests were also performed and strains recorded.

The contralateral femur provided mid-diaphyseal cross-sections and ash weights. Total bone length (L), major (a) and minor (b) axes dimensions at mid-diaphysis were recorded. Sectional properties (Area, I_{xx} , I_{yy} , I_{xy} , $I_p = I_{xx} + I_{yy}$) are determined using a computerized numerical procedure (2). Assuming that the femora cross-sections can be approximated by a hollow ellipse of major axis (a), minor axis (b) and thickness (t), then t can be calculated such that $I_p(\text{ellipse}) = I_p(\text{true section})$. The maximum shear stress is then calculated as $\tau = T/Q$, where $Q(\text{m}^3)$ is a function of a, b, and t. The shear modulus $G = \tau/\gamma$ is determined where γ is the maximum shear strain obtained from the strain gage recordings. Nonfailure torsion tests agreed within 5% with the failure torsion tests. $K(\text{m}^4)$, a function of a, b, and t is also determined, from which section torsional stiffness, GK, can be computed.

Results indicate that changes in the structural properties of the rat femora cease at an age of approximately 110 days. From an age of 21 to 110 days the torsional strength increased 1650% and the torsional stiffness increased 1280%. The increase in structural properties was caused by both geometrical and material property changes in the bones. Over the age range examined, the shear strength of the bone tissue increased by approximately a factor of 3 and the shear modulus increased by a factor of 2. Log-log plots of T, K, and G versus bone length, animal age or weight revealed allometric relationships ($y = ax^b$) which indicate that bone geometry and material are being regulated to optimize structural properties.

(1) Burstein, A.H., and Frankel, V.H. J. Biomech. 4:155-158, 1971.

(2) Nagurka, M.L., and Hayes, W.C. J. Biomech. 13:59-64, 1980.

* VA Medical Center, Orthopaedic Research Lab, Seattle, WA 98108

** University Hospital, Dept of Orthopaedics, Seattle, WA 98195

*** Mass. General Hospital, Orthopaedic Research Laboratory, Boston, MA 02214

† Research funded by the Veterans Administration.

Mechanical Properties of Osteopetrotic Bone

R.P. Robinson (Section of Orthopedics, The Mason Clinic, Seattle, WA)

F. Vosburgh (Rockefeller University, New York, NY)

A.H. Burstein (Biomechanics Department, The Hospital for Special Surgery, New York, NY)

Introduction: Osteopetrosis is a rare inherited disorder of human bone which is clinically associated with frequent low energy transverse fractures. An abnormality in osteoclastic activity appears to prevent normal remodeling and results in a skeleton composed mainly of calcified cartilage and immature bone.¹ In order to more completely understand the mechanism of pathologic fractures in patients with osteopetrosis, bone material property specimens were made and tested to failure to determine ultimate stress and elastic modulus. Apparent density determinations and morphologic evaluations were also carried out.

Method: A postmortem formalin fixed segment of distal femoral metaphysis was obtained from a patient with osteopetrosis. Gross preliminary histologic evaluation revealed a dense homogeneous bone without a medullary canal or an outer cortical shell. After transferring the bone into normal saline, longitudinal and transverse material property specimens were milled and tested to failure in compression as described by Reilly and Burstein.² Ultimate stress, elastic modulus and apparent density were determined. Microscopic morphology in the longitudinal and transverse planes were assessed with a Zeiss MOP digitizer.

Results and Conclusions: The apparent density of osteopetrotic bone was comparable to that reported for human cortical bone ($1.80 \pm .09 \text{ gm/cm}^3$). Load versus displacement graphs revealed an elastic and brittle material. Ultimate stress and modulus of elasticity were lower than that of cortical bone ($58 \times 10^6 \pm 14 \times 10^6 \text{ N/M}^2$ and $2.1 \times 10^9 \pm 0.7 \times 10^9 \text{ N/M}^2$ respectively for longitudinal specimens). Elastic modulus was isotropic (longitudinal $2.1 \times 10^9 \pm 0.7 \times 10^9 \text{ N/M}^2$ and transverse $2.2 \times 10^9 \pm 0.6 \times 10^9 \text{ N/M}^2$, $p < .05$) while ultimate stress was not (longitudinal $58 \times 10^6 \pm 14 \times 10^6 \text{ N/M}^2$ and transverse $33.9 \times 10^6 \pm 5.0 \times 10^6 \text{ N/M}^2$, $p < .05$). More area in transverse sections was occupied by skeletal tissue than in longitudinal sections ($90.3\% \pm 3.31$ and $73.0\% \pm 4.48$ respectively, $p < .01$). A vague longitudinal orientation of tissue could be seen histologically.

Calcified cartilage and immature bone which make up the skeleton of patients with osteopetrosis combine to form a dense bone like tissue with inferior material properties than human cortical bone. This is true despite taking into account the distortion of formaline fixation. These properties can explain the frequent fractures seen in patients with this disease.

¹Shapiro, F., Glemcher, M.J., Marijke, E.H., Tashjian, A.H., Brickley-Parsons, D., Kenzora, J.E., "Human Osteopetrosis," J. Bone and Joint Surg., 62-A: 384-399, 1980.

²Reilly, D.T., Burstein, A.H., Frankel, V.H., "The Elastic Modulus for Bone," J. Biomechanics, 7: 271-275, 1974.

THE DISTRIBUTION OF TIBIAL TRABECULAR BONE PROPERTIES
AS DETERMINED BY COMPUTER ASSISTED AXIAL TOMOGRAPHY

Steven A. Goldstein, Ph.D., Larry S. Matthews, M.D., Ethan M. Braunstein, M.D.,
and Byron W. Marks, M.D.
Orthopaedic Biomechanics Laboratory and Department of Radiology, University of
Michigan, Ann Arbor, Michigan

Our early studies on the mechanical properties of trabecular bone in the human tibial metaphysis have shown that the quality of bone varies greatly with metaphyseal location; both the distance from the subchondral plate and the cross sectional location are important. These studies indicate the presence of concentrations of strength arising from the medial and lateral contact regions. While the experimental determination of ultimate stress and tangent elastic moduli provided discrete values for more precise analytical modeling, the transitional and boundary properties of these location specific parameters were still unclear. The first plane of trabecular bone and the centroids of the load bearing surfaces were identified on five fresh human cadaver tibias. With metallic markers transfixed at the defined planar points, the tibias were placed on the table of a General Electric CT/T 8800 computer assisted tomographic scanner equipped with a high resolution detector array. The proximal tibias were then scanned transversely at 5 mm intervals. A matrix of approximately 100 voxels (volume elements) was defined on each tibia which exactly corresponded to the matrix locations assigned in the previous mechanical experiments. The mean densities and standard deviations in CT numbers (-1000 = air density; + 1000 = cortical bone density) were recorded for each voxel.

Utilizing the voxel densities and locations, a relationship between the mechanical properties and CT density numbers was investigated. From linear least squared regression techniques, a statistically significant relationship between the mechanical properties measured and the CT density numbers (stratified by location) was found.

The results of the study support the concept of internal concentrations of strength distributing loads to the diaphysis. This study provides a higher resolution of specific trabecular bone property distributions. This study also indicates that high resolution CT scanning can be utilized to estimate the mechanical properties of trabecular bone and may be valuable for future investigation of interfacial properties with implants.

PHYSICS OF FLUID FLOW THROUGH CONNECTIVE TISSUES

by

V. C. Mow, E. R. Myers and W. M. Lai

Department of Mechanical Engineering,
Aeronautical Engineering & Mechanics
Rensselaer Polytechnic Institute
Troy, New York 12181

Cartilages, meniscus, tendons and ligaments are hydrated tissues. Usually, 60 to 80% of the weight of these tissues is water; the remainder is a solid matrix composed of collagen, proteoglycans, cells, and other non-specific proteins. The type and amount of collagen and its structural arrangement and the conformation of the proteoglycan macromolecules and the relative amount with respect to collagen are tissue specific, and these characteristics determine the intrinsic mechanical properties of the organic solid matrix of the tissue. However, the organic solid matrix of these tissues is porous and filled with water. Most of the interstitial fluid is free to move upon deformation or when a hydraulic pressure gradient is applied across a segment of the tissue. The interaction caused by the frictional drag of interstitial flow and matrix compaction governs the "viscoelastic" behavior of most of these connective tissues. This presentation will focus upon the phenomenon of interstitial fluid flow controlling the compressive creep and stress-relaxation behaviors of articular cartilage, nasal cartilage and meniscus. Also, because proteoglycans are polyanions which attract a high concentration of free cations within the interstitial fluid, the concentration and movement of these free counter-ions will influence the "viscoelastic" behavior of these connective tissues. We have developed a mechanochemical model which incorporates the interactions between interstitium electrolyte concentration, interstitial fluid flow and matrix deformation. These topics will be motivated by our ion-induced isometric stress-relaxation experiment. Although these concepts have been applied to only a few of the connective tissues mentioned above, the composition and structure of all connective tissues argue that such theories and experiments can also be used for various tendons and ligaments.

REGIONAL LEFT VENTRICULAR ASYNERGETICS: A QUESTION OF BALANCE
BETWEEN INTRAMYOCARDIAL AND INTRACAVITARY PRESSURE

Hani N. Sabbah and Paul D. Stein, Departments of Medicine
and Surgery, Henry Ford Hospital, Detroit, Michigan.

With the capability of altering patterns of regional left ventricular contraction by medical and surgical means, a greater understanding of the relation between the degree of myocardial ischemia and the qualitative analysis of regional contraction is currently needed. Although postulates have been presented by some investigators, the mechanics of regional left ventricular wall abnormalities are not completely understood. The purpose of this study was to investigate the relation between abnormalities of left ventricular wall thickening during systole in ischemic regions, and the interaction of left ventricular intracavitary pressure and regional intramyocardial pressure. Wall thickness was measured in 10 open-chest dogs with ultrasonic dimension gauges, left ventricular pressure, aortic pressure, and intramyocardial pressure in the subendocardium were measured with catheter-tip micromanometers. Regional ischemia was produced by occlusion of the left anterior descending coronary artery. During the control period, peak subendocardial pressure exceeded peak left ventricular pressure by 44 ± 6 mm Hg (Fig. 1). With hypokinesia, defined as a 50% to 89% reduction of systolic wall thickening, peak subendocardial pressure exceeded peak left ventricular pressure but to a lesser extent (15 ± 1 mm Hg) (Fig. 1). During akinesia, defined as a 90% to 100% reduction of systolic wall thickening, there was less than 1 mm Hg difference between peak subendocardial pressure and peak left ventricular intracavitary pressure (Fig. 1). During dyskinesia, defined as systolic thinning of the ischemic wall, peak left ventricular pressure exceeded peak subendocardial pressure by 29 ± 6 mm Hg (Fig. 1).

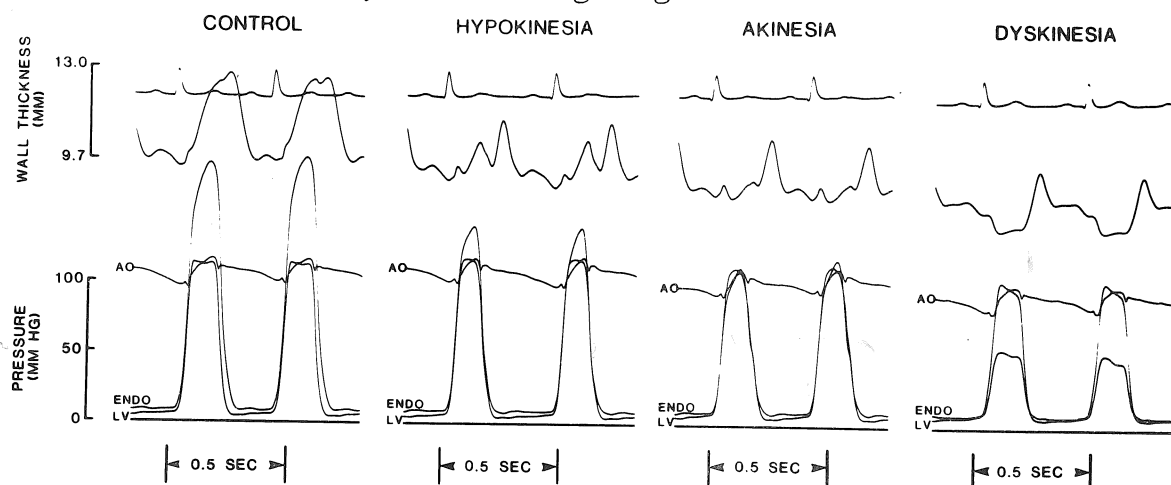


Fig. 1. AO = aortic pressure, LV = left ventricular pressure, ENDO = subendocardial pressure

These observations indicate that regional changes of left ventricular wall thickness characterized by hypokinesia, akinesia, and dyskinesia are associated with pressure gradients between the left ventricular cavity and the left ventricular wall. It appears, that regional abnormalities of systolic left ventricular wall thickening that occur during various levels of myocardial ischemia reflect regional changes of intramural forces. These changes, in turn, affect the normal direction and magnitude of the opposing forces between the ventricular cavity and the wall.

REGIONAL VARIATIONS OF INTRAMURAL PRESSURE WITHIN THE CANINE LEFT VENTRICLE

Paul D. Stein and Hani N. Sabbah, Departments of Medicine and Surgery
Henry Ford Hospital, Detroit, Michigan

Numerical analyses of left ventricular dynamics may lead to potentially useful information regarding myocardial contraction and the transmural distribution of regional stresses within the left ventricular wall. A greater understanding of regional cardiac dynamics, however, is necessary to achieve a useful model. Recent measurements of pressure within the left ventricular wall (intramyocardial pressure) may be helpful in this regard. Such measurements have been made possible by the use of modified catheter-tip micromanometers. In 26 open chest dogs, pressure within the deep subendocardial layers of the left ventricular wall during systole, 190 ± 5 mmHg, exceeded left ventricular intracavitary pressure, 134 ± 4 mmHg ($P < .001$) (Fig. 1). Systolic pressure in the superficial subepicardial layers, 100 ± 3 mmHg, was lower than intracavitary pressure. It would seem, therefore, that a gradient of pressure exists across the left ventricular wall during systole. During diastole (18 open chest dogs) a pressure gradient was also observed across the left ventricular wall; but the direction of the gradient was opposite to that of the systolic gradient. During diastole, pressure was highest in the subepicardium, 26 ± 1 mmHg, lower in the subendocardium, 14 ± 1 mmHg, and lowest within the left ventricular cavity (Fig. 1). These values in the beating intact heart differed in magnitude and direction from the gradient of intramural pressure observed in arrested passively distended heart. Passive distention of the arrested heart failed to produce a higher pressure in the subepicardium, such as was observed in the functioning heart during diastole. These observations suggest dynamic effects within the left ventricular wall during diastole, which perhaps may represent diastolic tone, and which are not predicted on the basis of the characteristics of passively distended tissue. Finally, systolic pressure within the papillary muscle of 12 open chest dogs, 348 ± 25 mmHg, was higher than either within the subendocardium or subepicardium.

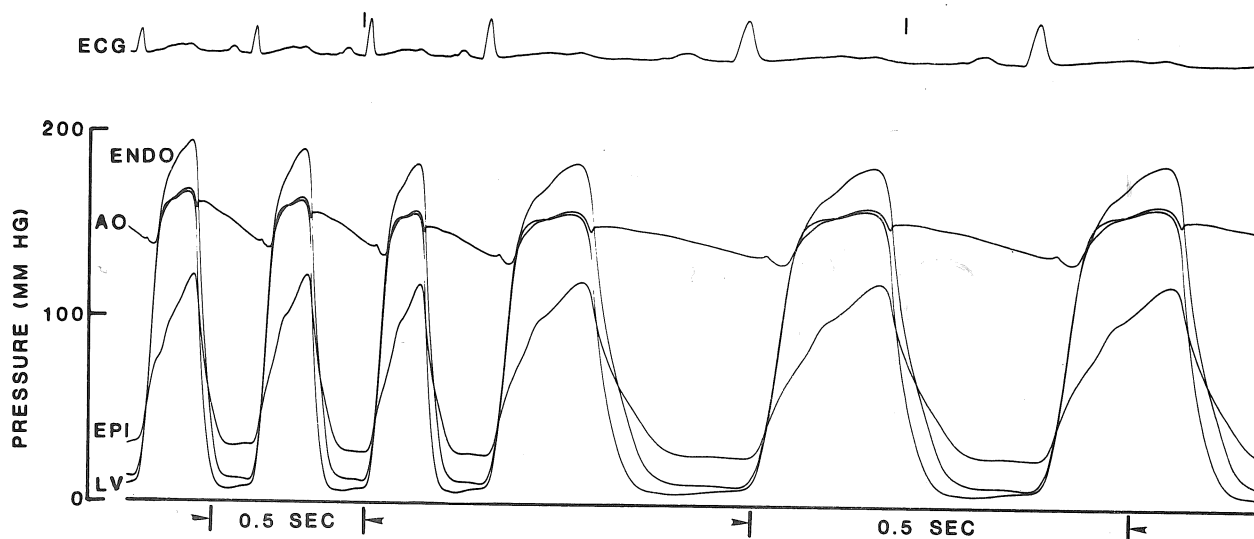


Fig. 1. AO = aortic pressure, LV = left ventricular pressure, ENDO = subendocardial pressure, EPI = subepicardial pressure

These observations suggest a nonuniformity of contraction across the left ventricular wall which should be considered when numerical analyses of left ventricular mechanics is attempted.

THE TWO-BURST PATTERN REVISITED

M.H. Sherif*, R.J. Gregor**, L.M. Liu***, R.R. Roy**, and C.L. Hager**

*Brain Research Institute, University of California, Los Angeles, CA 90024

**Department of Kinesiology, University of California, Los Angeles, CA 90024

***Department of Quantitative Methods, University of Illinois, Chicago, IL 60680

The two-burst pattern of myoelectric activity has been observed in many instances. For example, the ankle, knee and hip extensors of the cat exhibit two-distinct bursts of activity during treadmill locomotion.¹ Some results in the literature suggest that forces generated during early stance (i.e. just after foot contact) depend greatly on the muscle state during late swing.² To test this hypothesis, a tendon "buckle-transducer"³ was used to measure the medial gastrocnemius force from a cat during unrestrained treadmill locomotion. Myoelectric signals were also collected with wire electrodes. An intervention analysis⁴ was performed to correlate myoelectric activity to force output.

Results indicate that the total force output is the sum of two components. The first--and major--part depends on activity which precedes the movement by 35-80 msecs. The second part is depicted by a second order response and is not significantly correlated with the force. The first burst seems to be responsible for setting muscle stiffness prior to ground contact. The second burst could be attributed to local muscle properties (e.g. actin-myosin binding and calcium uptake). It is conceivable then, that the pause between the two volleys is due to a switching from a predominantly central neuro control to a control at the muscle level. In any event, this work demonstrates that mechanical performance cannot be always related to the concomitant myoelectric activity.

References

1. Engberg, I. and Lundberg, A. (1969). "An electromyographic analysis of muscular activity in the hindlimb of the cat during unrestrained locomotion," Acta Physiol. Scand. 75, 614-630.
2. Grillner, S. (1972). "The Role of muscle stiffness in meeting the changing postural and locomotor requirements for force development by the ankle extensors," Acta Physiol. Scand. 86:92-108.
3. Gregor, R.J., Hager, C.L., Roy, R.R., and Whiting, W.C. (1981) "In-vivo force velocity characteristics of fast ankle extensors in the cat hind limb," Med. Science Sports Exerc. 13, 128.
4. Box, G.E.P. and Tiao, G.C. (1975). "Intervention analysis with applications to economic and environmental problems," J. Amer. Statist. Assoc. 70, 70-79.

Funding: NIH Grant NS 16333-03 and a grant from the College of Business Administration at the University of Illinois at Chicago.

ACOUSTIC EMISSION: A NON-INVASIVE MONITORING TECHNIQUE FOR TOTAL JOINT REPLACEMENT PATIENTS

T.M. Wright, D.L. Bartel and A.H. Burstein, The Hospital for Special Surgery (Affiliated with New York Hospital-Cornell University Medical College)

Total joint replacement of diseased and damaged joints is successful in relieving pain and restoring function. Complications do exist, however, and are often associated with mechanical damage (e.g., loosening and fracture). The need exists for a technique to detect such damage at its earliest stage.

Acoustic emission (AE) is a proven method for nondestructive monitoring of loaded structures. It involves the detection of stress waves emanating from sources of mechanical damage. AE signals, together with knowledge of the applied loads, can be used to determine the onset of damage, the damage source location, and, in some cases, the damage mechanism itself. AE monitoring of total joint replacement patients provides a non-invasive method for detecting damage which is easy to perform and of minimum risk to the patient. Development of AE monitoring has involved work in three areas: in-vivo monitoring of patients, determination of soft tissue attenuation characteristics of AE signals, and in-vitro experiments to identify the AE characteristics of specific damage mechanisms.

In-vivo monitoring has centered on total knee patients. To date, 125 total knee joints in 89 patients have been monitored using conventional AE equipment. The results have shown excellent agreement between the AE characteristics (measured while loading the joint) and the clinical diagnosis based on patient symptoms and radiographic findings.

AE monitoring of total knee patients is aided by the fact that the AE transducer is placed over the tibia with little soft tissue interposed. To apply the same technique to total hip patients requires understanding of the soft tissue attenuation of acoustic emission. A clamp was designed by which two transducers (one emitting and the other receiving an AE pulse) were placed in opposition with varying amounts of soft tissue interposed. The results of tests on volunteers show that AE waveform characteristics such as peak amplitude and energy are attenuated exponentially with soft tissue thickness. The attenuation coefficient for amplitude ranged between 0.32 and 0.45 in^{-1} (depending on frequency) and for energy varied between 0.53 and 0.81 in^{-1} (corresponding to thicknesses of 4 and 5 cm to attenuate by one half the energy and the amplitude, respectively). Though such data do not preclude the use of AE monitoring in total hip patients, they must be accounted for in using waveform characteristics to identify damage mechanisms.

Identification of specific damage mechanisms from patient monitoring is the most promising capability of acoustic emission. Development of this capability has involved stress analysis and in-vitro experimentation. Stress analysis has been done on simple models to find load and boundary conditions for which the initiation and location of damage can be controlled. An analysis of an axially loaded stem cemented into a hollow cylinder has been promising in this regard. In-vitro experiments have been conducted using cadaver tibias with total knee components implanted. The tibias were loaded in a materials testing system and the load recorded along with AE characteristics from a transducer attached to the tibia. Test results were similar to in-vivo monitoring in terms of the acoustic emission characteristics. Of interest is the fact that significant damage was recorded without any accompanying discontinuity in the load-displacement curves.

This research was supported by NIH Grant No. AM 26211 and by a grant from the Clark Foundation.

THE ANALYSIS OF POSITION AND MOTION

Edward S. Grood
Sports Medicine Institute
Department of Orthopedic Surgery
University of Cincinnati
Cincinnati, OH

Jesus Dapena
Department of Exercise Science
University of Massachusetts
Amherst, MA

Segment Interaction during the Swing Phases of Walking and Running

C.A. Putnam, Dalhousie University, Halifax, Nova Scotia

The patterns of motion of the lower extremity segments during the swing phases of walking and running are functions of the resultant joint moments acting on each segment and the interaction between adjacent segments. The purpose of this study was to examine the interaction between the thigh and shank during the swing phase of gait and to compare the influence of the segment interaction on the motion of the lower extremity segments with that of the resultant joint moments. The recovery phases of the thigh and shank were broken into two parts. For each segment these included the initial positive angular acceleration phase (PAAT and PAAS for the thigh and shank, respectively) and the remaining negative angular acceleration phase (NAAT and NAAS for the thigh and shank, respectively), where positive is in the direction of hip flexion and knee extension. PAAT occurred during the first 20% of the swing phase of walking and the first 30% of the swing phase of running, while PAAS occurred during the first 60% of the swing phase of both walking and running. The segment interaction during these phases was quantified in terms of the moments of the resultant joint forces expressed as functions of the linear acceleration of the hip, the angular velocity and acceleration of the thigh and shank and the segment weights.

It was found that the relative influences of the segment interaction and the resultant joint moments on the thigh and shank motions were very similar, in many respects, for walking and running. During PAAS, the shank was angularly accelerated primarily by the resultant knee moment and the interactive moments associated with the thigh angular velocity and the segment weights, with the latter having the greatest effect of these three factors. During NAAS, the resultant knee moment had by far the greatest influence on the angular acceleration of the shank. During walking only, the interactive moments associated with the segment weights, angular acceleration of the thigh and linear acceleration of the hip all had some influence on the angular acceleration of the shank but in each case, it was considerably smaller than that due to the resultant knee moment. The resultant hip moment plus interactive moments associated with the segment weights and, for running only, the hip linear acceleration played major roles in angularly accelerating the thigh during PAAT. The interactive moments associated with the angular acceleration of the thigh and shank were also very large during this phase but tended to angularly accelerate the thigh in the negative direction. Finally, during the NAAT, the resultant hip moment and interactive moments associated with the segment weights, angular velocity of the shank and the linear acceleration of the hip all played important roles in angularly accelerating the thigh in the negative direction, while the interactive moments associated with the angular acceleration of the thigh and particularly the angular acceleration of the shank played large roles in countering these effects, tending to accelerate the thigh in the positive direction.

To summarize the factors influencing the thigh and shank motions for both walking and running, the resultant knee moment was not nearly as important as the interactive moments in angularly accelerating the shank in the positive direction during the initial part of the swing phase, but was considerably more important than the interactive moments in negatively accelerating the shank during the latter part of the swing phase. The resultant hip moment played an important role in angularly accelerating the thigh throughout the swing phase and often worked in opposition to the interactive moments.

LINEARIZED APPROXIMATIONS FOR THE SIMULATION
OF SWING LEG MOTION DURING GAIT

W.H. Lee and J.M. Mansour*

Department of Orthopaedic Surgery,
Children's Hospital Medical Center and
Harvard Medical School, Boston, MA 02115

Numerous techniques, based on mechanical analyses, have been employed to study human gait. The simulation of human gait is one such technique. Simulating gait is a potentially valuable tool since it yields a cause and effect relationship between a change in an input variable, such as a joint moment, and the output which is the limb kinematics. The equations of motion needed to perform a simulation of human gait are nonlinear. Depending on the number of degrees of freedom to be modeled these equations can become quite complex. Thus, simulating human gait can require sophisticated computer software and hardware.

The purpose of this investigation was to evaluate the validity of simplified linear systems approximations for nonlinear swing leg motion during gait. If a linearization was found to be valid it was then employed to systematically analyze the interdependency of the state variables and controls.

Exact, nonlinear equations of motion for the swing leg moving with a specified hip trajectory were previously developed using a Lagrangian formulation (1). Two different linearizations were developed. A linear time varying (LTV) approximation was developed by linearizing about a set of nominal displacement, velocity, acceleration and control trajectories. Three linear time invariant (LTI) approximations were developed by linearizing about fixed limb positions (see Fig. 1): 1) $\theta = \phi = 0, \psi = \frac{\pi}{2}$, 2) $\theta = \phi = \psi = 0$ and 3) the joint angles at heel strike.

Overall, simulations performed with the LTV systems yielded a closer approximation to the exact nonlinear system simulations of subject motion than the LTI system simulations. Using the LTV system, the initial angular velocity of the thigh was found to be an important determinant of normal swing leg motion as was shown previously using the nonlinear system. The sensitivity of the foot to system perturbations, as noted with the nonlinear system, was also apparent in the LTV case but to a far greater extent. In contrast, the LTI simulations yielded limb trajectories with greater deviations from the nominal than the LTV simulations. Since the LTI system was unable to adequately reproduce the nominal trajectories, no further study of the LTI case was pursued.

The results of this study suggest that the LTI approximation will yield an accurate representation of the exact swing leg dynamics for small perturbations of the system from the nominal trajectories. Thus, the well developed methods of linear systems analysis may be applied to study the swing phase of human gait.

References:

1. Mena, D., Mansour, J.M. and Simon, S.R. (1981) Analysis and synthesis of human swing leg motion during gait and its clinical application. *J. Biomechanics*, 14, 12, 823-832.

*Current address: Dept. of Mechanical and Aerospace Engineering, Case Western Reserve University, Cleveland, Ohio 44106

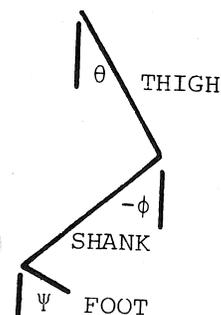


FIG. 1

MECHANICS OF ORIENTATION IN SEA PENS: A ROTATIONAL ONE LINK JOINT

Barbara A. Best
Department of Zoology
Duke University
Durham, NC 27706

Passive filter-feeding invertebrates depend on ambient water movements for feeding and exhibit a wide diversity of morphologies and habitat distributions in response to the predictability and amplitude of current conditions. Organisms exposed to predictable uni- or bi-directional flow may assume a fixed rigid body orientation to facilitate the processing of water. To utilize unpredictable, multi-directional flow, some animals are radially symmetrical, while others have means of adjusting their orientation to suit the varying conditions.

This study reports on one form of invertebrate orientation by use of a rotating joint system. The ability to orient in the filter-feeding sea pen, Ptilosarcus gurneyi (Coelenterata: Pennatulacea), is examined with particular emphasis on the mechanics of orientation, the fluid dynamics of the system, and the biomechanical properties of the structural elements. Ptilosarcus passively maintains a perpendicular orientation to the flow, stabilized in this position by drag forces acting upon the bilaterally symmetric filter. A calcified axial rod functions as the axis of rotation and constitutes a one link joint which allows rotation of the body without bending. The geometry of the body wall delineates the 'joint'; presence of a constriction determines the point of rotation by maximizing torsional stresses.

Three basic functions can be ascribed to joints in general: 1) transfer loads, 2) allow relative movement of the elements, and 3) determine the direction of movement, i.e. the degrees of freedom. The role of both the axial rod and the body wall in each of these three functions are discussed for individuals of various sizes, from 2cm to 60cm in length. Both the geometry and the material properties of the joint elements change in response to increasing drag forces as the organism grows. Field recordings of the ambient currents indicate continuous small-scale deviations in current directions, superimposed on a large-scale bi-directional tidal flow. Under these conditions, a passively rotating joint increases the volume flow rate of water through the filter, thus enhancing feeding.

H. KUROSAWA, M.D., & P.S. WALKER, PH.D.
 Orthopedic Biomechanics, Brigham & Women's Hospital,
 Boston, & V.A. Medical Center, West Roxbury: Affiliated
 with Harvard Medical School.

Several methods have been used to describe knee motion: planar instant centers of rotation, instant centers of the medial and lateral sides, instant axes of rotation, the screw axis, and Eulerian angles. Two dimensional analysis inadequately describes the variation rotations and translations. The other methods sometimes produce erratic results, are difficult to interpret, and difficult to relate to anatomical landmarks. We attempted a simple description which would give a pictorial visualization and which could be applied to internal and external prosthesis design.

The Concept From previous and present studies, it was found that the posterior femoral condyles could be modelled as parts of spheres, and the tibial surfaces as flat, to good accuracy. The line joining the centers is considered as the axis of the knee. Thus, tracking the motion of this axis with respect to the tibial surfaces, as a function of flexion, describes the motion of the knee. The model is shown in Figure 1.

Results Fourteen fresh knees were sequentially radiographed using a similar rig to Harding et al. (J. Biomech., 10: 517, 1977), where the quadriceps was loaded. Seven volunteers were video-x-rayed in the action of climbing a step. From digital input of the tibial axes and the curves of the posterior femoral condyles, a computer program determined various angles. The specimen results were as follows. From 0° to 120° flexion, the medial condyles center moved anteriorly 4.5 ± 2.2 mm, and the lateral center moved posteriorly 17.0 ± 5.5 mm. Total transverse rotation was 20.2 ± 6.0 degrees, $d(\text{tr. rot.})/d(\text{flexion})$ decreasing with flexion. Adduction was $4.3^\circ \pm 2.1^\circ$. The results from the volunteers was similar but with less transverse rotation. The average specimen results were plotted using computer graphics (Figure 2). The transverse tibial axis is parallel to the two posterior condyles. It is noted that when the axis is projected beyond the medial and lateral boundaries, the medial motion is distinctly anterior with flexion and the lateral motion distinctly posterior.

H. Kurosawa is visiting from University of Tokyo. We thank A. Garg for computer programming and Howmedica, Inc. for computer equipment.

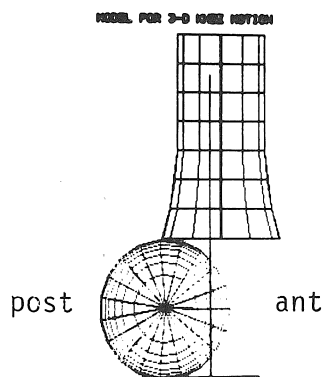


FIGURE 1

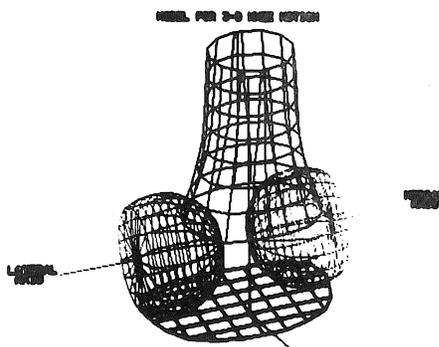
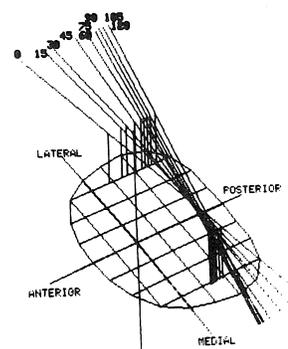


FIGURE 2



Evaluation of Data Smoothing Techniques for Biomechanical Data

R.J. Bentham, Dalhousie University, Halifax, N.S.

A study was undertaken to determine the effectiveness of various smoothing techniques on biomechanical data taken from Pezzack(1977), Lanshammar(1982), and Vaughan(1980). That of Pezzack were derived from angular motion of an aluminum arm moved by wrist abduction and adduction. Lanshammar added pseudo random white noise to Pezzack's data, while Vaughan's data was derived by digitizing a ball dropped freely through space.

In the present study, displacement-time data were smoothed by digital filtering, natural cubic splines, and quintic splines. In addition, another technique, not commonly employed, was investigated. This involved applying first order finite differences to the raw displacement-time data to arrive at acceleration. This raw acceleration data were then smoothed with the aforementioned techniques. Each technique was judged according to its ability to precisely match the known acceleration curves of the test data.

Each smoothing technique gave similar results when applied to Pezzack's data as well as when applied to Lanshammar's data. Only the quintic spline smoothed the ball drop data accurately. The natural cubic spline's property of forcing the second derivative to zero at the endpoints introduced problems for all data sets. For the ball drop data, it was noted that thirteen (at the beginning) to eighteen (at the end) endpoints were deflected from the true acceleration curve. With Pezzack's and Lanshammar's data only the three points nearest the endpoints were affected. In all cases, the endpoint problems associated with the cubic spline could be eliminated by linear extrapolation of a sufficient number of points. With digital filtering, Vaughan's data required a great deal of oversmoothing to keep the last 7 to 10 points from peaking unrealistically. Extrapolating the data did not seem to correct this problem. Some endpoint problems were also associated with the technique of smoothing raw acceleration-time data.

The task of choosing the "best" smoothing factor with each technique has usually been a solely qualitative process. An effort was made to overcome this limitation. Based on the assumption that the noise in the raw data was random and normally distributed, probability plot correlation coefficient tests for normality were applied to the raw versus residual data. Oversmoothing was evidenced by a significant deviation of the residuals from the normality. Problems are still encountered with this technique, particularly in deciding what constitutes the minimum acceptable level of normality in the residuals.

A TRIPLE PENDULUM MODEL OF THE GOLF SWING

Kevin R. Campbell, Biomechanics Research Lab, University of Illinois, Urbana, Illinois 61801.

In the analysis of the dynamics of the golf drive, researchers have often employed a double pendulum model of the swing. Although this model has provided useful information concerning the relationships between the arms, club and wrist dynamics, no information has been gained with regard to shoulder and upper body motion during the golf swing. In this study, a triple pendulum model of the golf swing was developed to investigate the kinetics of the shoulders, arms and club segments in the golf drive as described in modern golf theory.

The upper level of this model, the shoulders, was fixed to rotate about its midpoint and was represented by the upper torso segment of Hanavan (1964). The middle or second link was the left arm which was hinged at the shoulder. The lower link of the triple pendulum was the club which rotated about a hinge at the wrist. The right arm serves mainly in a stabilizing capacity at the top of the backswing and is assumed to be relatively passive in the down swing and therefore is not included in this model. The main contribution of the right arm in striking the golf ball is providing a torque at the wrist to aid in extension near impact. This torque was incorporated into the net torque between segment two and three of the model. The triple pendulum model had three degrees of freedom and its configuration was completely described by the generalized coordinates which were defined by the angle each link made with a vertical reference. The Lagrangean method was employed to determine the equations of motion for the model.

Four highly skilled golfers (mean handicap of 1.25) served as subjects. High speed cinematography was employed to obtain continuous displacement measures of the generalized coordinates. These data were then treated with a cubic spline to obtain the smoothed displacement, velocity and acceleration functions. This data was then input into the equations of motion to determine the torque on each segment. The instantaneous power flow due to the generalized forces (torques) was then determined. It was then possible to determine the mechanical work of the total system and of each torque by integrating the instantaneous power functions.

For all subjects, peak clubhead velocity ($V=45.666$ M/S) was achieved before impact (0.01582s), the average clubhead velocity at impact was 44.462 m/s. The maximum torque on the upper-torso segment ($T_1=118.88$ NM) occurred at an average time of .1467 seconds before impact. The average time before impact for the peak shoulder torque ($T_2=75.17$ NM) was .1375 seconds. The peak wrist torques ($T_3=30.46$ NM) occurred later in the swing with an average time interval of .1322 seconds to impact. The average percent work done by the upper-torso, shoulder and wrist torques were 62.44, 11.69 and 25.87 respectively. In all cases, the power flow due to the wrist torque increased as the power due to the other generalized forces became negative. This indicates a transfer of energy to the third segment as the velocity of the upper segments decreased. The results of this study indicate that the proposed triple pendulum model is an appropriate model for analyzing the golf swing.

SPEED-CORRELATED CHANGES IN LIMB ORIENTATION, STRIDE FREQUENCY AND
MOVEMENT COMPONENTS IN A GENERALIZED LIZARD.

J.A. Peterson, Department of Biology, University of California, Los Angeles

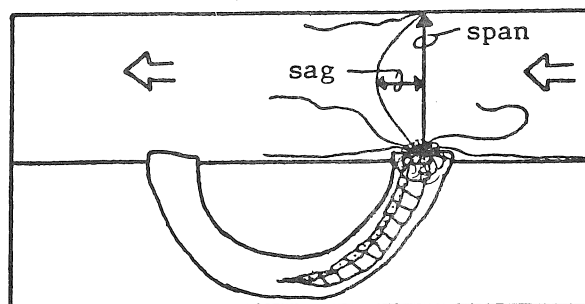
Generalized lizards, such as Dipsosaurus dorsalis, can use a wide range of speeds (from less than 10cm/sec to 600cm/sec for an animal of 60-70gms and 10-11cm body length). Stride frequency and stride length reach 12Hz and 4.8 body lengths, respectively. At the highest speeds the duration of hindlimb contact may be only 18msec (14% of the stride time). Unlike cursorial mammals, Dipsosaurus achieves high speeds with a single gait or rhythm of limb movement. Analysis of high speed cine films of locomotion on a treadmill shows that the behavioral strategy for increasing speed differs significantly from that of cursorial mammals. An increase in hindlimb step length from .45 cm to 1.1cm correlates with an increase in the excursion arc of the limb coupled with a decrease in the effect of undulatory excursion and with a threefold increase in the effective length of the hindlimb (from 20mm to 60mm). The increase in effective limb length is achieved i) as the limb shifts from a sprawling orientation, in which the humerus and femur operate close to the horizontal plane, to a nearly vertical, more mammal-like orientation, and ii) as the knee/elbow and wrist/ankle joints adopt more extended positions (the latter is associated with the transition from plantigrady to digitigrady). The changes in limb orientation occur gradually and those in the forelimb occur at lower speeds. At the highest speeds Dipsosaurus runs bipedally. The contribution of lateral undulation and knee/elbow extension to step length decreases as the limb becomes more vertical. At higher speeds excursion of the humerus and femur in or near the sagittal plane becomes the most significant component of step length. Essentially, Dipsosaurus shifts from "reptilian, sprawling posture" into more mammal-like limb orientation and excursion as speed increases. The behavioral strategy for increasing speed in Dipsosaurus emphasizes changes in the effective length of the limb and in the types of excursion, rather than a change in gait.

Amy S. Johnson, Department of Zoology, U.C. Berkeley, Berkeley, CA 94724
 "Coping with stress and strain: the mechanics of feeding with extensible tentacles (Eupolytmnia heterobranchia)"

Sedentary marine invertebrates, such as the terebellid polychaete worm Eupolytmnia heterobranchia, are limited by their immobility in the ways that they can capture and retain food. E. heterobranchia lives in U-shaped tubes on mud-flats and feeds by means of tentacles that can be extended over the surface of the substratum or into the water column. In either case, the longer the tentacles, the greater the access to food resources. Extension of the tentacles requires stretching the material of the tentacles. One way that terebellid worms can exert the force required to extend their tentacles along the surface of the substratum is by means of cilia located in a food groove on the ventral surface of the tentacles. The results of this study indicate that these worms can decrease the force required to pull a tentacle to any given extension by extending the tentacle, pausing and allowing relaxation to occur, and then pulling to that extension. This means that terebellids can pull their tentacles to greater lengths before reaching a critical breaking stress than they could if they did not exhibit this type of stop and start behavior.

E. heterobranchia that extend their tentacles into the water column expose the tentacles to drag forces. One way that the worm suspends its tentacles into water flow is with the tentacle attached at two points along its length, similar to the cables of suspension bridges. From standard engineering equations for the force acting on the cables of suspension bridges, it can be seen that stress (or the force per cross-sectional area) is proportional to the drag, and it might therefore be expected that the stress would increase as water velocity increases. However, the results from experiments done in a flow tank indicate that the stress remains relatively constant over the range of velocities that the tentacles would remain suspended, with the mean value of stress around 0.02 MN/m^2 . From tensometer experiments, the mean breaking stress of these tentacles was found to be around 0.04 MN/m^2 , so that it appears as if the stress may be regulated below the breaking stress. From these same engineering equations it can be seen that the stress in the tentacles should also be proportional to the ratio of the span distance between the points of attachment to the sag of the tentacle (Figure 1). Calculations from the changes in span and sag of a tentacle that occur as the tentacle is exposed to a range of velocity indicate that the span-to-sag ratio decreases as velocity increases. This means that for a given span, the sag of a tentacle will increase as velocity increases. The stress in the tentacles can be regulated by the worms by either changing the sag of the tentacles (perhaps by muscular contraction) or by changing the length of span exposed to flow by changing the points of attachment. It would be expected that at some velocity terebellids could not maintain tentacles in water flow without breaking. Since there is greater suspended matter in the water column at high flow velocities, it would be predicted that greater suspension feeding behavior with tentacles extended into flow should occur as a function of velocity, up to the point at which the benefits of feeding from flow are outweighed by the risks of breakage due to drag forces. At very high velocities terebellids would be expected to feed only from the surface of the substratum.

Figure 1: Span and sag are the distances shown in the adjacent sketch of a suspended tentacle of Eupolytmnia heterobranchia. The \leftarrow indicates the direction of water flow.



MECHANICAL PROPERTIES OF HUMAN NECK/TORSO SKIN AND VESSEL REPLICATIONS
by W. Goldsmith and L. J. Frankel, Dept. Mech. Engin., Univ. Calif., Berkeley

Human impact response can be analyzed from kinematic, stress and deformation data of the components of an appropriate physical model subjected to dynamic loads (1). A major problem here is the use of soft tissue replications with correct mechanical properties. In general, the quasi-static stress-strain behavior of *in vitro* human soft tissue is bilinear with a concave-upward knee whose location along the strain axis is determined by the ratio and arrangement of collagen and elastin; all such tissues are under tension in the relaxed state. Proper model response demands embodiment of the correct initial *in situ* load to correctly place this knee; this has been carried out for muscle, tendon and ligament replicas in the neck and upper torso area (2).

Skin and major arteries should be added to ascertain the effect on model response and blood flow, respectively, due to dynamic loading. A suitable substitute must have a stress-strain curve close to that of the prototype. After much experimentation, a double knit synthetic skin of 85 % Fortral polyester and 15 % wool provided good correspondence with cited human mechanical properties (3). Fig. 1 shows the stress-strain curve for this material in and transverse to the direction of the fibers, as well as longitudinal and transverse data on human thoracic tissue. For an applied prestrain of the human tissue of about 30 %, agreement between the curves is satisfactory. Prototype and model material are both stiffer in the cross direction. The ultimate tensile strength and elongation of the material corresponded closely with cited averages of 12.9-14.4 MPa and about 90 %, respectively, for the human cervical and thoracic regions (3). The material also exhibits suitable viscoelastic characteristics, with stabilized hysteresis loops after a few cycles.

Fig. 2 presents a comparison of the stress-strain curve of the carotid artery (3) and woven Veri-Soft (8 mm dia) and knitted Cooley Dacron (10 mm dia) Meadox Medical Co. grafts. There is a large region of strain for a very small change in load for the grafts, with a stiffer domain entered only at 125-150 % elongation. To correspond, the graft must be first tensioned by 50-60 % and then further strained by 20 % for the preload upon inclusion in a model. The presence of both skin and arteries in a head/neck/upper torso model and dynamic testing with impact energies up to 7 J, applied to both head and base showed no significant danger of blood vessel damage, but requires a careful regimen of synthetic skin attachment to avoid anomalies in the structural behavior of the model (4).

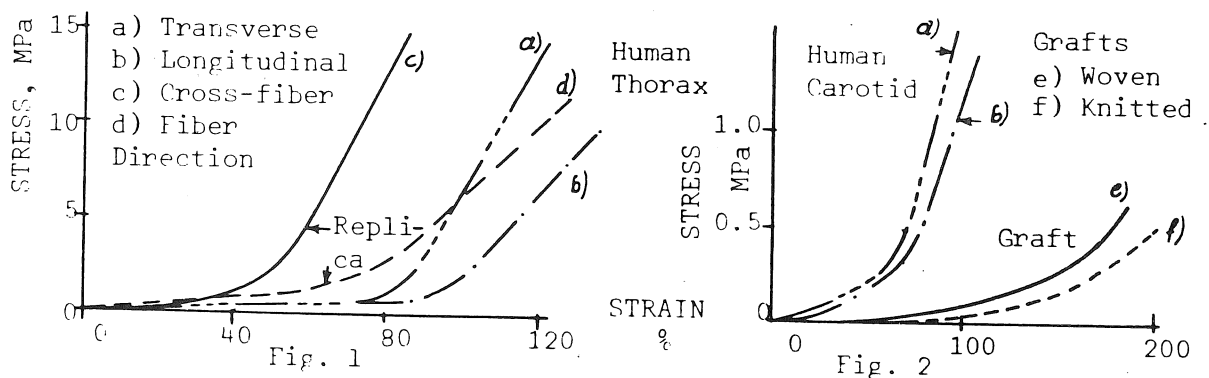
(1) J. M. Kabo, Response of a Head-Neck System to Saggital Plane Loading, Dissertation (Ph.D.), Univ. of California, Berkeley, 1980.

(2) J. M. Winters, Mechanical Response of an Advanced Head-Neck System to Transient Loading, Thesis (M.S.), Univ. of California, Berkeley, 1980.

(3) H. Yamada. Strength of Biological Materials. Williams/Wilkins, 1970.

(4) L. J. Frankel, Three-Dimension Response of a Humanoid Head-Neck System to Dynamic Loading, Thesis (M.S.), Univ. of California, Berkeley, 1981.

Work supported by the National Institutes of Health under Grant 5R01AM 18284.



Mechanical Properties of the Liverpool Artery:

I. Uniaxial Properties

T.V.How, R.M.Clarke, D.Annis, Bioengineering and Medical Physics Unit,
University of Liverpool, P.O.Box 147,
Liverpool L69 3BX, England.

Most commercially available synthetic grafts are made from PTFE and PET which are relatively inextensible polymers. The failure rate of these grafts of diameter less than 6mm is high and has been associated with their high circumferential stiffness (1,2). This has led to the suggestion that the failure of these grafts may be the result, in part, of a mismatch in compliance between the graft and the natural artery to which it is attached.

There is a clinical need for the design and development of a small diameter graft with compliant walls. An electrostatic process has been developed, at Liverpool, for producing microfibrinous grafts from a polyurethane elastomer (3). The grafts are anisotropic as a result of their structure, which may be described as a layered two-dimensional fibre network. By controlling the process variables it is possible to alter the structure and consequently, the mechanical properties of the graft.

Uniaxial stress-strain and stress relaxation tests were carried out on standardized dumb-bell shaped specimens obtained from 10mm I.D. grafts. The electrostatic process was characterized by investigating the effect of the process variables on the tensile properties. The results are compared with published data on the properties of the natural arteries and other vascular prostheses.

The initial tensile moduli of the Liverpool graft were dependent on the manufacturing variables and the values ranged from 1.03×10^6 to $1.85 \times 10^6 \text{ Nm}^{-2}$ in the circumferential direction (E_{θ}) and from 1.33 to $2.23 \times 10^6 \text{ Nm}^{-2}$ in the longitudinal direction (E_z). It was possible to control the ratio E_{θ} / E_z between 0.53 and 1.39.

The graft was relatively insensitive to strain rates over the range of 0.14/min. to 2.22/min. There was no significant difference between the relaxation patterns of circumferential and longitudinal specimens. This suggests that the viscoelastic properties were a function of the elastomeric material and did not depend upon the fibre distribution in the graft.

The results show that grafts may be produced with a wide range of mechanical properties. It is therefore possible to design and manufacture grafts with compliance similar to that of the natural artery.

References

1. Kidson, I.G., and Abbot, W.M., 1978, Cardiovascular Surgery, 58, Suppl., Circulation II - I4.
2. Walden, R., L'Italien, G.J., Megerman, J., Abbot, W.M., 1980, Arch.Surg. 115, 1166.
3. Annis, D., Bornat, A., Edwards, R.O., Higham, A., Loveday, B., Wilson, J., 1978, Trans.Am.Soc.Artif.Intern.Organs 24, 209.

Mechanical Properties of the Liverpool Artery:II Multi-axial properties

R.M. Clarke, T.V. How, Bioengineering and Medical Physics Unit, University of Liverpool, P.O. Box 147, Liverpool L69 3BX, England

The three-dimensional static elastic properties of the Liverpool artificial artery have been studied by a series of experiments on cylindrical segments. A mathematical model for the material has been derived. The model expresses the strain energy function of the material as a polynomial in the principal strains. The model assumes the artificial artery to be homogeneous, incompressible and orthotropic. Both thin and thick-wall derivations of stresses have been evaluated for use in the model. The model is based upon one used by Patel and Vaishnav (1972) to characterize the properties of natural arteries.

Data from the experiments are used to derive the constants of the constitutive equation. The correlation between measured and predicted response to load is good. The model therefore provides a means of predicting the behaviour of an artificial artery with known unstressed dimensions under a given set of loading conditions, in particular those encountered in the living vascular system. This allows the design of an artificial artery whose mechanical properties closely match those of the natural artery. By manipulating conditions of manufacture accordingly, it is possible to produce an artificial artery with the desired mechanical properties.

Ref. Patel, D.J. and Vaishnav, R.N., "The rheology of large blood vessels", in "Cardiovascular Fluid Dynamics" Vol. II, Bergel, D.H. (ed.) Academic Press, pp.1-64.

MECHANICAL PROPERTIES OF CEPHALOPOD ARTERIES

Robert Shadwick and John Gosline, University of British Columbia, Vancouver, B.C., CANADA.

The mechanical properties of the systemic aortae of six cephalopod molluscs, Nautilus pompilius, Nototodarus sloani, Loligo opalescens, Ilex ilecebrosus, Sepia latimanus and Octopus dofleini were investigated by in vitro inflations of isolated arterial segments. As expected, all aortae exhibit non-linear, "J-shaped" stress-extension curves and all are highly extensible in the circumferential direction. Differences in the longitudinal extensibility appear to be correlated with specific features of the connective tissue architecture. In the squids Nototodarus, Ilex and Loligo, and to a lesser extent in Sepia and Octopus, the arteries are reinforced longitudinally by a relatively thick layer of longitudinally oriented elastic fibres. These fibres are composed of a protein-rubber which is chemically and mechanically distinct from the vertebrate protein-rubber elastin.

Analysis of the form of the incremental wall stiffness data for the cephalopod arteries indicates that the in vivo blood pressures for Nautilus and Octopus fall in the range of 20 to 60 cm H₂O, and this is in agreement with measured values for these species. A similar analysis suggests that the blood pressure in the squids are higher, about 100 to 200 cm H₂O. Although direct measurements for these animals are not yet available, squids undoubtedly require a high pressure circulatory system to support the very rapid aerobic locomotion of which they are capable.

Pulse wave velocities, calculated from vessel wall elasticity, indicate that Nautilus and Octopus arterial systems act as true "Windkessels", whereas it appears possible that wave propagation effects may be important in large squids during periods of maximal activity.

MINERAL DEPOSITS IN CONNECTIVE TISSUES:
THE MECHANICAL DESIGN OF SPICULE-REINFORCED ANIMALS

M. A. R. Koehl
Department of Zoology
University of California, Berkeley, California 94720



Many animals from different phyla have embedded in their pliable connective tissues small bits of stiff material known as spicules.¹ The tensile behavior of spicule-reinforced connective tissues from various cnidarians and sponges, as well as of model spiculated "tissues", was investigated in order to elucidate the effects on mechanical properties of spicule size and shape, and of their packing density and orientation within a tissue. The main results of the study are:

Spicules increase the stiffness of pliable connective tissues probably by mechanisms analogous to those by which filler particles stiffen deformable polymers: local strain amplification, and interference with molecular rearrangements in response to a load.

The greater the volume fraction of spicules, the stiffer the tissue.

The greater the surface area of spicules per volume of tissue, the stiffer the tissue. Thus, a given volume of spicules of high surface-area-to-volume-ratio (S/V) have a greater stiffening effect than does an equal volume of large spicules of low S/V . Furthermore, a high volume fraction of large spicules in a tissue can have the same stiffening effect as a lower volume fraction of smaller spicules.

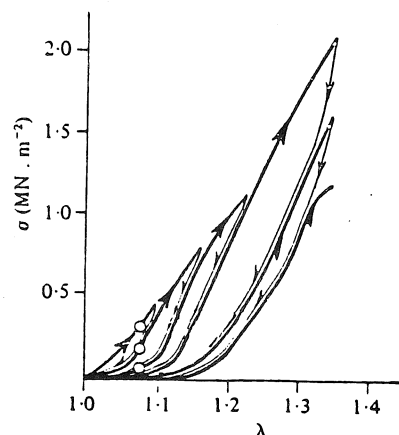
Spicules that are anisometric in shape have a greater stiffening effect parallel to their long axes.

Spicules with very high aspect ratios appear to act like reinforcing fibers -- stress is transferred by shearing from the pliable matrix to the stiff fibers, which thus bear in tension part of the load on the composite.

Spicule-reinforced tissues exhibit stress-softening behavior, which is more pronounced in heavily-spiculated tissues.²

The distribution and morphology of spicules (and therefore of stiffness) within the body of an animal or colony can affect the way in which the whole structure responds to mechanical loads, such as those imposed by flowing water.

² Stress-softening: Stress (σ)-extension (λ) curves for spiculated connective tissue from a soft coral, *Alcyonium*, subjected to cyclic tests until it broke. The tissue was being pulled when arrows point upwards to the right and was being returned to its original length when arrows point downwards to the left. Note that the stress in the tissue at a give extension is greater on the first pull than on subsequent pulls (compare circles) and less work (area under the curve) is required to pull the tissue to a given extension once it has been thus softened. ($\dot{\epsilon} = 0.04 \text{ s}^{-1}$).



IONIC REGULATION OF TISSUE MODULUS: ELECTROSTATIC OR CHEMICAL?

John P. Eglers
 Zoology
 Duke University*

Alan R. Greenberg
 Mechanical Engineering
 University of Colorado, Boulder

Sea cucumbers (phylum: Echinodermata) are remarkable for their ability to increase the elastic modulus of dermal connective tissues in response to attack. The dermis is a collagen meshwork enveloped in an aqueous gel of randomly coiled proteoglycan macromolecules and bounded by inner and outer cell layers. Evidence indicates that a neurochemical message initiates the defence by instructing surface cells to alter the ionic environment of the interstitial water. The modulus can be manipulated experimentally by diffusing ions into exposed tissue, but it is not known whether the effect arises from ion-polymer electrostatic interactions alone or if chemical bonding is also involved.

Assuming that there is no change in the network bonding pattern, the theory of random coil polymers yields the following propositions: 1) the density of the material (D) must increase with the ionic strength ($dD/dI > 0$); and 2) the elastic modulus (E) must increase with the density ($dE/dD > 0$). To test these propositions the moduli of tissue strips from *Thyonella gemmata* were measured by constant strain-rate loading in an Instron testing device. Matched samples were run in either distilled water (DW) or isotonic solutions of sodium chloride (.55M NaCl) or calcium chloride (.39M CaCl₂), after which the density of each was determined by pycnometer.

	O	I	E	D	n
DW	0	0	18 (7)*	1.32 (.06)*	16
NaCl	550	0.55	6 (5)	1.28 (.06)	17
CaCl ₂	550	1.16	17 (6)	1.40 (.04)	15

O-osmolality (mOs); I-ionic strength (Eq/l); E-elastic modulus (MPa); D-density (g/ml); *-standard deviation; n-number

Comparing DW to NaCl reveals a violation of proposition 1. Likewise CaCl₂ vs. DW violates proposition 2. However, the differences between sodium and calcium treated tissues are entirely consistent with both. Thus we conclude that although isotonic changes in ionic composition may have only electrostatic effects on the polymers, the complete removal of free ions appears to affect chemical bonds within the matrix as well.

* present address: 36 Whittier Blvd., Foughkeepsie NY 12603

THE INTERACTIVE EFFECTS BETWEEN FOOT TYPE AND SHOE CHARACTERISTICS

B.T. Bates, P.R. Francis, and H. Kinoshita, Biomechanics/Sports Medicine Lab., University of Oregon, Eugene, OR, 97403

The foot forms the dynamic base upon which the runner performs. The actions that occur at the foot-shoe-surface interface are of critical importance since they influence the functional mechanisms of the entire lower extremity. Since individuals are anatomically and functionally different, it would seem reasonable to expect that people might respond differently to various shoes. The purpose of this study was to examine the footfall characteristics of two extreme foot types and the interaction between these two foot types and three selected shoes during running.

The experimental set-up consisted of a force platform, a high speed movie camera, and a photoelectric timing system. Six individuals who were classified as having pes cavus (PC) foot types and six who were classified as having pes planus (PP) foot types were selected from volunteers following a clinical examination. All subjects were provided with the same models (basic, soft and firm) of running shoes in appropriate sizes. Following a brief warm-up and familiarization period, each subject performed 10 acceptable trials in each of the three shoes. An acceptable trial required that the subject contact the force platform in a "normal" running pattern and achieve a criterion speed of 15 km/hr \pm 4% (5.75-6.25 min/mi) through the test area. Force data were collected for all trials and coincident film data were collected for five of the 10 acceptable trials. Testing order of the shoes was randomly assigned.

Data analysis consisted of evaluating selected variables describing the ground reaction force-time curves and the pronation-time curves. Mean values for individuals were obtained from the appropriate trials and averaged across subjects to obtain condition means. Following preliminary data evaluation it became evident that the original clinical classification scheme was not adequate in predicting dynamic foot function. The correlation coefficient between pronation and foot type was a non-significant 0.10. Consequently, a dynamic classification scheme based upon foot function while wearing the basic shoe was also incorporated. Three groups (D1, D2, D3) were formed over the continuum from minimum to maximum mean pronation. Group composition was as follows: D1 - 1PC, 3PP; D2 - 3PC, 1PP; D3 - 2PC, 2PP. Five variables were evaluated in addition to selected comparisons and rankings.

The PC group exhibited greater overall pronation (14.1 vs 12.0 deg) than the PP group contrary to expectation. Based upon dynamic classification, group D1 performed best in the basic shoe (7.9 deg) while D3 functioned best in the firm shoe (15.0 deg). Overall, performance in the soft shoe was poorest (14.0 deg) followed by the firm (12.8 deg) and basic (12.4 deg) shoes. Evaluation of the initial impact force resulted in slightly lesser values (20.7 vs 22.0 N/Kg) for the PP group. There were no significant differences between the soft (20.7 N/Kg) and firm (20.3 N/Kg) shoe results overall or by group breakdown. Overall, D1 forces (19.2 N/Kg) were less than those for D2 (23.8 N/Kg) and D3 (21.0 N/Kg). The poor overall performance by the D2 group could have resulted from the predominance of rigid foot types making up the group (3PC and 1PP). Rankings based upon the primary variables resulted in best overall performances for groups D1, D2 and D3 while wearing the basic, soft and firm shoes respectively. In conclusion, foot type as evaluated clinically did not produce a viable scheme for assessing dynamic function. In addition, evaluation of shoe effects independent of dynamic foot function knowledge produced limited useful information.

HIERARCHICAL DESIGN IN A FIBRE REINFORCED COMPOSITE;
THE EQUINE HOOF WALL

J.E. Bertram and J.M. Gosline
Department of Zoology, University of British Columbia,
Vancouver, British Columbia, Canada

The levels of structural organization of the equine hoof wall (stratum medium) are described as discerned through scanning electron, transmission electron and polarized light microscopy. This keratinous material is constructed on several separate but dependent levels of organization. The α -helical fibre/ disulphide X-linked matrix composite (molecular level) forms lamellar sheets at the ultrastructural level. These sheets are themselves organized as concentric cylinders (ca. 100 μ m diam.) running the height of the hoof wall (microstructural level). From the fibre orientation within the lamellar sheets to the general organization of the concentric cylinders this material system closely resembles the secondary osteons found in Haversian bone. The similarity between bone and hoof is especially surprising when considering the major differences between the two in terms of embryonic origin, composition and mode of deposition. It is proposed that the organization of hoof wall and Haversian bone represents convergent design among these fibre reinforced composites. As seen for bone, this specific design enhances the fracture toughness of hoof wall and may also contribute to its abrasion resistance. Some preliminary mechanical test data supporting this conclusion is provided.

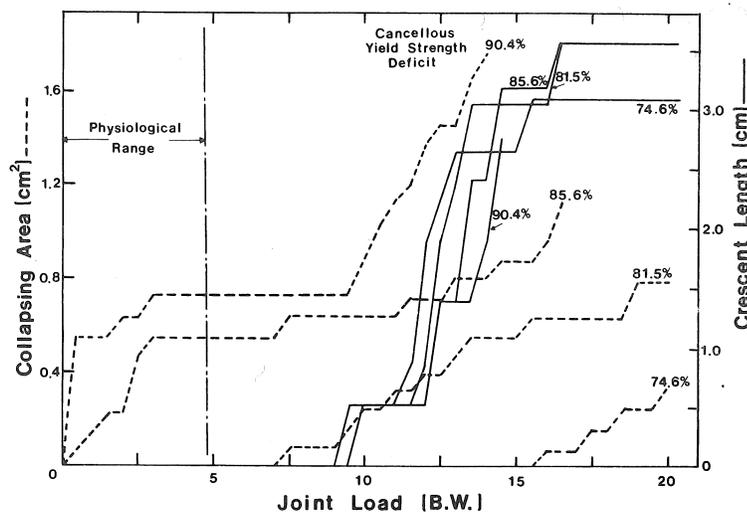
EARLY COLLAPSE PROCESSES IN FEMORAL HEAD OSTEO NECROSIS:
A MATERIALLY NONLINEAR FINITE ELEMENT FORMULATION

Thomas D. Brown, Ph.D.
Thomas A. Mutschler, M.S.
Albert B. Ferguson, Jr., M.D.

Department of Orthopaedic Surgery
986 Scaife Hall
University of Pittsburgh
Pittsburgh, Pa. 15261

Aseptic necrosis of the femoral head is a frequent complication of femoral neck fractures, and is also often seen in patients with a history of alcoholism or prolonged steroid administration. Despite the essentially mechanistic nature of the head collapse processes, rather little is presently known about the role of specific mechanical factors in the initiation and progression of bony failure. This study reports the development and application of a nonlinear finite element model of femoral head osteonecrosis, in which the experimentally observed post-yield behavior of cancellous bone in compression is approximated by a linear-strain-hardening elasto-plastic constitutive relationship. An 816 degree-of-freedom plane strain numerical formulation, based upon the initial stress solution technique, allows computation of sectional stress fields as a function of incrementally applied muscle and (distributed) articular surface loads. Lesion parameter effects explored were subchondral and intracapsular strength and modulus deficits (dependent on revascularization), as well as the depth, subchondral chord length, and orientation of wedge-shaped infarctions.

The computational results consistently demonstrated both subchondral and intracapsular failure patterns similar to those seen clinically. There was a clear distinction, however, between these two failure regimes (Figure 1), dependent primarily upon the relative strength deficits in these two zones. Failure progressively advanced with increasing joint load, but was observed to initiate within the physiological load range only if there was exceedingly severe bony strength compromise. The implied involvement of fatigue effects in the failure processes is, however, fully consistent with the multi-month nature of the clinical collapse process. The dependence of failure zone growth upon lesion geometrical parameters was found to be exceedingly complex. Regions of failure within a small lesion were usually not found to be regions of failure within an inclusive large lesion; rather, the failure zones tended to "migrate" in such a manner as to be concentrated, within a given lesion, near the necrotic/viable bone interfaces.



Biodynamic Considerations in Foot Slip Prevention

by: Don B. Chaffin, Robert Andres, Kwan Lee
Center for Ergonomics
The University of Michigan
Ann Arbor, MI 48109

This paper develops a dynamic, eight-link biomechanical model of a person pushing and pulling a cart. This model is validated by having subjects of varied anthropometry and strength push and pull a cart while three-dimensional, instantaneous hand and foot forces were measured. The validation experiments included a range of handle heights, walking speeds, and cart motion resistance forces.

The resulting model was found to predict instantaneous foot normal and shear forces with an r^2 value of about 0.6 (the mean normal force error was 60N and shear force error of 19N). Peak foot forces were predicted well enough to develop estimates of the maximum coefficient of friction required between the shoe and floor during a stride cycle. These estimates were shown to be significantly affected by, 1) subject body weight, 2) speed of walking, 3) hand force direction (pushing or pulling), and 4) handle height.

It is proposed that the use of biomechanical model of the type described can provide a rational means for determining the traction requirements of various walking surfaces when people must move heavy objects.

FLOW PROPERTIES AND RUPTURE STRENGTH
OF NAUTILUS SIPHUNCULAR TUBE

John A. Chamberlain, Jr., Department of Geology, Brooklyn College of the City University of New York, Brooklyn, NY 11210 and Osborn Laboratories of Marine Sciences, New York Aquarium, Brooklyn, NY 11224; William A. Moore, Jr., Dept. of Geology, Brooklyn College of CUNY; and Stephen W. Pillsbury, Dept. of Geology, Brooklyn College of CUNY

Measurement of flow rates and rupture strength of fresh Nautilus siphuncular tube at elevated pressures (10-85 bars) indicates that: 1) volume flow rate across the wall of the siphuncular tube increases linearly with pressure. 2) Flow rate increases in successively larger chambers of the shell as a result of size-related variation in surface area and thickness of the tube wall. Flow rate does not keep pace with ontogenetic increases in chamber volume and total body weight so that removal of fluid from new chambers may become increasingly time-consuming as the animal grows, and expensive metabolically. 3) Pumping rates in live Nautilus are considerably lower than flow rates induced in siphuncular tubes from empty shells. Pumping capacity of the live animal is apparently limited by the functional constraints inherent in its osmotic pump rather than by the fluid conductance properties of the tube wall. 4) Flow is not localized in the vicinity of the septal necks, as is commonly believed, but occurs uniformly along the length of the tube. 5) The siphuncular tube bursts at pressures of about 80-85 bars, which is equivalent to ambient hydrostatic pressure at the known depth limits of the live animals. Rupture usually occurs in the boundary zone of the siphuncle - septum junction. The contact of the tube to its mechanical supports is thus weaker than the tube itself. 6) Siphuncle rupture strength is constant in the last 20 chambers, as is tube thickness. Tube radius increases. This suggests that the geometry of the siphuncular tube can not be used as an index of living depth for fossil cephalopods.

ON THE BIOMECHANICS OF POLE VAULTING AND ANALYSIS OF DISLODGING OF THE BUTT PLUG

Ali E. Engin, Ph.D.
Department of Engineering Mechanics
The Ohio State University
Columbus, Ohio 43210 U.S.A.

and

Johnson Oladunni, Ph.D.
Engineering Analysis Department
University of Lagos, Nigeria

Review of the literature on the biomechanics of pole vaulting reveals two striking points. First, all efforts seem to be directed mainly in the direction of improving performance characteristics of the pole vaulter by studying bending and straightening of the pole while the kinetic and potential energies of the performing athlete change. Second, there appears to be no published work which deals with the consequences of improperly executed pole-vaulting. This paper therefore, focuses attention to some aspects of the second point.

Pole vaulting with a fiberglass pole is a continuous dynamic event which can be characterized by three phases. In the first phase the athlete attempts to gain as much horizontal momentum as possible by running with the pole. In the second phase he tries to convert most of the resulting kinetic energy to the potential energy by flexing of the pole. During this phase, the forward progress of the point of the pole is stopped by its placement in the box. However, forward motion of the upper part of the pole is reduced gradually as the pole flexes and swings like a pendulum to the vertical position. The swing-up, turn and push-up of the body defines the second pendulum action and constitute the third phase of the vaulting process.

The end of the pole which is placed in the box has a butt plug that should remain with the pole if the pole-vaulting is done properly according to the phases mentioned above. However, if the vaulter makes a bad vault and instead of letting loose grip of the pole, hangs onto it and takes it down on to the matts with him, he introduces the possibility of dislodging of the butt plug. In this paper, causes of dislodging of the butt plug are delineated by means of computation of the stored elastic strain energy in the pole and resulting whip-like motion of the bottom of the pole, thus, giving the plug high centrifugal acceleration. If the butt plug is not properly attached to the pole it is dislodged and behaves like a high speed projectile which can very easily hurt anyone nearby. In fact, dislodgement of the butt plug occurs frequently during improper vaulting and has already caused several eye injuries and resulted law suits. The paper is concluded with some suggestions on design modifications to prevent dislodging of the butt plug.

MAXIMIZING HEIGHT IN THE FOSBURY FLOP; EFFECTS OF INITIAL CONDITIONS

M. HUBBARD and J.C. TRINKLE Department of Mechanical Engineering
University of California Davis, California 95616

In a multisegment dynamic model of the high jump, the trajectories of the segments depend on their initial positions and velocities and on the jumper's actions throughout the event. Attaining maximum height, therefore, results from optimizing both takeoff conditions and muscle torques while airborne. It is of interest to investigate these two determinants of performance separately but in most cases this is impossible since they are inextricably intertwined (changing the takeoff conditions slightly will change the optimal muscle torques in flight). They can be separated, however, when the model for the jumper is a rigid body, containing no internal joints at which muscle torques may act. In this paper we calculate optimum initial conditions for a particular form of the high jump, the Fosbury Flop, where the jumper crosses the bar with the body extended and perpendicular to the bar. A similar approach has been used to study the simpler 'straddle' high jump techniques [1].

The mathematical model is shown schematically in Fig. 1. The jumper is assumed to be a single rigid body, a one dimensional rod of mass m , length l , centroidal mass moment of inertia I , and center of mass height d , and is assumed to move in a vertical plane perpendicular to the crossbar. At takeoff the jumper makes an angle θ with the horizontal plane and has components of velocity u and v , angular velocity ω , and kinetic energy T .

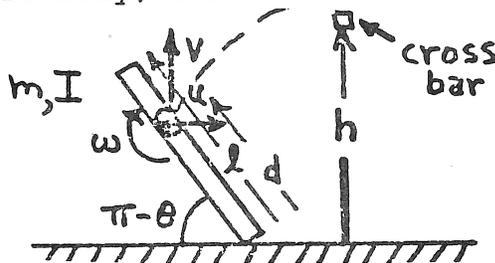


FIGURE 1. Schematic diagram

The problem may then be posed as the following: subject to a given initial kinetic energy $T = (mu^2 + mv^2 + J\omega^2)/2$, how should this be apportioned into u , v , and ω and what should the takeoff angle θ be in order to clear the maximum height? We define dimensionless variables $\tilde{T} = T/mg\ell$, $\tilde{I} = I/ml^2$, $\tilde{d} = d/\ell$, $\tilde{u} = u/\sqrt{lg}$, $\tilde{\omega} = \omega\sqrt{\ell/g}$, $\tilde{v} = v/\sqrt{lg}$ and (because optimal jumps always involve one or more brushes with the bar) the dimensionless brush time $\tilde{t} = t\sqrt{g/\ell}$. Nonlinear parameter optimization techniques with equality and inequality constraints are used to calculate optimal $\tilde{\omega}$, \tilde{u} , \tilde{v} , and θ . These results are presented as a function of the independent parameters \tilde{T} , \tilde{I} , and \tilde{d} . Interestingly, for $\tilde{d} = 0.5$ the solution space has two regions where there are, respectively, one and two brushes of the bar. In the latter region brush occurs at other than the center and the jumper c.m. reaches its peak significantly above the bar.

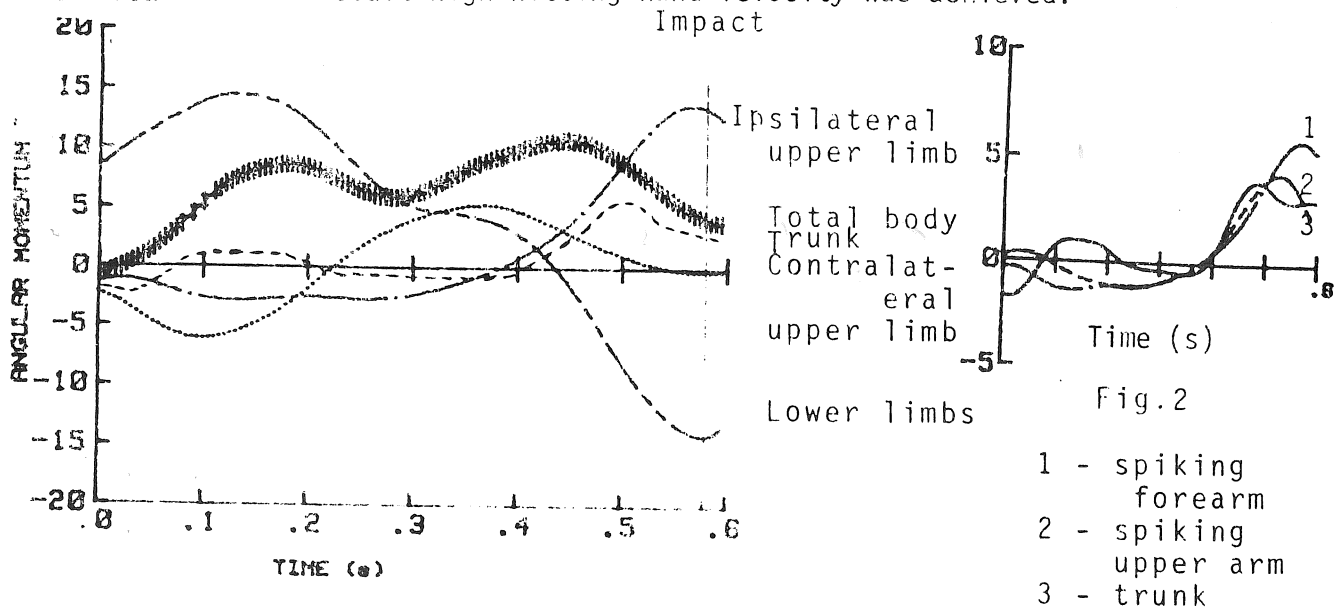
REFERENCES

1. M. Hubbard and J.C. Trinkle, Proc. 3d Conf. ESB, Nijmegen, The Netherlands, Jan. 1982.
2. P.E. Gill and W. Murray (eds.), Numerical Methods for Unconstrained Optimization, Academic Press, New York, 1974.

SEGMENT INTERACTION IN THE VOLLEYBALL SPIKE

- D.J. Kriellars, Dalhousie University, Halifax, N.S.

The sequencing and interaction of segment motion is an important factor in skill performance. In the aerial phase of the volleyball spike, segment interaction can be examined readily because of the simplification provided by the law of conservation of angular momentum in free fall. The purpose of this study was to investigate the segmental contributions to the velocity of the spiking hand, with particular emphasis on the temporal relationships of the segment angular momenta. Cine film was collected on two elite volleyball players (ten trials each). Two-dimensional kinematic and kinetic data were derived from the displacement data obtained from the film, using Dempster's body segment parameter data. Angular momentum was calculated relative to body mass centre with the following equation: $H_z^{cm} = I_{z,cm} \dot{\theta}_i + (\bar{r}_{cm,i} / cm \times m_i \dot{v}_{cm,i} / cm)$. A "forward somersaulting" (positive) total system angular momentum about the centroidal transverse axis of $7 \text{ kgm}^2/\text{s}$ was found. During the initial aerial phase, the angular momentum of the system was primarily restricted to both lower legs and the contralateral upper limb. The moment of the linear momentum of these distal segments relative to the total body mass centre (remote term) dominated these segments' contribution to the total system angular momentum. As a result, the trunk was maintained in a near vertical orientation. Later, during the hitting action of the spike, the contralateral limb's angular momentum decreased to zero. At the same time the local angular momentum of the upper trunk increased, the angular momentum of the spiking arm also increased such that it exceeded the system total and the angular momentum of the lower extremities decreased and eventually became directed opposite to that of the hitting arm and the system as a whole. An examination of the resultant knee and hip torques indicate that knee extension and hip flexion observed during the latter phase of the spike is an active process, much like a kick. This "kick" resulted in an increased backward (negative) angular momentum of the legs. The remaining segments reacted with an increase in their positive angular momenta and as a result high hitting hand velocity was achieved.



An increase in angular momentum and velocity from proximal to distal segments was found as a general pattern in the hitting phase (Fig. 2), with the more proximal segments decreasing in forward angular momentum and velocity as the distal segments increase. This sequential motion has previously been described as "transfer of angular momentum".

THE MEASUREMENT OF FOOT AND ANKLE KINEMATICS IN A SPORTS MEDICINE CLINIC. F.G. Lippert and R.M. Harrington, Dept. of Orthopaedics, Seattle VAMC; A.S. Woodle and S.G. Newell, Podiatry, Seattle; G.L. Scheirman, Dept. of Kinesiology, Univ. of Washington, Seattle, WA.

Running subjects the foot and ankle to high forces and large motions. Injuries such as achilles tendinitis, plantar fasciitis, shin splints, chondromalacia patellae, iliotibial band friction syndrome and popliteus tendinitis have been clinically linked to excessive pronation of the foot during ground contact. Pronation unlocks the foot for shock absorbing and adapting to uneven surfaces. The calcaneus everts and the medial longitudinal arch depresses. Several studies have measured this motion by filming the foot from the rear or medial side during ground contact. There is much interest in controlling the foot's motion either through the design of the shoe or by means of various orthotic devices placed in the shoe. The clinical application of these methods is usually based on static measurements or visual observation of walking and running. The purpose of this study was to adapt some of the methods of biomechanics research laboratories to clinical use in a podiatric sports medicine clinic.

Subjects are chosen from among the patients who are treated with plastic foot orthotics made over a plaster impression of their foot. Subjects run on a Quinton Instrument Co. treadmill and are filmed by a Polaroid Polavision high speed camera at 125 frames/second. The orthotics are designed to support the medial arch of the foot. In addition, posts may be added to the rearfoot, forefoot, or both areas to control the rocking and tilting motions of the foot during ground contact. Subjects are filmed barefoot, with shoes, with the orthotics in the shoes, and with the orthotic taped to the foot, but no shoes. For this study, orthotics were made with no posts, rearfoot posts and forefoot posts.

Various methods of measuring foot and ankle kinematics were compared. One common clinical method is to observe the subject as he walks or runs in a hall. The treadmill allows the clinician to observe multiple steps more closely and estimate the range of inversion/eversion of the heel. Next, the subject was filmed from the rear. Three reflective dots were placed in a line on both the midline of the calcaneus and the bisector of the lower Achilles tendon. The field of view of the camera included the foot and lower leg. The Polaroid system includes a viewer which develops the film in a few minutes and projects it at slow speeds or stop action. The angle between the calcaneus and lower leg, or the calcaneus and vertical can be measured directly on the viewer with a goniometer. For the final comparison, the film was digitized at the University of Washington Department of Kinesiology on a Hewlett-Packard 9864A digitizer linked to a 9810A computer which determined the angles. To evaluate digitizing error, film records were digitized twice. The resulting absolute error was 0.6° and the standard deviation of the error was 0.4° . As the results for a typical subject show, visual observation and goniometer measurements are not very accurate, but their magnitude follows the same trend as the values calculated by digitizing the film. It would appear desirable to include a digitizing tablet and microcomputer in the tools of a sports medicine clinic.

		RANGE OF INVERSION/EVERSION (DEGREES)							
		Leg/Calcaneus				Calcaneus/Vertical			
Condition	Foot	DIG	GON	OBS 1	OBS 2	DIG	GON	OBS 1	OBS 2
Barefoot	L	8.8±1.7	8	8	3	6.4±1.1	6	6	3
	R	9.8±1.5	9	7	3	7.6±1.1	5	5	0
Orthotics No Posts	L	7.1±2.7	9	8	2	6.4±2.1	7	6	2
	R	9.4±0.8	6	7	3	7.6±1.1	5	5	0
Orthotics RF Posts	L	7.9±1.6	4	6	2	5.9±1.4	4	3	0
	R	7.4±1.4	5	5	3	7.3±1.0	4	2	0
Orthotics FF Posts	L	4.8±1.5	1	4	2	3.5±0.8	0	3	0
	R	9.3±1.4	3	2	3	6.4±1.5	1	2	0

EFFECTS OF SHOE TYPE ON FOOT FUNCTIONING AND CONTACT PRESSURES DURING WALKING PERFORMANCE

D.R. McIntyre & B.F. Raley, Biomechanics Laboratory, Division of Physical Education and Dance, North Texas State University, Denton, Texas 76203

The purpose of this study was to evaluate the functional effectiveness of a selection of women's walking shoes. Nine female subjects each performed fifteen walking trials corresponding to three trials for each of five shoe/barefoot (BF) conditions. The shoes worn by each subject were: a flexible shank shoe (F), a ripple sole flexible shank shoe (R), a subject preferred shoe (P) and a rigid rockered sole shoe (RS). With the exception of the subject preferred shoe all shoes had comparable heel heights and uppers. During each trial, the pressures on the dorsum of the left foot in the region of the second metatarsal-phalangeal joint during a stance phase were recorded. Simultaneous film records were made of both the rear and lateral projections of the left lower limb. An ANOVA with repeated measures ($p < 0.5$) revealed no significant differences between the shoe/barefoot conditions for selected instantaneous values of the angles of the thigh, leg, foot, knee, ankle and a defined angle of pronation. The normalized absolute pressure impulses (N.sec./cm². kg.) were found to be of lesser magnitude for the RS (0.07) than for the F (0.13), R (0.10), P (0.15) and BF (0.14) conditions. Similar results were found for the maximum pressures although the RS was not significantly different from the R for this measure. The results of his study would lend support for the use of a rigid rockered sole shoe to reduce pressure concentrations in the forefoot region during walking performances. The concomitant potential exists for reducing the incidence of related foot problems.

ON SLOPE TESTING OF AN INSTRUMENTED ALPINE SKI BOOT

H. Medoff, MS, J. Pierce, M. Pope, PhD, R. Johnson, MD, D. Punia, BSEE
University of Vermont, Department of Orthopaedics & Rehabilitation
Burlington, VT 05405

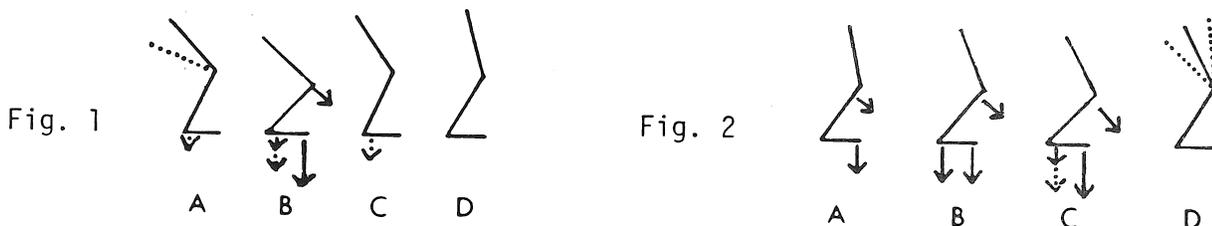
Alpine ski boots are the primary component of the force transmission system between a skier and the ski. During typical skiing maneuvers, forces are sent through the boot, the ski and ultimately to the snow. This process continues in a dual fashion, with "snow induced forces" moving up to the ski, through the boot and to the skier.

It was our goal during these tests to measure some of the forces on the foot/leg during actual skiing, as well as the knee angle and angular position of the tibia. These measured skiing forces on the leg will also be converted to bending stresses on the tibia and compared to the theoretical breaking strength.

Equipment: Ten transducers were monitored, six on the tongue area, two measuring gross pressure (one under the forefoot, another under the heel), two measuring ankle and knee angle respectively. The ten outputs went to a backpack worn by the skier which contained signal conditioning and amplification voltage to frequency conversion and a frequency multiplexor. The ten frequency signals were stored by a SONY TC5DM stereo cassette recorder that was strapped to the skier's chest. The total system weight was 6.4 kg, and is completely self-contained. In our laboratory, the frequencies were then "reconverted" to voltages and recorded on a 6-channel Gould chart recorder.

Test: A preliminary test was conducted with a collegiate racer of national caliber. The snow condition the day of this test can best be described as "Eastern slush". We instructed our skier to ski "normally" and take one run of slalom type turns and another of giant slalom type.

Test Results: We found that the slalom turns differed from the giant slalom (GS) in that some heel pressure usually preceded and coincided with the forward "weighting" (Fig. 1, phase A), unlike the GS turns which displayed an initial increasing forefoot and tongue pressure, followed by heel pressure (Fig. 2, phases A, B). GS turns also were distinguished by sustained heel pressures at phase B, which in the slalom run were very dynamic. In phase C of the GS and phases B and C of the slalom, the magnitude of heel forces appears to be a proprioceptive response to the terrain and/or the imaginary course. In some slalom turns, heel forces barely reach 5% of body weight (BW). In another, it reached 88% BW. High heel forces in the slalom were usually the result of a sudden weight shift from the forefoot at the end of the turn. The interplay of boot tongue forces with the other forces was similar in both runs, with the sensors nearest the top of the tongue reading the greatest force.



Figures indicate relative leg position, direction and magnitude of force. Dots indicate variable ranges.

AN INVESTIGATION OF MECHANICS OF BOXING AND HEAD INJURIES

L. Nguyen, P. K. Phung, Y. Youm, and S. C. Ling

Department of Mechanical Engineering
The Catholic University of America
Washington, D. C. 20064

Although boxing gloves are used, there has been increasing concern over injuries, especially brain damage, among the amateur and professional boxers in the sport of boxing.

Review of literature shows that there is an extreme scarcity in the field of scientific research of boxing. In this investigation, an analytical and experimental study was conducted. The main objectives were, firstly, to understand the mechanics of boxing, secondly, to determine the mechanical aspects of head injuries and, thirdly, to select the best suitable glove materials, among the manufacturers' lists, to reduce injuries.

For the analytical study, a mechanism of punching against the head of the boxer was simulated. A basic mechanical model was established. This model was then interpreted as an analogous electrical system which consisted of resistive, capacitive, and inductive elements; and, from this system, the equations of motions were derived. The currents were considered as the velocities of the arm of the boxer and the head of the opponent, the inductances as the masses of the arm and the head, and the capacitance as the compliance of the glove.

The compliance of the head was assumed as negligible compared to that of the glove. And from experiment, the compliance of the glove was obtained as a non-linear characteristic. Due to the non-linearity of the compliance, the finite difference solution method was employed to solve the equations.

Three different velocities of the punching arm were applied to the subject model to determine the critical acceleration of the brain during impact. This numerical analysis was done to the computer simulation.

Based on the severity index equation proposed by Gadd, the severity index values for three different velocities were computed. In this study, any value greater than 1000, the critical value, could cause severe brain damage.

In conclusion, this study enhanced the understanding of the mechanics of boxing and the head injuries in a quantitative manner.

Simon, Mark R., Department of Veterinary Biosciences, University of Illinois, Urbana, IL 61801. The Effect of Increased Intermittent Compressive Forces on Bone Growth.

The work of Hueter and Volkmann in 1862 showed an inverse relationship between static compressive forces parallel to the axis of epiphyseal cartilage and the rate of growth of that cartilage. In a previous study on the effects of compressive forces on the growth of condylar cartilage, I suggested that the normal compressive forces present during growth are necessary to stimulate condylar cartilage development. In a later work, experimental hindleg bipedalism was employed to study its effect on the growth and histomorphology of the epiphyseal growth plates of the metatarsals in the rat. Experimental bipedalism produces increased compressive stresses of an intermittent nature on the hindlimb bones because rats do not locomote continuously and, even during locomotion, the bones of a limb are stressed for only a fraction of each cycle. The results of that study suggested that increased, intermittent, compressive forces could prolong growth of the epiphyseal cartilage.

In this study, male and female Sprague-Dawley rats were used to see if increased, intermittent, compressive forces, produced by experimental bipedalism would have a compensatory effect in experimental-clinical situations known to inhibit bone growth, e.g., hypophysectomy, and cortisone injected rats. Half of the rats underwent amputation of both front legs at 10 days of age. At 21 days of age, half of the normal rats and half of the bipedal rats were subjected to the experimental-clinical situation. All rats were sacrificed at 55 days of age, and weighed. The hindlimb bones were removed, cleared of soft tissues, and fixed in 10% B.N.F. for 1 week. Each bone was blotter-dried, weighed on a Mettler scale with an accuracy of 0.0001 g, and the length of each bone was measured on a Helios caliper with an accuracy of 1/20 mm. The results of this study suggest that increased, intermittent, compressive forces can be instrumental in increasing long bone growth; however, that such treatment might be most effective among adolescent females.

THREE DIMENSIONAL GEOMETRIC MODEL OF THE FOOT

Sirois, J.P.⁽²⁾, Allard, P.^{(1),(2)}, Thiry, P.S.⁽¹⁾

(1) Department of Mechanical Engineering, Ecole Polytechnique, Montreal

(2) Pediatric Research Center, Ste-Justine Hospital, Montreal, Canada

Charting of bi-planar radiographs is a useful technique for the diagnosis of foot deformities. However, due to the complexity and variation of the bony structure of the foot, these studies must be compared with caution and are often of limited statistical value (Gamble and Yale, 1975). A recent study of cavus foot deformity using this approach has been performed on forty four Friedreich Ataxia patients (Allard et al., 1982). This work permitted the identification of three specific evolutionary patterns of the disorder. It pointed out also the difficulty of extracting three-dimensional characteristics of bony structures from non standardized bi-planar projections. This paper presents the standardized radiography technique and the geometric model used in the tri-dimensional reconstruction of the foot.

STANDARDIZED RADIOGRAPHY TECHNIQUE

An apparatus has been designed in our laboratory for standardizing bi-planar radiographs of the foot (Sibille et al., 1981). It is used to comfortably immobilize the patients' feet while a pair of radiographs are taken. Calibration spheres and reference axes on the surface of the film cassette allow the reconstruction of the internal orientation of each projection. For reasons of ease of execution, a 15° angle stereo-photogrammetric technique is used rather than an orthogonal technique.

THREE DIMENSIONAL MODEL

A three-dimensional "stick diagram" type model of the bony structure of the foot has been developed. The essential element of this model is the identification, from two radiographs, of distinct anatomical features on every bone. Each specific point is then located in a three dimensional cartesian coordinate system. An example of the simplest form is the spatial reconstruction of the metatarsals. These bones are modeled by their central axis which originates at the head of the bone and terminates at its base. This reconstruction allows us to calculate distances between points or the spatial angle between metatarsals.

RESULTS

As an illustration, the following parameters were calculated from a human foot skeleton and compared satisfactorily to the corresponding measurements made with a vernier caliper:

	calculated	measured
width of the forefoot:	71 mm	69 mm
length of the 1st metatarsal:	59 mm	56 mm
length of the 2nd metatarsal:	67 mm	66 mm
length of the 5th metatarsal:	58 mm	60 mm

The model is presently being used to describe the pes cavus deformity of Friedreich Ataxia patients at the Ste-Justine Hospital in Montreal.

ACKNOWLEDGEMENTS

Financial support from the Friedreich Ataxia Association of Canada is gratefully acknowledged.

REFERENCES

1. Gamble, F.O., Yale, I., Clinical Foot Roentgenology, 2nd ed., R.E. Krieger Co., New York, 1975.
2. Allard, P., Sirois, J.P., Thiry, P.S., Geoffroy, G., Duhaime, M., Roentgenographic Study of Cavus Foot Deformity in Friedreich Ataxia Patients, Can. J. Neur. Sciences, accepted for publication in 1982.
3. Sibille, J., Tremblay, C., Thiry, P.S., Allard, P., Reference Apparatus for Normalized Bi-Planar Radiographs of the Foot, Vth Ann.Meet.Am.Soc.Biomech., Cleveland, 1981.

BIOMECHANICS OF WOODSPLITTING

David G. Wilder, MSME, Steven W. Arms, BS,
Dennis D. Donnermeyer, BMET, Ian A.F. Stokes, Ph.D., Malcolm H. Pope, Ph.D.
University of Vermont, Department of Orthopaedics & Rehabilitation
Burlington, VT 05405

Use of wood for domestic space heating is increasing. It has been said that wood heats one twice: once during the burning, but also once during the chopping. Therefore, we investigated the mechanics of woodsplitting with an ax to gain insight into the energetics and kinetics of this activity.

Five healthy males were studied while splitting representative samples of Vermont maple. Forces in the ax handle were transduced by means of electrical resistance strain gauges wired to transduce the bending moment. Sagittal plane motion was recorded by means of a 16mm Bolex cine camera running at 24 frames/sec. Subsequently, positions of five points on the subject and the center of mass of the ax were digitized on a "Summagraphics" digitizer. The loci of these points were smoothed by means of a five-point moving average algorithm. Potential energies were then calculated, and velocities were calculated by differencing.

From the kinematic analysis of the films of successful and unsuccessful splitting attempts, peak kinetic energy of the ax was found to occur just prior to impact with the wood. The average kinetic energies produced for unsuccessful and successful splits were 1063.5 Joules (SD: 255.2 Joules) and 1124.1 Joules (SD: 319.7 Joules) respectively. The average elapsed times for the unsuccessful and successful ax swings were 2.56 sec (SD: 0.63 sec) and 2.47 sec (SD: 0.84 sec) respectively. Neither the kinetic energies nor the ax swing times were significantly different between the unsuccessful and successful splitting attempts.

Fracture energies of the wood were found by driving the ax into similar samples using an MTS machine, running at 1.27mm/sec. Energy was calculated by integrating the force/distance recordings. The mean fracture energy to create a fracture surface was 257.4 Joules/m². This corresponded to an energy of about 7.2 Joules for a typical log. Therefore, the manual method was highly inefficient, since the final energies of the ax were of the order of a kilojoule. Previously the value of a blunt ax has been noted (1). Average rate of working during a swing was about 440 watts or about 0.6 H.P. Kinematic analysis indicated a complex transfer of both kinetic and potential energy from subject to ax. We propose a new stationary bicycle driven hydraulic ram machine to improve the energy efficiency of muscle-powered woodsplitting. However, this would detract from one of the traditional benefits of chopping wood, that is, the thermodynamic heating of the body that the activity of chopping wood provides.

Reference:

1. Twitchell M: Wood Energy: A Practical Guide to Heating with Wood. Garden Way Publishing, Charlotte, Vermont, 1978, pp 81

DEVELOPMENT OF THE IN-VIVO
PROCEDURE FOR THE ORTHOTIC EVALUATION

A. S. Voloshin and C. P. Burger
Department of Engineering Science and Mechanics
Iowa State University
Ames, IA 50011 USA

J. Wosk
Hillel Hospital
Hadera, ISRAEL

It has become more and more recognizable during the last few years that proper cushioning of a subject's foot may make a big difference to his or her comfort. In response to this recognition, many companies now produce diverse orthotic devices. Some attempt to equalize pressure distribution, while others provide different support at various parts of the foot. The only test for effectiveness is the subjective feeling of the patient. This communication introduces a simple technique which allows for non-invasive, in-vivo measurement of the foot-orthotic interaction.

The technique is based on accelerometric measurements of the bone vibrations that result from heel strike during normal gait. A healthy subject wears a particular orthotic device for a time sufficient to feel himself comfortable. A low mass accelerometer is then strapped to the tibial tuberosity with a commercially available knee brace. The brace has a special construction that assumes uniform, constant and equal strapping force during each test. The subject is asked to walk naturally along a hard walkway, eight meters long, at approximately 100 steps/min.

The resulting vibrations are fed into an LSI-11/2 computer through a 12-bit resolution Analog-to-Digital Converter. The signals are processed through a Fast Fourier Analysis program, and the resultant frequency spectrum is studied to characterize the gait. The signals have frequency components ranging from 1 to 100 Hz. The data is recorded over a period of four seconds to include three or four complete walking cycles.

Preliminary experiments were run first with a barefoot subject and then with the same person wearing his own shoes and wearing shoes with a commercially available insert. The results revealed that shoes reduce the amplitude of the vibration measured on the tibial tuberosity by about 30%. Shoes with inserts reduced the amplitude by nearly 40%. These signals were analyzed by Fast Fourier Transform. The results show significant attenuation of the higher frequency components, above 10 Hz (from 10-35 Hz). No significant additional attenuation in the frequency domain occurred when the shoes were filled with inserts.

The results obtained show that this procedure can supply quantitative data for better design of shoes and inserts.